Falls Lake Nutrient Response Model

Provisional Draft Report

10/29/2009
Modeling & TMDL Unit
Division of Water Quality
North Carolina Department of Environment and Natural Resources

Acknowledgements

The Falls Lake nutrient response model was developed under the guidance of Falls Lake Technical Advisory Committee (TAC). We appreciate the helpful advice and recommendations provided by TAC members regarding model selection, choices of critical parameters, model statistics, and performance criteria. TAC members included representatives from Neuse Riverkeeper Foundation, City of Durham, City of Raleigh, Wake County, NC Division of Soil and Water Conservation, NC Department of Transportation, Triangle J. Council of Governments, South Granville Water and Sewer Authority, Durham County, and NC Division of Water Quality.

The Falls Lake Nutrient Response Model was thoroughly reviewed by Tetra Tech under contract from NC Department of Transportation. The review included model code, model application, and results. We appreciate the timely comments and feedback from Tetra Tech reviewers.

Contents

Figures

Tables

I. Introduction

I-1. Background

Falls of the Neuse Reservoir (also commonly referred to as Falls Lake), a multi-purpose man-made reservoir, is located in the upper portion of the Neuse River Basin, near the fast-developing Triangle Area in North Carolina (NC). The reservoir was constructed and filled by 1983, and is currently operated by the United States Army Corps of Engineers (USACE). Falls Dam is located just outside of Raleigh, immediately upstream of the village of Falls in Wake County, NC. Falls Lake stretches about 22 miles upstream to the confluence of the Eno, Flat, and Little Rivers near Durham. The reservoir covers almost 12,500 acres (50,585,000 m^2) with water and is surrounded by approximately 25,500 acres (103,193,400 m^2) of public land (Tetra Tech, 2003).

Falls of the Neuse Reservoir is the primary water supply for the City of Raleigh, and surrounding towns in Wake County, NC. The lake drains a watershed area of 494,600 acres or approximately 770 square miles, including all or part of the following six counties: Person, Durham, Orange, Wake, Franklin, and Granville. The watershed includes nine public drinking-water supply reservoirs for approximately 450,000 people.

Falls Lake has been categorized by NC Environmental Management Commission (EMC) as Nutrient Sensitive Waters (NSW) since 1983. As a result of this classification, NPDES discharge limits on phosphorus were put into effect. A statewide phosphate detergent ban was adopted by the General Assembly in 1988 to help further address phosphorus water quality problems in the Falls Lake watershed area and for other impoundments and estuaries in the state. The entire Neuse River Basin was classified as NSW in 1988. The 1993 Neuse River Basinwide Water Quality Plan recognized the achievement of total phosphorus load reduction, but identified that eutrophication continued to be a problem in Neuse River Estuary. Extensive fish kills were reported in 1995, drawing more attention to the water quality problem in the Neuse. A 30% reduction in nitrogen loading was recommended by

scientific committees and through the TMDL process to bring chlorophyll-*a* concentrations in the Neuse River to no more than 10% exceedance of the 40 ug/l state standard. In 1998, the EMC adopted the Neuse River Basin NSW Management Strategy to achieve the 30% reduction goal (the Neuse Riparian Buffer Protection rules became effective in 2000). As a result of the Strategy and the TMDL implementation, point sources and agriculture sources reduced their nitrogen contributions to the estuary by greater than 30% from the period of 1991-1995 by 2004.

In July 2005, the North Carolina General Assembly passed Session Law 190 (www.ncleg.net/sessions/2005/bills/senate/html/s981v5.html). Session Law 2005-190 requires the EMC to study drinking water supply reservoirs and develop nutrient control criteria to manage these reservoirs. In addition, a nutrient management strategy was required for certain reservoirs, including Falls of the Neuse Reservoir.

I-2. Purpose of Modeling Project

The primary objective of this modeling project is to develop and calibrate a combined hydrodynamic, sediment transport, and nutrient response model for Falls of the Neuse Reservoir in the Neuse River Basin. The nutrient response model will be used to assist DWQ in developing a nutrient management strategy for Falls Lake watershed.

Data collected during and prior to the modeling study indicate sufficient violations for turbidity and chlorophyll-*a* such that Falls Lake is placed on the 2008 draft 303(d) list of impaired waters. The model developed in this project can also be utilized for future TMDL development.

I-3. Field data used for the modeling project

The Falls Lake nutrient response model is developed based on field data collected by various State and Federal agencies, including: 2005-2007 data collected by DWQ Intensive Survey Unit at multiple stations in the lake; DWQ ambient monitoring stations located at the major tributaries; USGS flow and water quality data; climate

data from NC State Climate Office; and atmospheric deposition data from National Atmospheric Deposition Program (NADP) and Clean Air Status and Trends Network (CASTNET).

More information about available data for this study can be found in the Field Study and Modeling Plan for the Falls of the Neuse Reservoir Nutrient Management Strategy (http://h2o.enr.state.nc.us/tmdl/documents/FallsLakeNMSv8.3.pdf). Details on how the data are used are provided in section II-2 of this report.

II. Model Introduction

The three-dimensional, coupled hydrodynamic and water quality model Environmental Fluid Dynamics Code (EFDC), was selected to simulate water quality variations in the Falls Lake. A three-dimensional approach was recognized by the Falls Lake Technical Advisory Committee (TAC) as necessary to have a reasonable representation of the complicated bathymetry of Falls Lake. In addition, preliminary data showed multiple dominant algal groups were present in Falls Lake at different seasons; therefore, the TAC suggested that the model have the capability to represent different algal groups. EFDC was selected to meet these requirements.

EFDC has been identified as an acceptable tool for the development of Total Maximum Daily Loads by US Environmental Protection Agency (US EPA, 1997). It has been successfully applied in many types of water courses in previous studies, including estuaries, lakes, and coastal seas (e.g., Kuo et al., 1996; Shen et al., 1999; Ji et al., 2001; Lin and Kuo, 2003; Shen and Haas, 2004; Park et al., 2005; Lin et al., 2007, 2008; Xu, et al., 2008).

II-1. EFDC Model

EFDC has four sub-models: hydrodynamic, sediment transport, eutrophication (water quality model), and other transport model (Fig. II-1). The hydrodynamic model is the foundational sub-model, which simulates water surface elevation, current, salinity (not used in the current study), and temperature. These parameter inputs are provided to the other sub-models, and at the same time, biogeochemical processes regarding the concerned variables (e.g., sediments and nutrients) are calculated in the corresponding sub-models. A brief description of the hydrodynamic, sediment transport, and water quality sub-models follows.

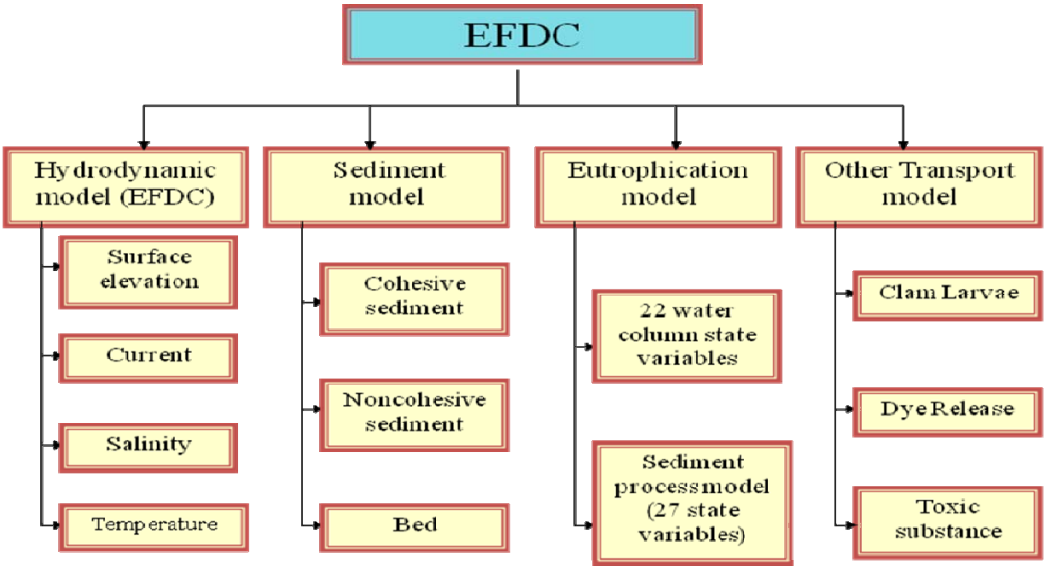

Fig. II-1. The EFDC Model Structure

a. Hydrodynamic model

The hydrodynamic sub-model was developed by Hamrick (1992; 1996). The model solves the Navier-Stokes equations for a water body with a free surface. In the vertical direction, sigma coordinates, with the hydrostatic assumption, are used in the model. Horizontally, curvilinear orthogonal grids are used. The following description of the hydrodynamic model of EFDC closely follows Hamrick (1992).

Transforming the vertically hydrostatic boundary layer form of the turbulent equations of motion and utilizing the Boussinesq approximation for variable density results in the momentum and continuity equations and the transport equations for salinity and temperature in the following form:

$$\partial_t(mHu) + \partial_x(m_y Huu) + \partial_y(m_x Hvu) + \partial_z(mwu) - (mf + v\partial_x m_y - u\partial_y m_x)Hv$$
$$= -m_y H\partial_x(g\zeta + p) - m_y(\partial_x h - z\partial_x H)\partial_z p + \partial_z(mH^{-1}A_v\partial_z u) + Q_u \qquad (1)$$

$$\partial_t(mHv) + \partial_x(m_y Huv) + \partial_y(m_x Hvv) + \partial_z(mwv) + (mf + v\partial_x m_y - u\partial_y m_x)Hu$$
$$= -m_x H\partial_y(g\zeta + p) - m_x(\partial_y h - z\partial_y H)\partial_z p + \partial_z(mH^{-1}A_v\partial_z v) + Q_v \qquad (2)$$

$$\partial_z p = -gH(\rho - \rho_o)\rho_o^{-1} = -gHb \qquad (3)$$

$$\partial_t(m\zeta) + \partial_x(m_y Hu) + \partial_y(m_x Hv) + \partial_z(mw) = 0 \tag{4}$$

$$\partial_t(m\zeta) + \partial_x(m_y H\int_0^1 u dz) + \partial_y(m_x H\int_0^1 v dz) = 0 \tag{5}$$

$$\rho = \rho(p, S, T) \tag{6}$$

$$\partial_t(mHS) + \partial_x(m_y HuS) + \partial_y(m_x HvS) + \partial_z(mwS) = \partial_z(mH^{-1}A_b\partial_z S) + Q_S \tag{7}$$

$$\partial_t(mHT) + \partial_x(m_y HuT) + \partial_y(m_x HvT) + \partial_z(mwT) = \partial_z(mH^{-1}A_b\partial_z T) + Q_T . \tag{8}$$

In the above equations, u and v are the horizontal velocity components in the curvilinear, orthogonal coordinates x and y, mx and my are the square roots of the diagonal components of the metric tensor, m = mxmy is the Jacobian or square root of the metric tensor determinant. The vertical velocity, with physical units, in the stretched, dimensionless vertical coordinate z is w.

The total depth, H= h + ζ, is the sum of the depth below and the free surface displacement relative to the undisturbed physical vertical coordinate origin, z* = 0. The pressure p is the physical pressure in excess of the reference density hydrostatic pressure, $\rho_0 gH(1 - z)$, divided by the reference density, ρ_0. In the momentum equations (1, 2), f is the Coriolis parameter, Av is the vertical turbulent or eddy viscosity, and Qu and Qv are momentum source-sink terms which will be later modeled as subgrid scale horizontal diffusion. The density, ρ, is in general a function of temperature, T, and salinity or water vapor, S, in hydrospheric and atmospheric flows respectively and can be a weak function of pressure, consistent with the incompressible continuity equation under the anelastic approximation. The buoyancy, b, is defined in equation (3) as the normalized deviation of density from the reference value. The continuity equation (4) has been integrated with respect to z over the interval (0,1) to produce the depth integrated continuity equation (5) using

the vertical boundary conditions, w = 0, at z = (0,1), which follows from the kinematic conditions. In the transport equations for salinity and temperature (7,8) the source and sink terms, QS and QT include subgrid scale horizontal diffusion and thermal sources and sinks, while Ab is the vertical turbulent diffusivity.

The system of eight equations (1-8) provides a closed system for the variables u, v, w, p, ζ, ρ, S, and T, provided that the vertical turbulent viscosity and diffusivity and the source and sink terms are specified.

Mellor and Yamada's level 2.5 turbulence closure scheme (Mellor and Yamada, 1982), which was modified by Galperin et al. (1988), is used in the model. Both turbulent kinetic energy and turbulent length scale are solved using dynamically coupled transport equations.

A wetting and drying scheme (Ji et al., 2001) is also included in the model. A detailed description of the EFDC hydrodynamic model and its numerical solution scheme can be found in Hamrick (1992; 1996).

b. Sediment transport model

The sediment transport model is coupled with the hydrodynamic model with the same time resolution. A multiple-class sediment transport model (Kim et al., 1998; Lin and Kuo, 2003) is included in the model. In this study, three sediment classes were selected to represent washload, clay, and silt/fine sand.

The governing equation for each class of the total suspended sediment concentration in the water column is:

$$\frac{\partial mHC}{\partial t}+\frac{\partial m_y HCu}{\partial x}+\frac{\partial m_x HCv}{\partial y}+\frac{\partial mC(w-w_s)}{\partial z}$$
$$=\frac{\partial}{\partial x}(\frac{m_y}{m_x}k_h H\frac{\partial C}{\partial x})+\frac{\partial}{\partial y}(\frac{m_x}{m_y}k_h H\frac{\partial C}{\partial y})+\frac{\partial}{\partial z}(k_z\frac{m}{H}\frac{\partial C}{\partial z}) \quad (9)$$

where C is the TSS concentration in the water column; H is the water depth; u, v, and w are the water velocity components in x, y, and z directions, respectively; w_s is the typical sediment settling velocity, and k_h and k_z are the horizontal and vertical turbulent diffusion coefficients, respectively. m_x and m_y are the square roots of the

diagonal components of the metric tensor for the scale factors of the horizontal coordinates, $m = m_x m_y$ is the Jacobian or square root of the metric tensor determinant. At the water surface, no sediment flux is allowed, and the boundary condition is:

$$w_s C + k_z \frac{\partial C}{\partial z} = 0 \qquad (10)$$

The bottom boundary condition for sediment flux is:

$$w_s C + k_z \frac{\partial C}{\partial z} = D - E \qquad (11)$$

where E is the mass of sediment eroded from bottom per unit bed area per unit time, also known as the erosion or resuspension rate; D is the mass of sediment deposited to bottom per unit bed area per unit time, or the so-called deposition rate. The erosion rate for cohesive sediment is simulated as:

$$E = \begin{cases} M\left(\frac{\tau_b - \tau_{ec}}{\tau_n} - 1\right)^{\exp} & for\ \tau_b > \tau_{ec} \\ 0 & for\ \tau_b \le \tau_{ec} \end{cases} \qquad (12)$$

where τ_b is the bed shear stress, M is an empirical constant with the same unit as E; and τ_{ec} is the critical shear stress for erosion.

The deposition rate D is calculated as: $D = Pw_sC_b$. P is the probability of deposition; different forms have been adopted by different modelers (Sanford and Chang 1997; McDonald and Cheng, 1997; etc.). C_b is the sediment concentration near the bed. A commonly used formulation to define P is $P = \frac{\tau_{dc} - \tau_b}{\tau_{dc}}$ if bed shear stress is less than a critical shear stress for deposition (τ_{dc}) and P = 0 if the bottom shear stress is higher. The model calculates D as:

$$D = \begin{cases} w_s C_b \frac{\tau_{dc} - \tau_b}{\tau_{dc}} & for\ \tau_{dc} > \tau_b \\ 0 & for\ \tau_{dc} \le \tau_b \end{cases} \qquad (13)$$

Constant values of the empirical parameters (e.g. M, τ_{ec}, τ_{dc}) were used within the model domain. Table II-1 lists the parameter values used in the model.

In calculating the bed shear stress, τ_b, it was assumed that τ_b is a linear summation of current-induced bed shear stress, $\tau_{current}$, and wind-wave-induced bed shear stresses, τ_{wave}:

$$\tau_b = \tau_{current} + \tau_{wave} \quad (14)$$

$$\tau_w = 1/2\, f_w \rho U_b^{\,2} \quad (15)$$

where f_w is the wave drag coefficient, ρ is water density, and U_b is the maximum orbital velocity near the bottom (Sanford et al. 1999; Nakagawa et al. 2000).

In predicting wind waves, the empirical formulation (Eq. 16) suggested by Shore Protection Manual (1984) was used.

$$\frac{gH}{U_A^{\,2}} = 0.283 \tanh[0.530(\frac{gd}{U_A^{\,2}})^{3/4}] \tanh\{\frac{0.00565(\frac{gF}{U_A^{\,2}})^{1/2}}{\tanh[0.530(\frac{gd}{U_A^{\,2}})^{3/4}]}\}$$

$$\frac{gT}{U_A} = 7.54 \tanh[0.833(\frac{gd}{U_A^{\,2}})^{3/8}] \tanh\{\frac{0.0379(\frac{gF}{U_A^{\,2}})^{1/3}}{\tanh[0.833(\frac{gd}{U_A^{\,2}})^{3/8}]}\} \quad (16)$$

Where H and T are the predicted significant wave height and period, U_A is the wind speed, d is the water depth, and F is the fetch.

A bed sediment model in EFDC keeps track of the deposited sediments at the bed of each cell of the model grid; therefore, sediment resuspension can be limited by the amount of sediments at the bed.

Table II-1. Parameters used in TSS simulation

Parameter	w_s (m/s)	M	τ_{ec} (m^2/s^2)	τ_n (m^2/s^2)	exp	τ_{dc} (m^2/s^2)
Class 1	5.e-7	0.01	1.e-2	1.e-2	1.0	1.e-2
Class 2	5.e-6	0.006	1.e-4	1.e-4	1.0	1.e-4
Class 3	5.e-5	0.004	1.e-3	1.e-3	1.0	1.e-3

c. Eutrophication model

The water quality sub-model of EFDC (Park et al., 1995a; Tetra Tech, 2007) consists of a water column water quality model and a sediment diagenesis model linked internally. The water column water quality model simulates the spatial and temporal distributions of 22 state variables in the water column (Table II-2). Their

interactions are illustrated in Fig. II-2. These variables include: suspended algae (3 groups: cyanobacteria as model state variable Bc, diatoms as Bd, and green algae as Bg); a stationary or non-transported algae (has been used to simulate macroalgae); organic carbon (refractory particulate organic carbon as RPOC, labile particulate organic carbon as LPOC, dissolved organic carbon as DOC); nitrogen (refractory particulate organic nitrogen as RPON, labile particulate organic nitrogen as LPON, dissolved organic nitrogen as DON, ammonium nitrogen as NH_4, nitrite plus nitrate nitrogen as NO_3); phosphorus (refractory particulate organic phosphorus as RPOP, labile particulate organic phosphorus as LPOP, dissolved organic phosphorus as DOP, total phosphate as PO_{4t}); silica (particulate biogenic silica as SU, available silica as SA); dissolved oxygen (as DO); chemical oxygen demand (as COD); total suspended solids (as TSS, which is simulated in the hydrodynamic model); total active metal (as TAM); and fecal coliform bacteria (as FCB).

For each state variable, a mass conservation equation is solved:

$$\frac{\partial C}{\partial t}+\frac{\partial (Cu)}{\partial x}+\frac{\partial (Cv)}{\partial y}+\frac{\partial (Cw)}{\partial z}=\frac{\partial}{\partial x}(K_x\frac{\partial C}{\partial x})+\frac{\partial}{\partial y}(K_y\frac{\partial C}{\partial y})+\frac{\partial}{\partial z}(K_z\frac{\partial C}{\partial z})+S_c \quad (17)$$

where C is the concentration of a water quality state variable and u, v, and w are the water velocity components in the x, y, and z directions, respectively. K_x, K_y, and K_z are the turbulent diffusivities in the x, y, and z directions, respectively. S_c is the internal and external sources and sinks of the water quality state variable.

Internal sources/sinks are those generated/consumed by kinetic processes. External sources/sinks refer to point sources and non-point sources fringing the system. The simulated kinetic processes in the water quality model include algal growth, metabolization, predation, hydrolysis, mineralization, nitrification, and denitrification.

Table II-2. EFDC model water quality state variables

(1) cyanobacteria: Bc
(2) diatom algae: Bd
(3) green algae: Bg
(4) stationary algae: Bm
(5) refractory particulate organic carbon: RPOC
(6) labile particulate organic carbon: LPOC
(7) dissolved organic carbon: DOC
(8) refractory particulate organic phosphorus: RPOP
(9) labile particulate organic phosphorus: LPOP
(10) dissolved organic phosphorus: DOP
(11) total phosphate: PO4t
(12) refractory particulate organic nitrogen: RPON
(13) labile particulate organic nitrogen: LPON
(14) dissolved organic nitrogen: DON
(15) ammonia nitrogen: NH4
(16) nitrate nitrogen: NO3
(17) particulate biogenic silica: SU
(18) dissolved available silica: SA
(19) chemical oxygen demand: COD
(20) dissolved oxygen: DO
(21) total active metal: TAM
(22) Fecal coliform bacteria: FCB

The kinetic formulations in the model are mostly from CE-QUAL-ICM (Cerco and Cole, 1993; 1994; Cerco, 1995), with differences listed in Park *et al*. (1995a; 1998; 2005). A detailed description of kinetic processes and their mathematical formulations used in the eutrophication sub-model can be found in Park et al. (1995a), Tetra Tech (2007), and Ji (2008).

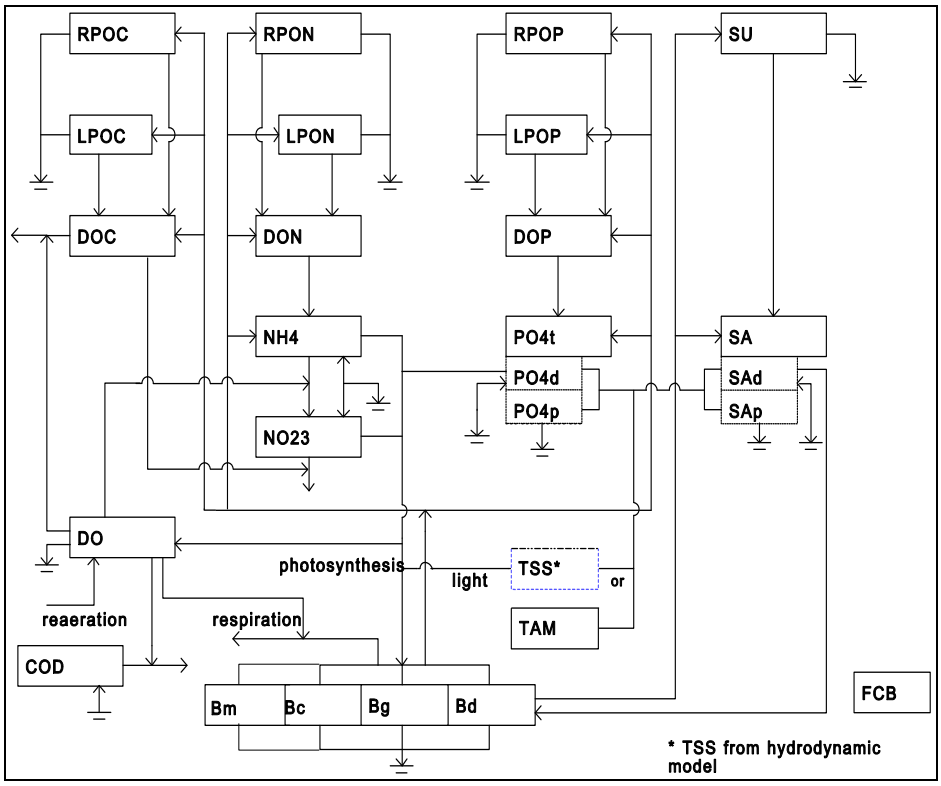

Fig. II-2. State variables simulated in the EFDC water quality model

II-2. Model Configuration

a. Model Grid

The main stem of the Falls of the Neuse Reservoir extends from relatively deeper channels close to the dam up to shallower arms downstream of the confluence of the Eno, Little, and Flat Rivers. The channel winds around especially at the confluence between the New Light creek and Falls Lake. To better fit the bathymetry of Falls Reservoir, orthogonal curvilinear grids were used. Cell sizes varied from around 60 m to about 1000 m. A total of 519 cells were used in the model (Fig. II-3).

Vertical stratification of water temperature and dissolved oxygen were usually observed during summer. Therefore, four vertical layers were used in the model in order to represent the vertical differences in the water column and, at the same time, to manage the cost of computational time. These four vertical layers divide the water column equally.

Bathymetry data used include 17 transects (spreading across the entire Falls Reservoir) conducted in 2005 by DWQ, USGS 24K TOPO map, and DEM data from the Flood Plain Mapping Program. These data were used to assign depth for each model cell. Linear interpolations of closest available data points were used to calculate the depths of cells where data were not available.

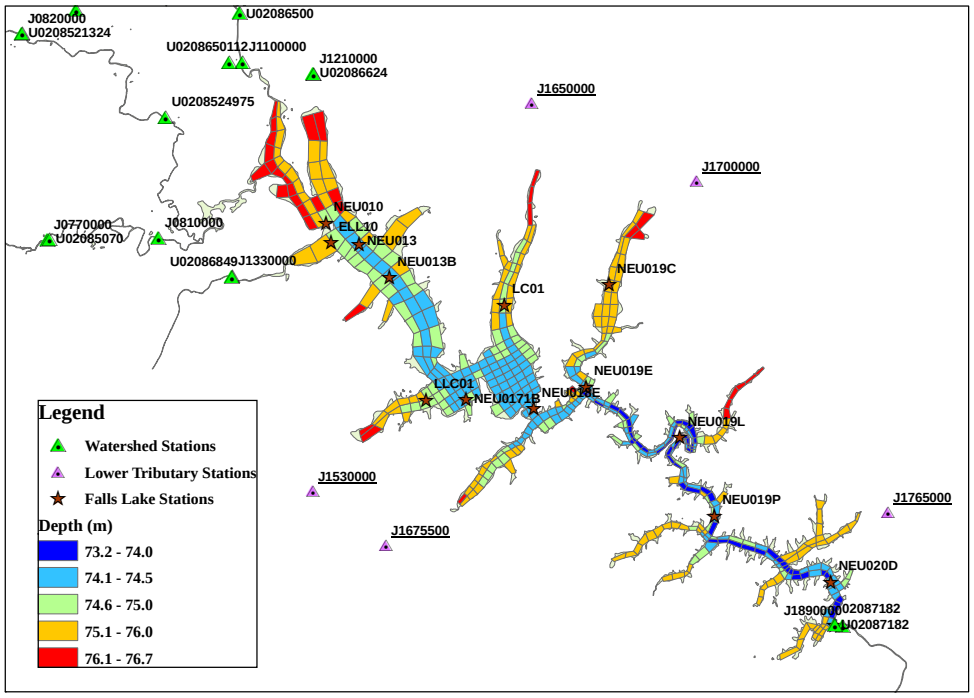

Fig. II-3. Falls Lake model grid and monitoring stations

b. Surface Boundary Condition

Surface boundary was specified for both the hydrodynamic and the eutrophication sub-models of EFDC.

Air temperature, wind, cloud cover, relative humidity, solar radiation, and rainfall data were needed for calculation of the heat flux, water mass flux, and surface drag at the interface between air and water. These data were obtained from the NC State Climate Office at RDU airport station. In cases of missing data from RDU station, data from Reedy Creek Station was used.

In the eutrophication model, air depositions of NH4 and NO3 are included as nutrient sources into the surface layer of the water column. Two forms of air deposition were considered here: dry deposition and wet deposition. Dry depositions are the depositional nutrient fluxes during dry (non-raining) days. Wet depositions are the depositional nutrient fluxes accompanied with rainfall. Dry and wet deposition nutrient fluxes suggested by a data survey study from the Highway Stormwater Program of the NC Department of Transportation were used in this model study (NCDOT, 2008).

For wet depositional flux, weekly wet chemistry data from National Atmospheric Deposition Program (NADP) station NC41 (Finley Farms, Wake County, North Carolina) were used in the model (Fig. II-4).

For dry chemistry inputs, Clean Air Status and Trends Network (CASTNET) station PED108 (Prince Edward, Prince Edward County, Virginia) was found to be the best available source of weekly average data for sulfate, SO_x, NO_x, nitrate and ammonium (Fig. II-5). The weekly fluxes calculated by Multi Layer Model and downloaded from http://www.epa.gov/castnet/data.html were used. The Prince Edward station is located approximately 65 miles north of the Falls Lake watershed in Prince Edward County, Virginia.

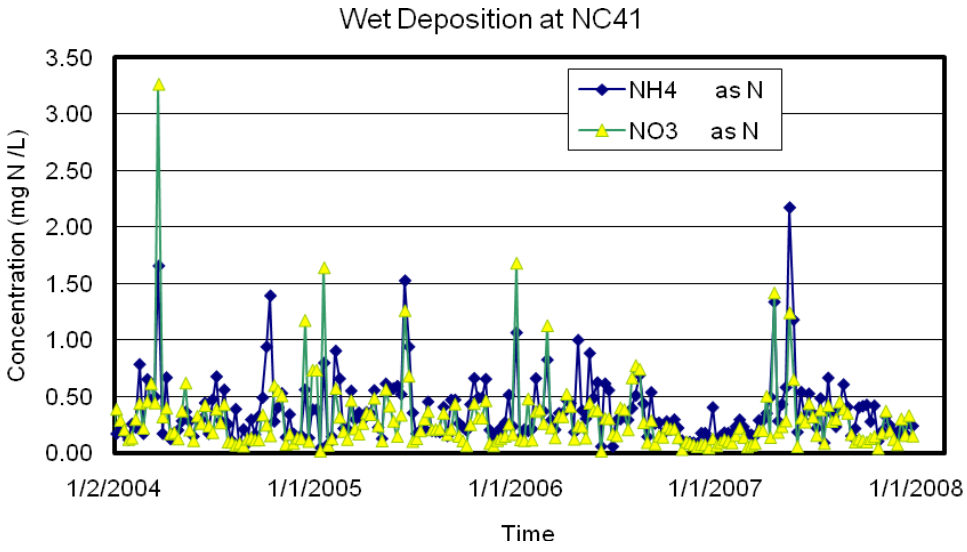

Fig. II-4. Time series of nutrient concentrations (from NADP) for the calculation of wet atmospheric deposition.

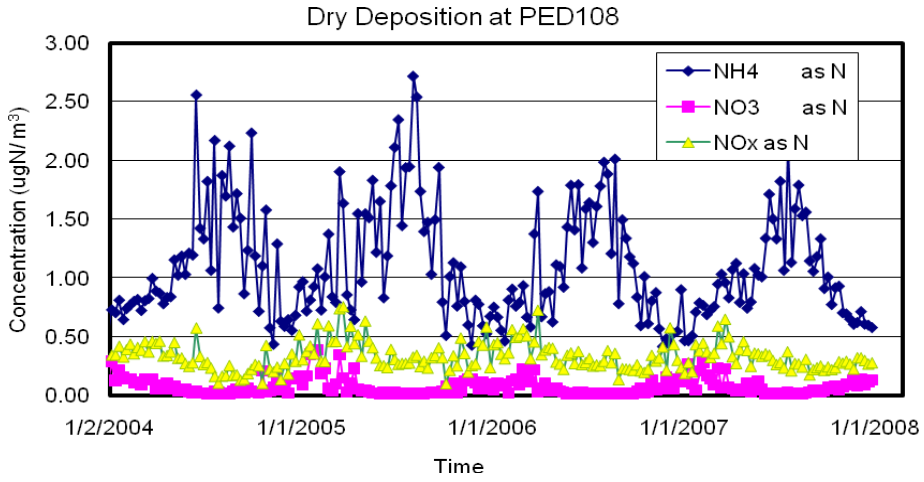

Fig. II-5. Time series of nutrient concentrations (from CASTNET) for the calculation of dry atmospheric deposition.

c. River Boundary Conditions

Eighteen river inputs/outputs were specified in the Falls Lake modeling domain to represent 17 tributaries and one outward discharge at the dam (Fig. II-6). For gaged and monitored tributaries, observational data were used to derive the river inputs. The river inflow data was downloaded from the USGS web site at: http://waterdata.usgs.gov/nwis. The water quality observational data can be downloaded from EPA STORET Program at: http://www.epa.gov/storet/dbtop.html.

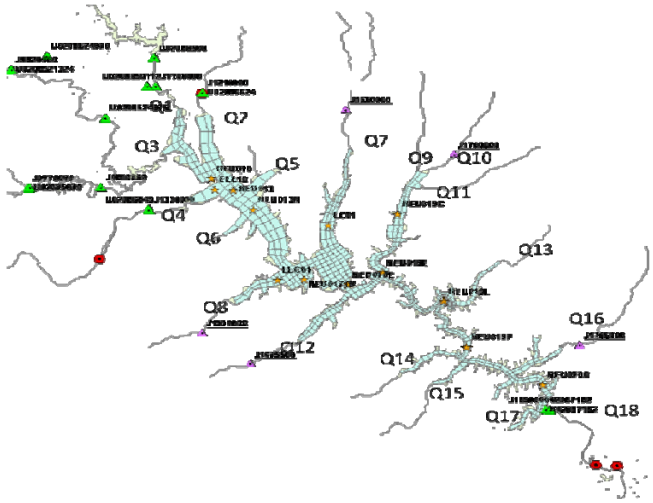

Fig. II-6. Falls Lake Model River Inputs

For un-gaged and un-monitored tributaries, concentration data from a close-by tributary were used and flow data from a close-by tributary multiplied by a distribution ratio were specified. The distribution ratio was calibrated based on the ratio between the un-gaged drainage basin area and the close-by tributary basin area. Table II-3 – II-6 lists the estimated drainage area (based on the DWQ WARMF segmentation) and monitoring stations used for each river inputs/outputs.

Table II-3. Estimated drainage areas (in m^2) from WARMF model segmentation for un-gaged tributaries

River Input	*Estimated Area*	*River Input*	*Estimated Area*
Q2	11600	Q11	3500
Q4	7500	Q12	4000
Q5	1600	Q13	4000
Q6	1500	Q14	2500
Q7	5800	Q15	2700
Q8	4500	Q16	4000
Q9	4000	Q17	2400
Q10	3500		

Table II-4. Monitoring stations used for water temperature river inputs

River input	*Station (-0000)*	*River input*	*Station (-0000)*
Q1	J110	Q10	J121
Q2	J121	Q11	J121
Q3	J081	Q12	J133
Q4	J133	Q13	J121
Q5	J121	Q14	J133
Q6	J133	Q15	J133
Q7	J121	Q16	J121
Q8	J133	Q17	J133
Q9	J121	Q18	J121

Table II-5. Monitoring stations used for TSS river inputs (values are listed as used for 2005/2006/2007)

River input	*Station (-0000)*	*River input*	*Station (-000022)*
Q1	J110/J110/J110	Q10	J121/J121/J121
Q2	J121/J121/J121	Q11	J121/J121/J121
Q3	J189/J107/J189	Q12	J189/J107/J189
Q4	J133/J133/J133	Q13	J110/J110/J110
Q5	J077/J077/J077	Q14	J110/J110/J110
Q6	J133/J133/J133	Q15	J110/J110/J110
Q7	J082/J082/J082	Q16	J110/J110/J110
Q8	J110/J110/J110	Q17	J110/J110/J110
Q9	J121/J121/J121	Q18	J110/J110/J110

Table II-6a. Monitoring stations used for river inputs of N, P, and DO.

River input	*Station*	*River input*	*Station*
Q1	J1100000	Q10	J1700000
Q2	J1210000	Q11	J1700000
Q3	J0810000	Q12	J1675500
Q4	J1330000	Q13	J1700000
Q5	J1650000	Q14	J1675500
Q6	J1530000	Q15	J1675500
Q7	J1650000	Q16	J1765000
Q8	J1530000	Q17	J1765000
Q9	J1700000	Q18	J1890000

Table II-6b. Monitoring stations used for river inputs of TOC and chl-*a* (values are listed as used for 2005/2006/2007)

River input	*Lake Station*	*River input*	*Lake Station*
Q1	NEU010/NEU010/NEU010	Q10	NEU019C/NEU019C/NEU019C
Q2	NEU010/NEU010/NEU010	Q11	NEU019C/NEU019C/NEU019C
Q3	NEU010/NEU010/NEU010	Q12	NEU018E/NEU018E/NEU018E
Q4	NEU013/ELL10/ELL10	Q13	NEU019L/NEU019L/NEU019L
Q5	NEU013B/NEU013B/NEU013B	Q14	NEU019P/NEU019P/NEU019P
Q6	NEU013B/NEU013B/NEU013B	Q15	NEU019P/NEU019P/NEU019P
Q7	NEU017B/LC01/LC01	Q16	NEU020D/NEU020D/NEU020D
Q8	NEU017B/LLC01/LLC01	Q17	NEU020D/NEU020D/NEU020D
Q9	NEU019C/NEU019C/NEU019C	Q18	NEU020D/NEU020D/NEU020D

d. Benthic Nutrient Flux

Benthic nutrient fluxes were measured by DWQ in April 2006 at two sites:

Site 1: NEU018E - NH3 flux from sediment to water column was reported at a rate of 0.0103 $g/m^2/day$. No significant net flux of NO2+NO3, or TP was found. SOD average flux rate was -0.7811 $g/m^2/day$ (negative implies sediment removing oxygen from the water column).

Site 2: NEU013B - NH3 flux from sediment to water column was reported at a rate of 0.0501 $g/m^2/day$. No significant net flux of NO2+NO3 or TP was found. SOD average flux rate was -1.3868 $g/m^2/day$.

Since certain temporal and spatial variations of the nutrient flux rates were reported, and neither the spatial nor the temporal resolutions of the data were enough to develop a dynamic representation of sediment nutrient fluxes for model use, constant values were specified in the model. The measured nutrient flux rates were used as an indication of the ranges of the parameter values and their order of magnitudes. The exact nutrient flux values were selected through model calibration processes and are listed in Table II-7.

Table II-7. Constant benthic nutrient fluxes specified in the model (unit: $g/m^2/day$)

	NH3	PO4	NOx	SOD
2005	0.02	0.0023	0.00	-1.2
2006	0.01	0.001	0.00	-1.2
2007	0.02	0.0023	0.00	-1.2

e. **Model Period**

Intensive surveys in the lake and at the ambient monitoring stations were conducted from March 2005 to September 2007; the models were set up to run during these periods.

Long-term (1984-2007) averaged rainfall tends to be evenly distributed among different months; however, the estimated long-term lake inflow (data from USACE)

shows a seasonal pattern of higher inflows during winter-spring, and lower during summer-autumn (Fig. II-7).

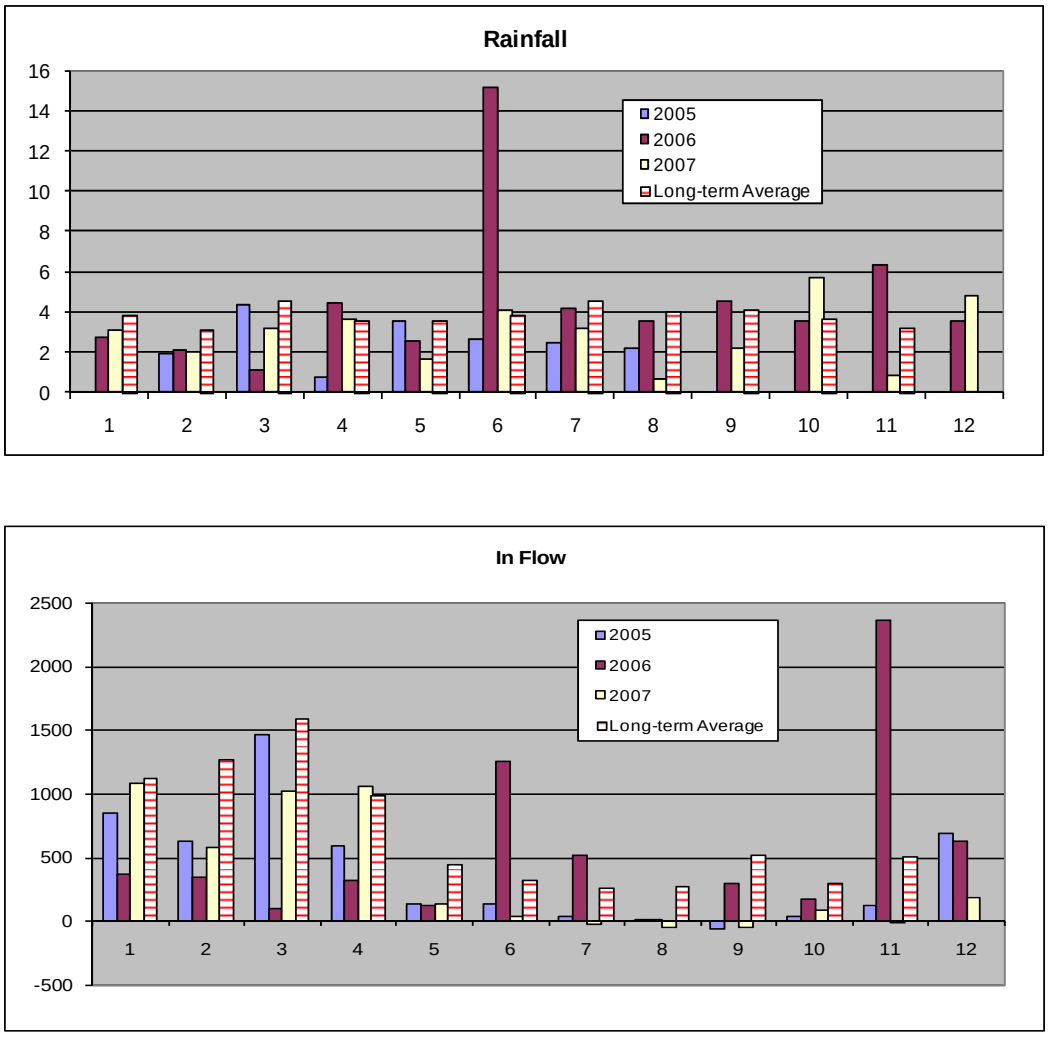

Fig. II-7. Monthly rainfall and inflow during 2005, 2006, and 2007, compared with long-term (1984-2007) data at Falls Lake.

Variations from the long-term average (denoted as abnormal values, Fig. II-8) are quite different among 2005, 2006 and 2007. Comparatively, 2005 and 2007 are dry years with negative abnormal inflows almost throughout; both significantly negative and positive abnormal inflows were observed during 2006, which resulted in a year with total rainfalls and inflows close to the long-term mean.

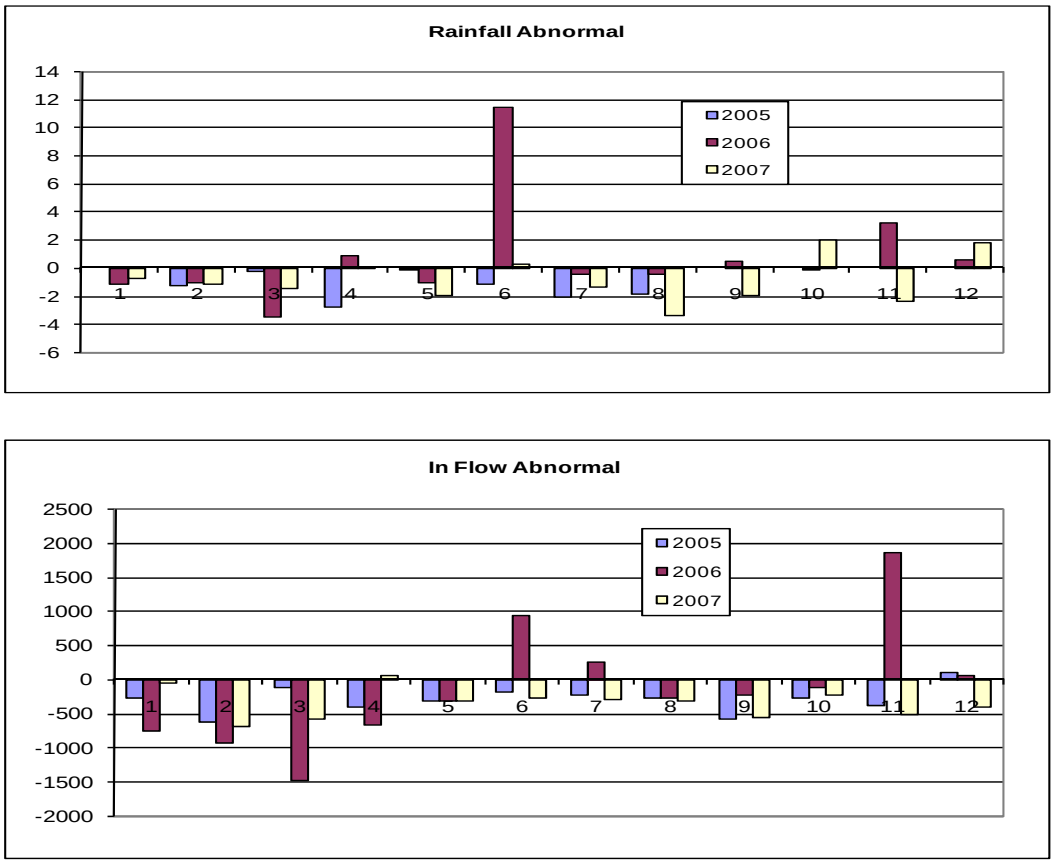

Fig. II-8. Monthly rainfall and inflow abnormal (from long-term mean) during 2005, 2006, and 2007 at the Falls Lake.

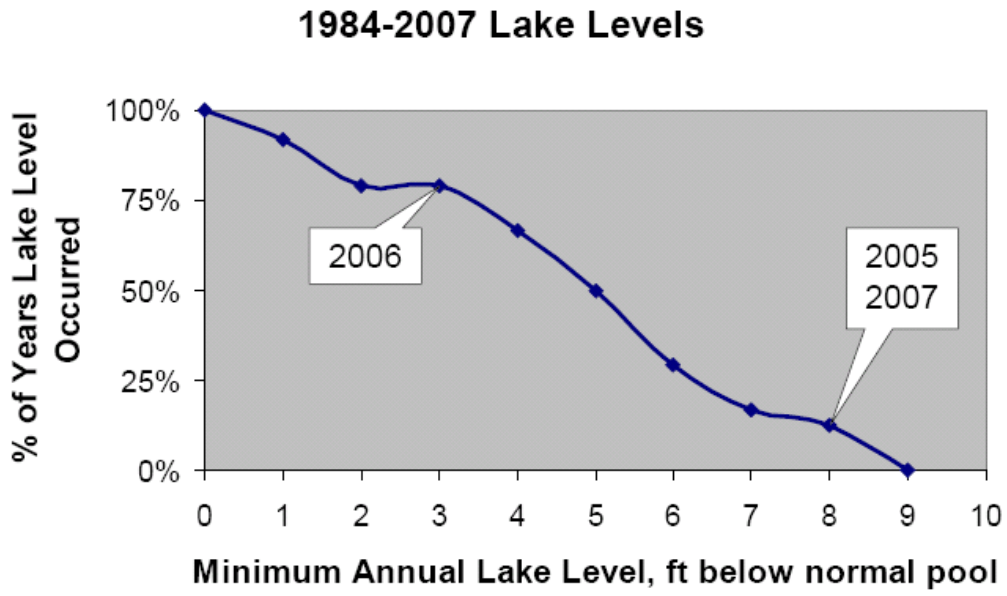

Fig. II-9. Percent of years minimum lake level occurred at different elevations.

Based on the inflow statistics and lake level representations (Fig. II-9), 2005 and 2007 are regarded as dry years in the model simulation period, and 2006 is regarded as a normal year. Considering computational time and model continuity, the lake model was set up to run year by year. Due to differences in hydrographs and rainfall patterns between 2005 and 2006, we decided to calibrate the lake model separately for the year of 2005 and 2006, and use 2007 as model validation period where all model parameters were taken from 2005 model calibration processes.

While calibrating 2005 and 2006 model runs separately, the goal was to not change model parameters as much as possible. The parameters that varied (between 2005 and 2006 model simulations) were river input representations and benthic nutrient fluxes.

f. Model Parameters

In cases where direct field data were not available, the selection of model parameters were based on literature review and model calibration processes. Table II-8 lists some critical model parameters used in this model project, together with values used in other studies.

Table II-8. Parameters used in the model

	Units	Fort Cobb Lake*	Chesapeake Bay**	Neuse River***	Pamlico Sound[#]	Cape Fear River##	Falls Lake
Maximum algal growth rate @ 20°C	1/day	1.5-1.8	2.25-2.5	2.0	2.5	2.3	2.6
Nitrogen half saturation for algal growth	g/m^3	0.05		N/A	0.01	0.05	0.05
Phosphorus half saturation for algal growth	g/m^3	0.002		N/A	0.001	0.005	0.002
Background light extinction coefficient	1/m	0.475	N/A	N/A	0.475	0.55	0.475
Light extinction for TSS	1/m per (g/m^3)	0.015	N/A	N/A	0.015	0.015	0.015
Light extinction for total suspended chlorophyll	1/m per (mg/m^3)	0.041	0.017	N/A	0.017	0.017	Riley (1956)
Optimum temperature for algal growth	°C	23.0-32.0 (Bc) 17.0-23.0 (Bd) 20.0-25.0 (Bg)	20.0-27.5	N/A	20.0-26.0	20.0-26.0	23.0-32.0 (Bc) 17.0-23.0 (Bd) 20.0-25.0 (Bg)
Algal basal metabolism rate @ 20°C	1/day	0.01-0.04	0.003-0.04	0.05 (as death rate)	0.01	0.01	0.01-0.04
Algal predation rate	1/day	0.01-0.1	0.01- 0.215		0.1	0.12	0.01-0.1
Algal settling velocity	m/day	0.01-0.25	0.0 - 0.35	0.015-1.5	0.15	0.15	0.01-0.1

PO_4 partition coefficient	L/mg	0.04	N/A	N/A	0.002	0.004	0.04
Carbon/chlorophyll	mg/µg	0.04-0.065	0.06	0.05	0.06	0.06	0.06-0.065
Nitrogen/carbon	mg/mg	0.167-0.176	0.167	0.14	0.14	0.16	0.167-0.176
PCprm1(constant for phosphorus/carbon)	mg/mg	N/A	42	50	40	30	30
PCprm2 (constant for phosphorus/carbon)	mg/mg	N/A	85	N/A	0	40	0
PCprm3(constant for phosphorus/carbon)		N/A	200	N/A	200	200	0
Minimum organic phosphorus hydrolysis rate	1/day	0.01-0.1	0.005-0.1	0.1 (rate @ 20°C)	0.005-0.1	0.005-0.1	0.01-0.1
Minimum organic nitrogen hydrolysis rate	1/day	0.005-0.075	0.005-0.075	0.1 (rate @ 20°C)	0.005-0.075	0.005-0.075	0.005-0.075
Maximum nitrification rate	1/day	0.2	0.07	0.05	0.07	0.09	0.06
Benthic PO_4 flux	g P/m^2/day	0.001	N/A	N/A	0-0.001	0.002	0.001-0.0023
Benthic NH_4 flux	g N/m^2/day	0.05	N/A	N/A	0-0.04	0.02	0.01-0.017
Benthic NO_3 flux	g N/m^2/day	0.002	N/A	N/A	0-0.004	0.002	0.000

*ODEQ, 2006; **Cerco and Cole, 1994; ***Lung and Paerl, 1988; #Lin et al., 2007; ##Lin et al., 2008

III. Model Calibration

Model calibration runs were set up for 2005 and 2006. Model calibration was conducted in the following sequence: hydrodynamic model, total suspended sediment (TSS) transport model, and finally, the eutrophication model.

A number of statistical methods were suggested by the TAC to guide the evaluation of model performance. The defining equations for the recommended statistical methods are listed as follows:

Relative Error (RE) - $RE = \frac{\sum(\mathrm{Pred} - Obs)}{\sum Obs}$

Average Error (AE) – $AE = \frac{\sum(\mathrm{Pred} - Obs)}{n}$

Standard deviation for observational data (SD_{obs}) - $SD_{obs} = \sqrt{\frac{\sum(Obs - \overline{Obs})^2}{n-1}}$

R-square (R^2) - $R^2 = \left(\frac{\sum_{i=1}^{n}(Obs_i - \overline{Obs})(\mathrm{Pred}_i - \overline{\mathrm{Pred}})}{\sqrt{\sum_{i=1}^{n}(Obs_i - \overline{Obs})^2}\sqrt{\sum_{i=1}^{n}(\mathrm{Pred}_i - \overline{\mathrm{Pred}})^2}}\right)^2$

Root Mean Square Error (RMSE) - $RMSE = \sqrt{\frac{\sum(\mathrm{Pred} - Obs)^2}{n-1}}$

Ratio between RMSE and SD_{obs} (RMSE/SD_{obs}) - $RMSE / SD_{obs} = \frac{RMSE}{SD_{obs}}$

Coefficient of Efficiency (CE) – $CE = 1 - \frac{\sum(\mathrm{Pred} - Obs)^2}{\sum(Obs - \overline{Obs})^2}$

Percent Biased (pBias) - $pBias = \frac{\sum(\mathrm{Pred} - Obs)}{\sum Obs} * 100\%$

Most of the observed data are analyzed from composite water samples at surface to twice the secchi disk depth, but the model predicts cell-averaged concentrations at

different layers. To calculate the corresponding model-predicted values for observations, the concentrations from the first two layers were averaged at deeper regions (cell depth greater than five meters) and averaged three (cell depth greater than three meters, but less than or equal to five meters) to four (cell depth less than or equal to three meters) model layers as the water column became shallower. In viewing the statistical values, one should be cautious about the natural discrepancies between field data and model predictions in the comparison process.

The use of a number of different statistical methods to assess model performance avoids biased interpretation from only one method. For example, AE is a measure of whether the model results are biased towards over- or, under-predicting observed values. R-squared describes the co-linearity between simulated and measured data. RMSE is a representation of uncertainties involved with model prediction.

The statistical performance measures should be viewed in context of each other and in a relative manner. Differences between model-predicted and observed values may be caused by patchiness of peak concentrations that are not well represented in the model (in which averaged-values within a model cell were calculated). Discrepancies can also be caused by slight time differences of the occurrence of peak concentrations, in which case model results can still be regarded as well representative of reality, while statistics alone would suggest poor model performance.

In calibrating the model, time serious plots were made at each monitoring station to compare the model-predicted and observed key water quality parameters. In addition, the goal in terms of statistics (as suggested by the TAC) was to have RMSE for predicted hydrodynamic model variables much less than one SD_{obs} (e.g. $RMSE \leq 0.5SD_{obs}$), and to have AE for predicted TSS and water quality model variables much less than one SD_{obs} (e.g. $AE \leq 0.5SD_{obs}$). In addition, the TAC also suggested that the RMSE for chlorophyll-*a* should be around one SD_{obs}.

III-1. Hydrodynamic Model

The hydrodynamic model was calibrated to simulate water level, flow, and temperature variations during 2005 and 2006.

a. Water level

As a result of different meteorological conditions such as the spatial and temporal differences in rainfall pattern, the distribution factors into un-gaged tributaries were expected to be different in 2005 and 2006. Such parameters were allowed to vary within around 15% of those generated directly from area ratio. Optimal values were selected based on model performance of water level simulations.

Rainfall directly to the lake surface was input as a time series and the evaporation rate was calculated internally within EFDC.

The model-simulated water level variations generally followed the observed values by US Army Corps of Engineers (Fig. III-1, III-2). During 2005, the Falls Lake water level was observed to vary between 74.1 to 77 meters above sea level. A slight over estimation of around 0.1 meters was predicted by the model. During 2006, the Falls Lake water level was observed to vary between 75.6 to 78.7 meters; the absolute error predicted by the model was 0.04 meters. In addition, at the end of model simulation, the predicted and observed lake water level were within 0.4 meters, which indicates that the water mass was well represented by the model for the entire years of 2005 and 2006. Other statistics values computed for the model results are also listed in Table III-1. The RMSE for the model prediction were much less than the corresponding SD for observations.

Table III-1. Statistics for 2005 and 2006 water level simulation

	RE	AE	SD_{obs}	R^2	RMSE	$RMSE/SD_{obs}$	CE	pBias
2005	0.001	0.10	0.89	0.99	0.17	0.17	0.96	0.14%
2006	0.0005	0.04	0.50	0.89	0.20	0.40	0.84	0.05%

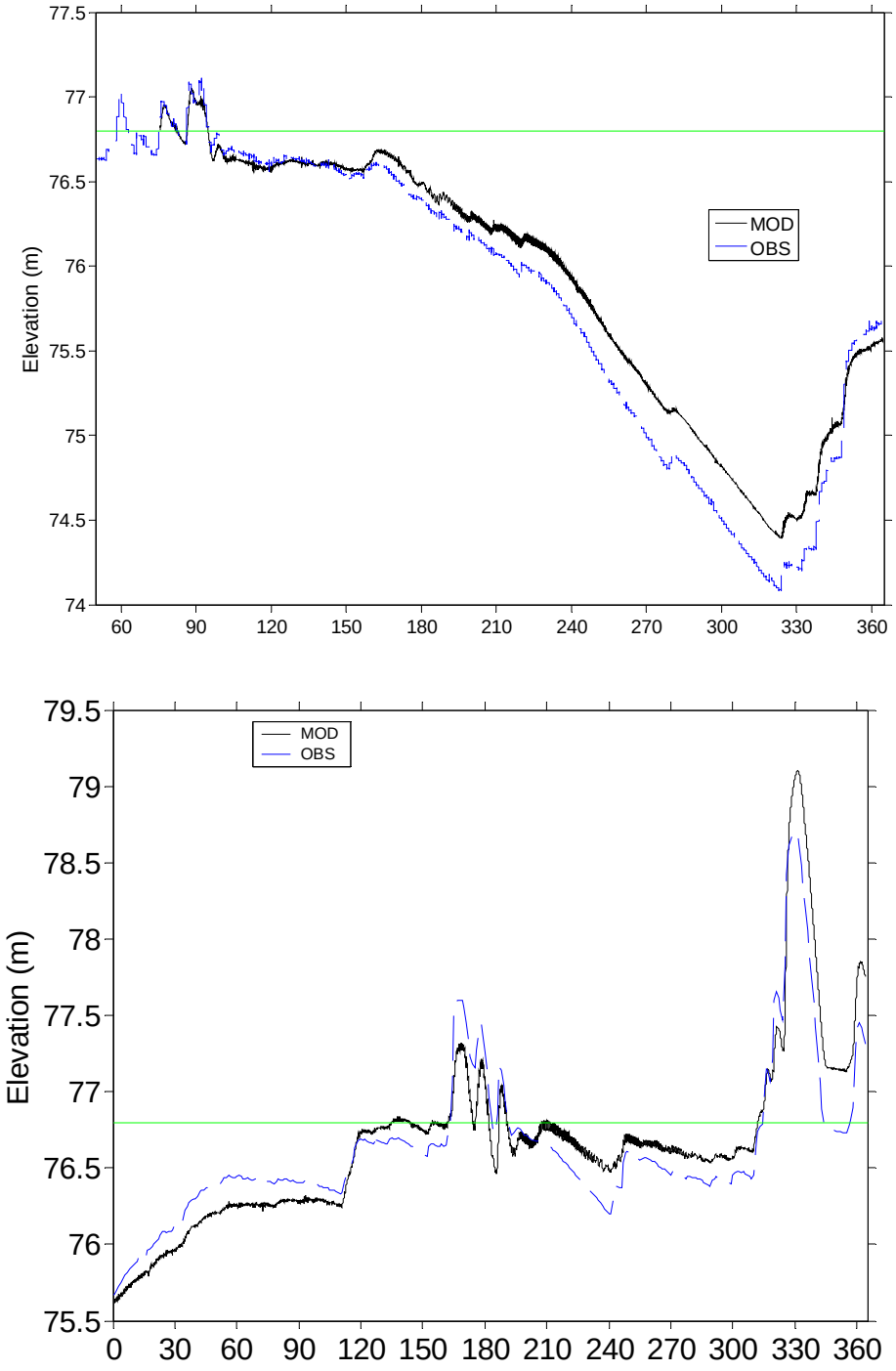

Fig. III-1. Time series of model-simulated and observed water level variation in 2005 (upper panel) and 2006 (lower panel).

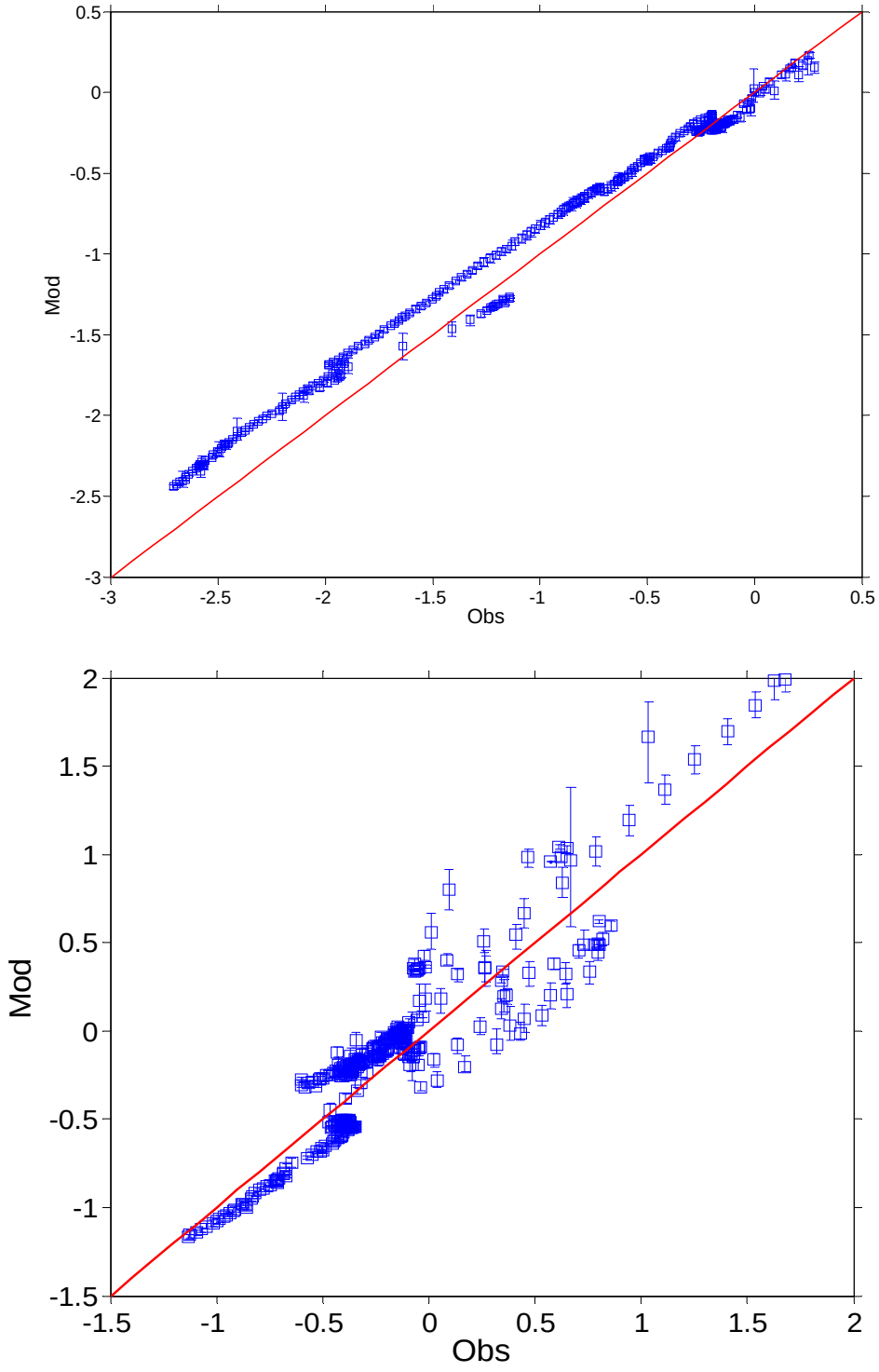

Fig. III-2. Scatter plots of model-simulated and observed water level variation in 2005 (upper panel) and 2006 (lower panel).

b. Water temperature

Water temperature is primarily a function of heat fluxes at the air-water interfaces. Time series of solar radiation, air temperature, and cloud cover were obtained from RDU international airport and specified in input files. The horizontal and vertical distribution of water temperature within the lake is also affected by flow and turbulences.

Fig. III-3 shows the time series of model-predicted and observed water temperature at station NEU013B. Seasonal variations of water temperature were well represented by the model for both 2005 and 2006. Time-series plots for other stations can be found at Appendix B. Fig. III-4 shows the scatter plots comparing the model-predicted water temperature with the observed values at all the lake stations for 2005 and 2006. The squares indicate the depth averaged values and the error bars indicate the temperature ranges within the water column. Both observed and model-predicted temperature ranged between around 5 to 33ºC. In both years, R^2 between modeled and observed values resulted above 0.95, indicating good model representations of the variations of water temperature in the lake.

Table III-2. Statistics for 2005 and 2006 water temperature simulation

	RE	AE	SD_{obs}	R^2	RMSE	$RMSE/SD_{obs}$	CE	pBias
2005	0.03	0.63	6.56	0.96	1.61	0.25	0.94	3.21%
2006	0.03	0.50	7.42	0.97	1.50	0.20	0.96	2.81%

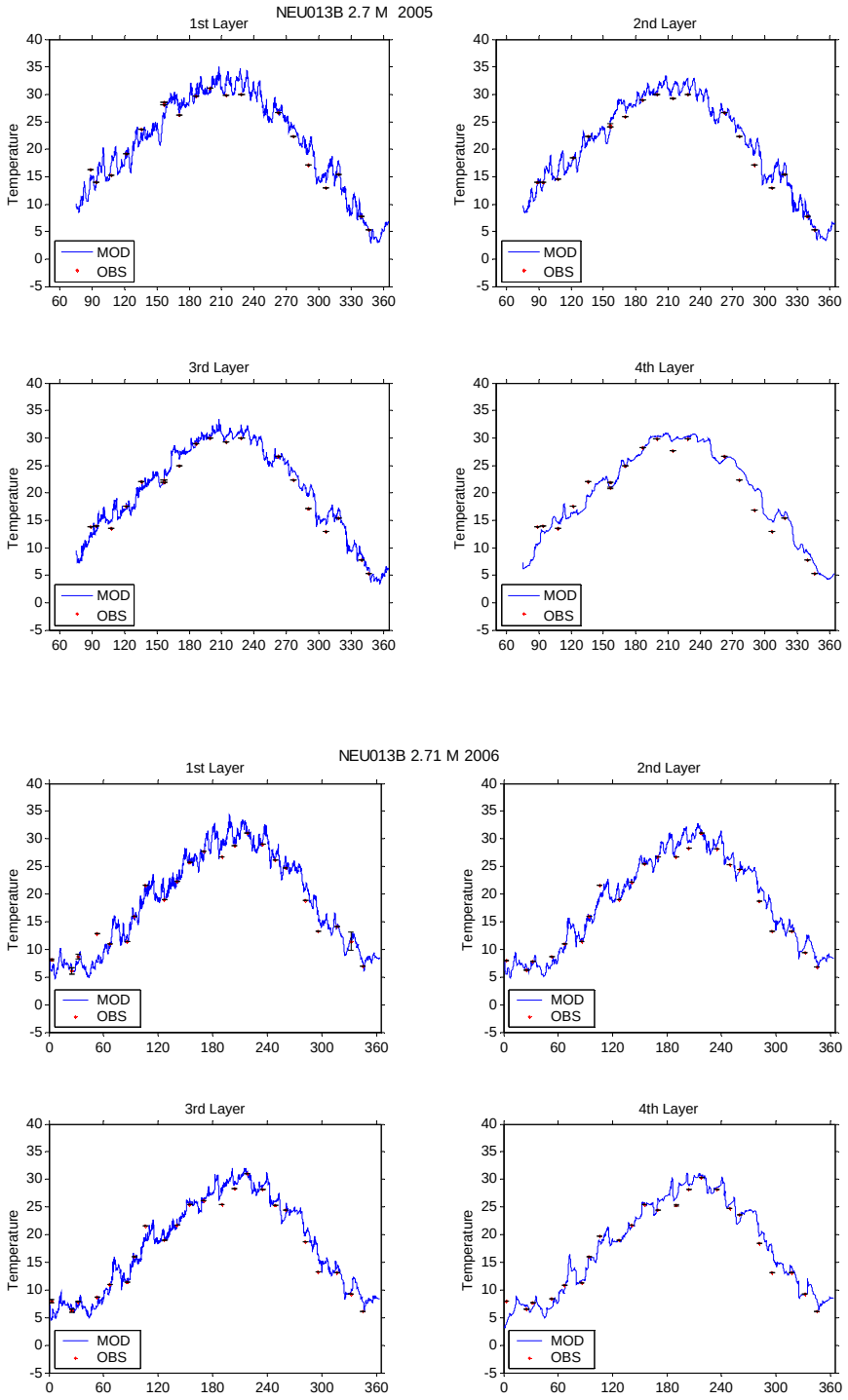

Fig. III-3. Time series of model-simulated and observed water temperature variations at different model layers at NEU013B in 2005 (upper panel) and 2006 (lower panel).

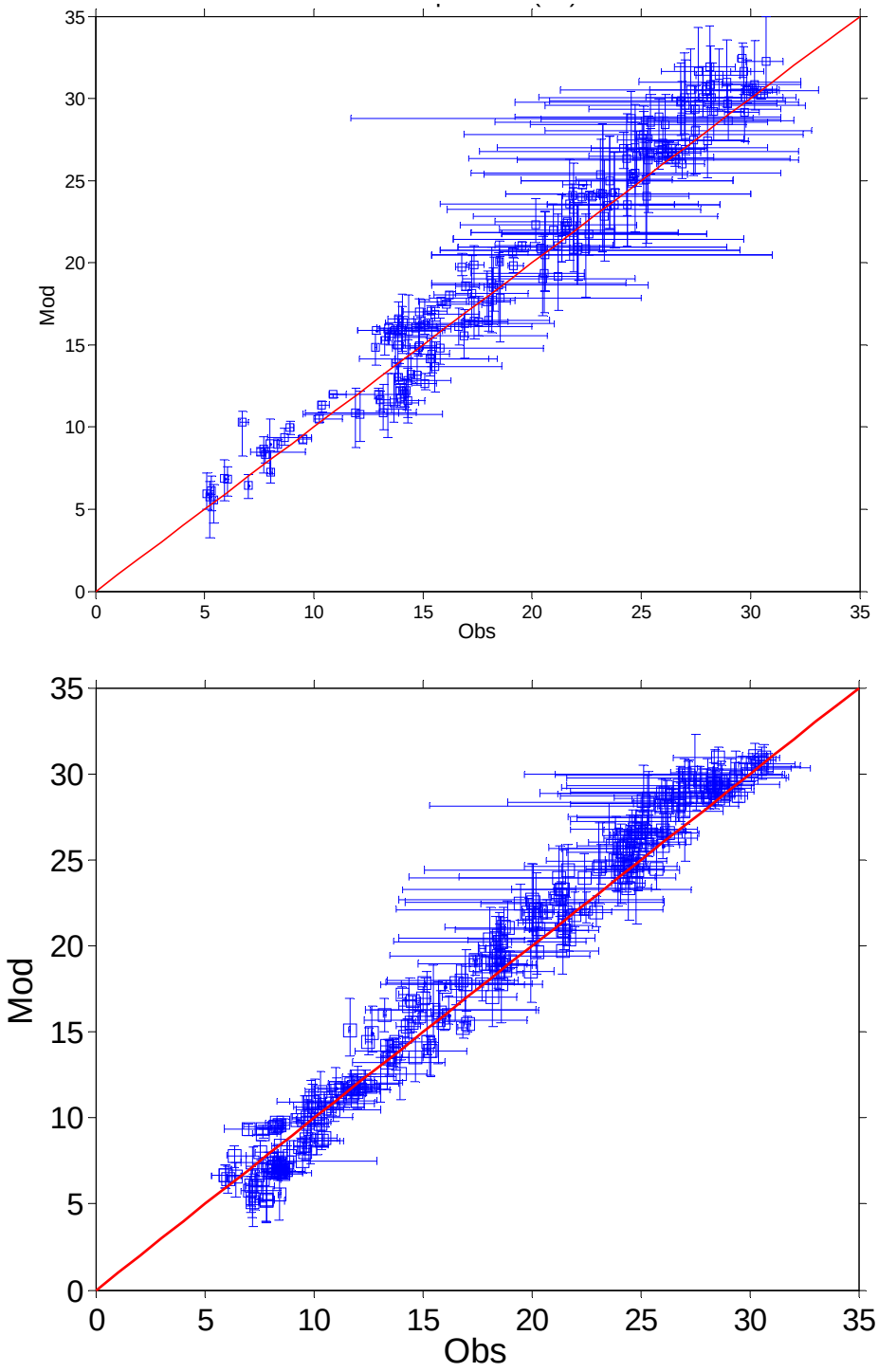

Fig. III-4. Scatter plots of model-simulated and observed water temperature variations at all stations in 2005 (upper panel) and 2006 (lower panel).

III-2. TSS Model

Three sediment classes were selected to be simulated in the TSS sub-model. Sediment erosion and deposition processes represented in the model were discussed in section II-2, and the parameters used were listed in Table II-1.

Figure III-5 to III-7 show time series of model-simulated vs. field-observed TSS concentrations at NEU013B, NEU0171B, and NEU019P, respectively. NEU013B is located at the upper portion of the Falls Lake and has a much higher TSS concentration than those at NEU 0171B and NEU019P, located at the middle and lower portion of the Falls Lake. The lines are model-simulated TSS concentrations at the four different layers. The stars indicate TSS concentrations from composite water samples collected at the depths from the surface to twice the secchi depth. A general pattern of higher TSS concentrations in the upper part of the lake and lower values in the lower part of the lake was also predicted by the model.

Secchi depths usually ranged from 0.5 to 2 meters at different stations and sampling times. Model-simulated TSS concentrations were averaged through the four layers at shallow stations (less than or equal to three meters) and averaged through the top three layers at deeper stations (greater than three meters, but less than or equal to five meters), and averaged through the top two layers at deepest stations (greater than five meters). These averaged values were compared with the observed TSS concentrations (Fig. III-8 and Table III-3). Due to temporal variations of secchi depth at each station and the large vertical differences in TSS concentrations in the water column, such model-data comparisons should be viewed only qualitatively.

Table III-3. Statistics for 2005 and 2006 total suspended sediment simulation

	RE	AE	SD_{obs}	R^2	RMSE	$RMSE/SD_{obs}$	CE	pBias
2005	-0.39	-7.09	21.76	0.07	22.82	1.05	-0.10	-39.46%
2006	-0.53	-6.57	10.21	0.05	12.14	1.19	-0.41	-52.6%

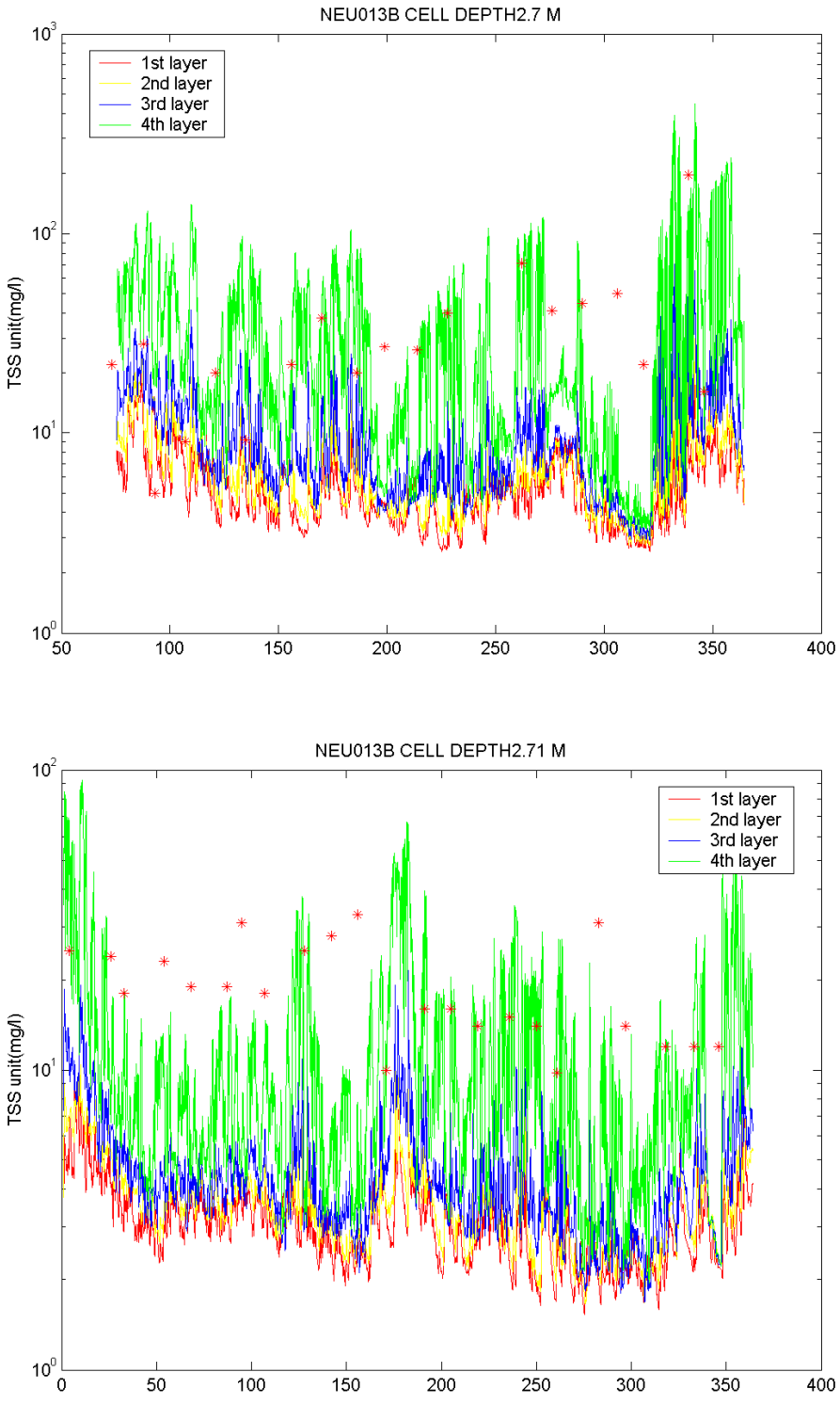

Fig. III-5. Time series plots of model-simulated (lines) and observed (stars) total suspended sediment concentrations at NEU013B in 2005 (upper panel) and 2006 (lower panel).

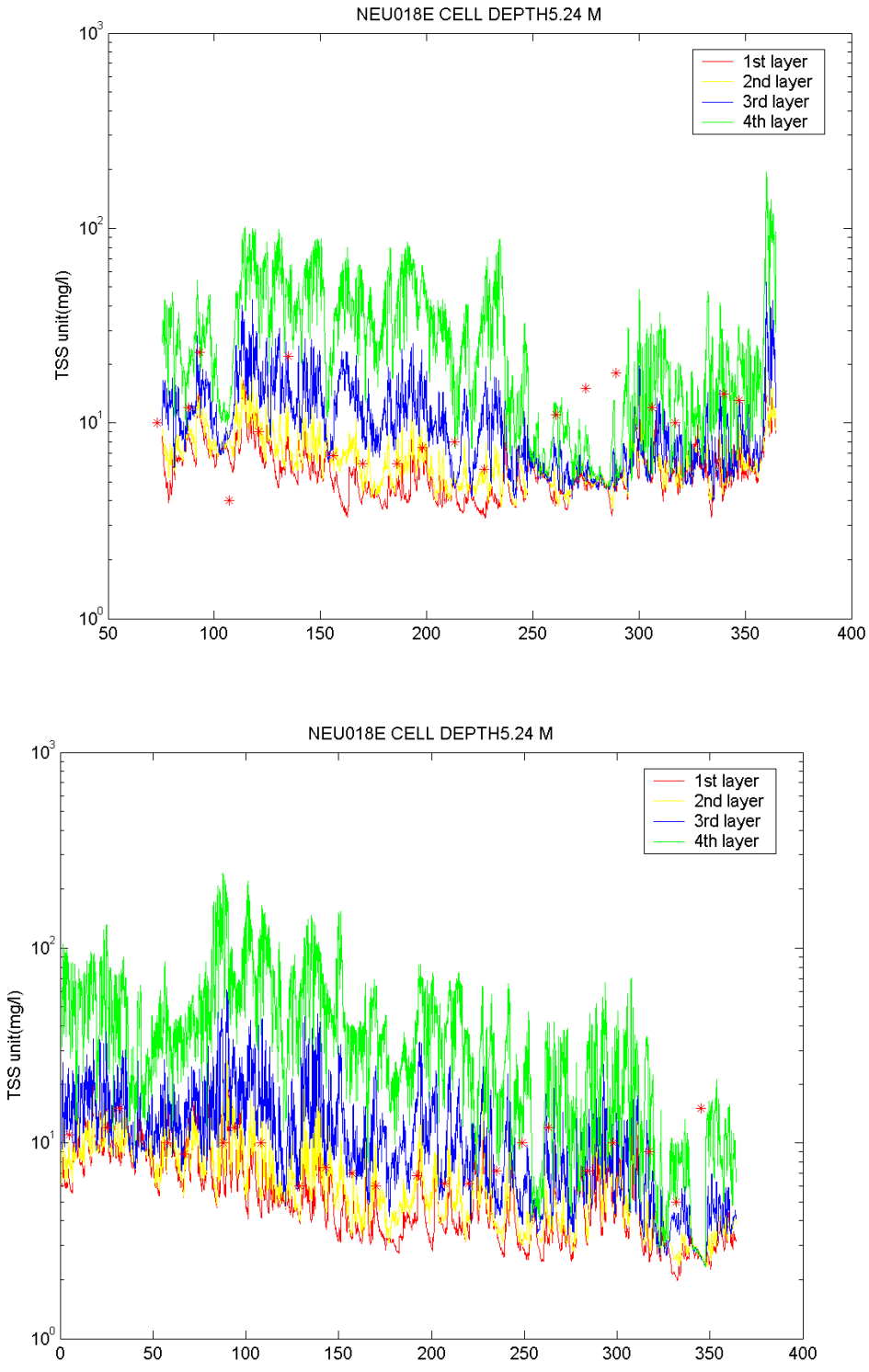

Fig. III-6. Time series plots of model-simulated (lines) and observed (stars) total suspended sediment concentrations at NEU018E in 2005 (upper panel) and 2006 (lower panel).

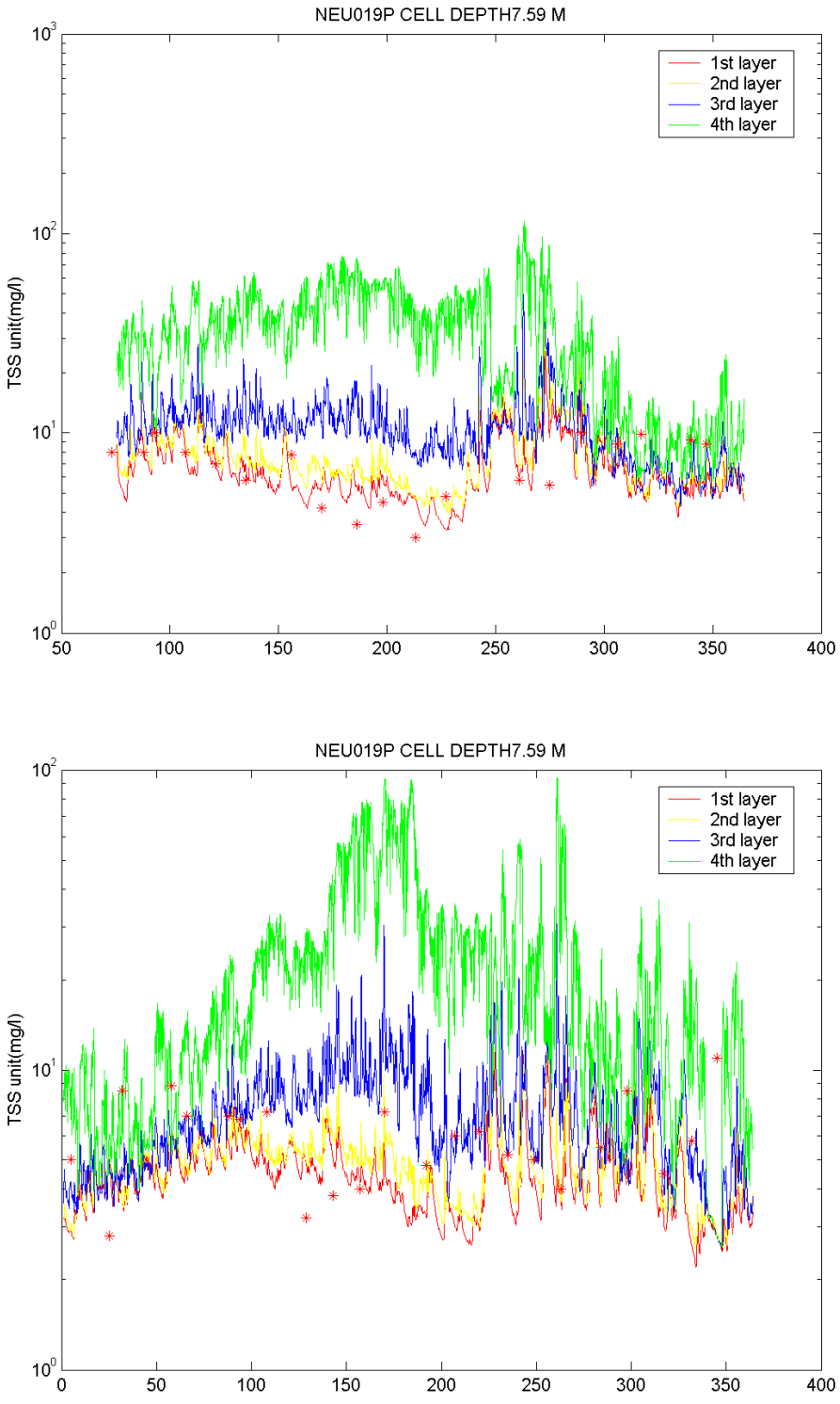

Fig. III-7. Time series plots of model-simulated (lines) and observed (stars) total suspended sediment concentrations at NEU019P in 2005 (upper panel) and 2006 (lower panel).

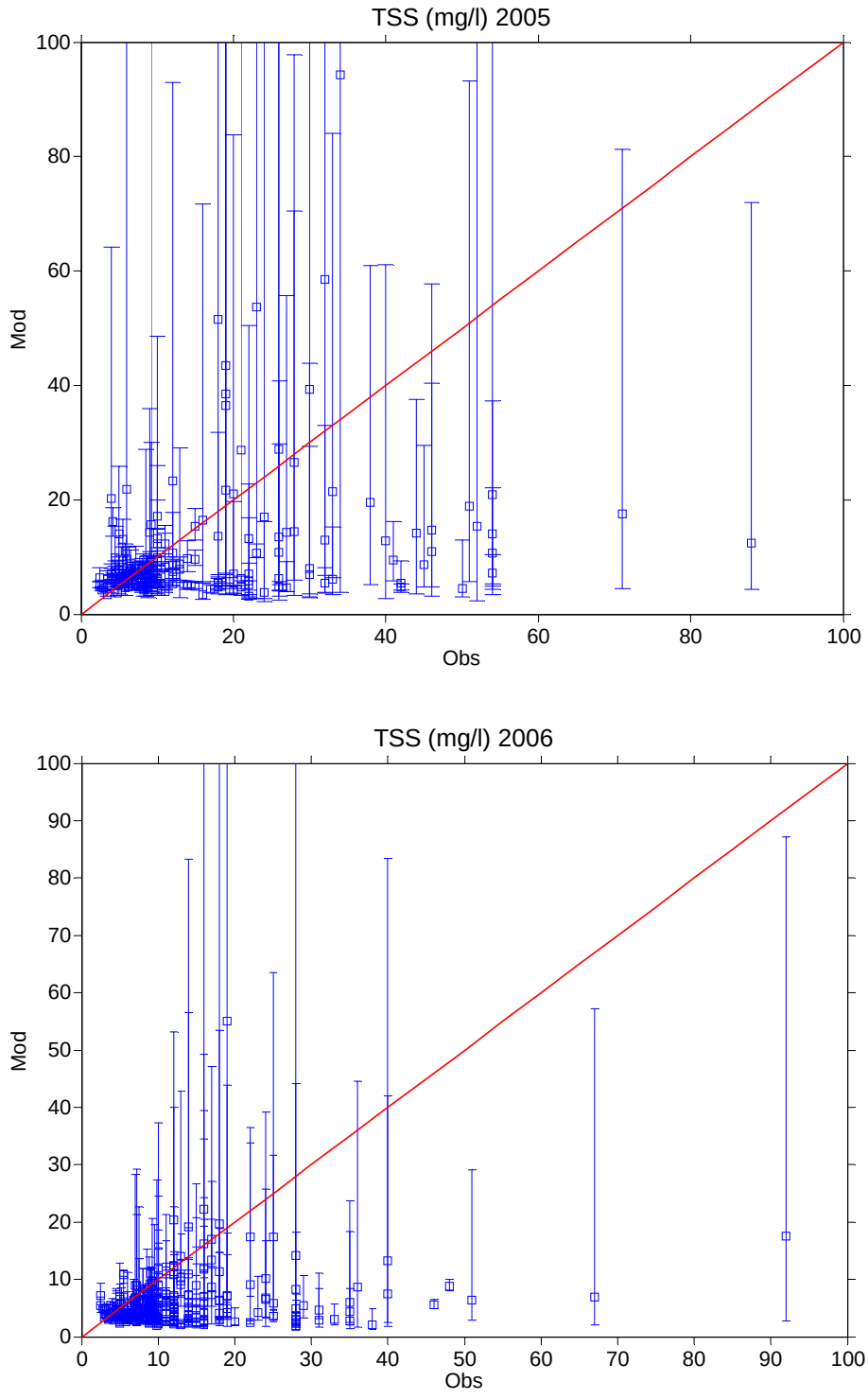

Fig. III-8. Scatter plots of model-simulated and observed total suspended sediment variations at all stations in 2005 (upper panel) and 2006 (lower panel).

III-3. Water Quality Model

The water quality model was calibrated for chlorophyll-*a* (chl-*a*), total organic carbon (TOC), total phosphorus, phosphate, nitrate, ammonia, total Kjeldahl nitrogen (TKN), and dissolved oxygen (DO) concentrations.

a. Chlorophyll-*a*

The primary concern for water quality in Falls Lake is the effect of nutrient load in promoting algal blooms. Such blooms can cause various nuisance effects in the lake, such as excessive accumulations of foams, scums, and discoloration of the water. Algal blooms may also cause treatability problems for drinking water supplies, and can lead to anoxia and fish kills during the summer. Chl-*a* standard violations (greater than 40 µg/l) were often observed in Falls Lake. One of the primary goals of the model project was to have reasonable representation of chl-*a* variations in the lake.

Figures III-9 to III-11 show time series plots of model-predicted and observed chl-*a* variations during 2005 and 2006, at stations NEU013B, NEU018E, and NEU019P, respectively. The three stations represent the upper, middle, and lower portions of the lake. The model agreed reasonably well with the observations, representing the same order of magnitude, and revealing a similar spatial trend.

The observed chl-*a* concentrations at all stations in the Falls Lake ranged from less than 10 to 103 µg/l during 2005 and 2006. Chl-*a* data were not available during spring and summer of 2005. Historical records show that chl-*a* concentration could reach as high as 280 µg/l at station NEU013 (7/16/1986). The model-predicted chl-*a* concentration ranged between less than 10 to 156 µg/l during 2005 to 2006 at the monitoring stations (Fig. III-12). Highest values were simulated at upstream stations where chl-*a* violations were most frequently observed.

The average errors predicted by the model are below 4 µg/l (much less than their corresponding SD_{obs}) during both years and a good R^2 between modeled and observed chl-*a* concentrations were obtained from the 2006 model simulation (Fig. III-13, Table III-4).

Table III-4. Statistics for 2005 and 2006 chlorophyll-*a* simulation

	RE	AE	SD_{obs}	R^2	RMSE	$RMSE/SD_{obs}$	CE	pBias
2005	0.10	2.99	15.64	0.07	16.79	1.07	-0.15	9.95%
2006	0.10	3.57	19.07	0.40	17.89	0.94	0.12	9.97%

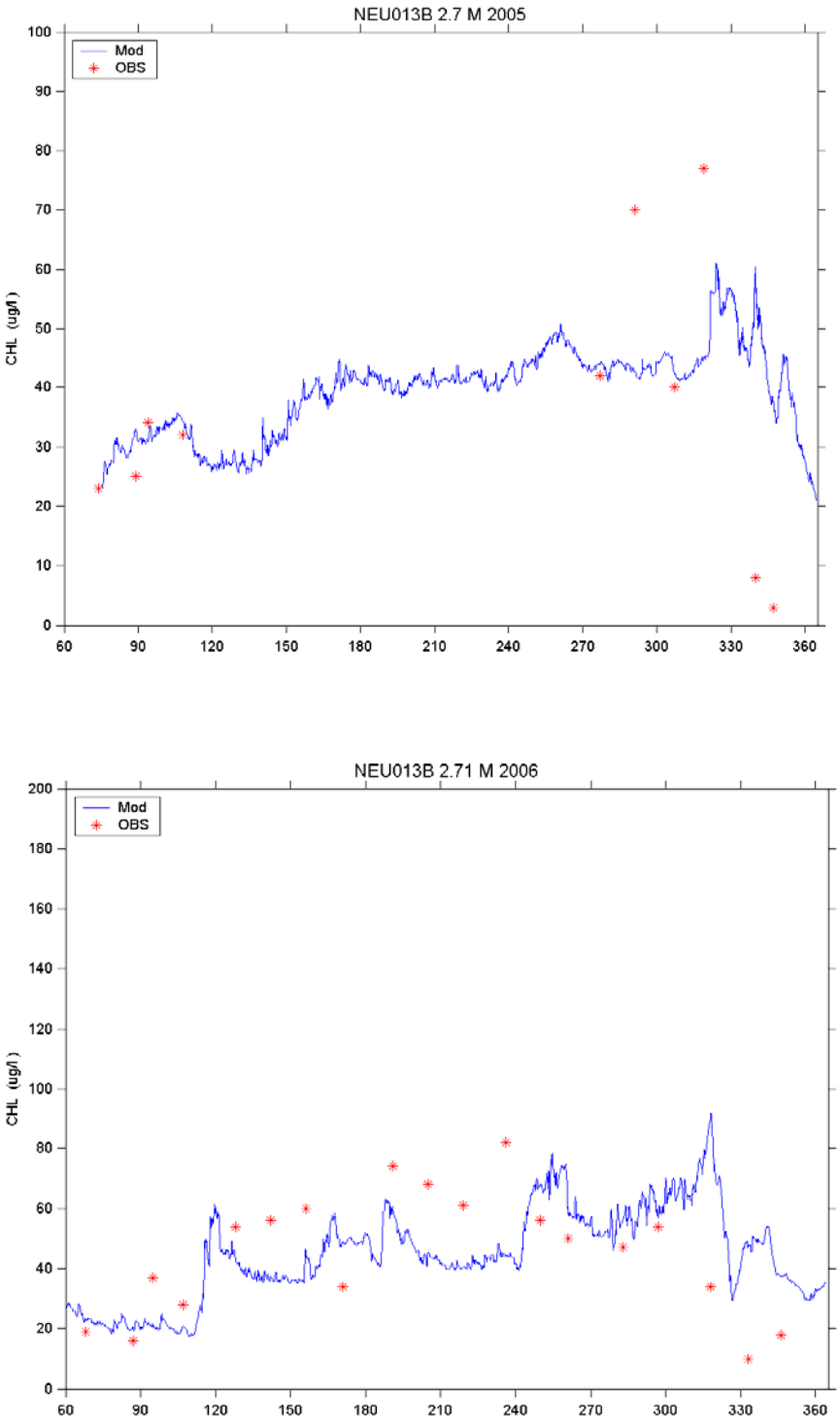

Fig. III-9. Time series plots of model-simulated (lines) and observed (stars) chlorophyll-*a* concentrations at NEU013B in 2005 (upper panel) and 2006 (lower panel).

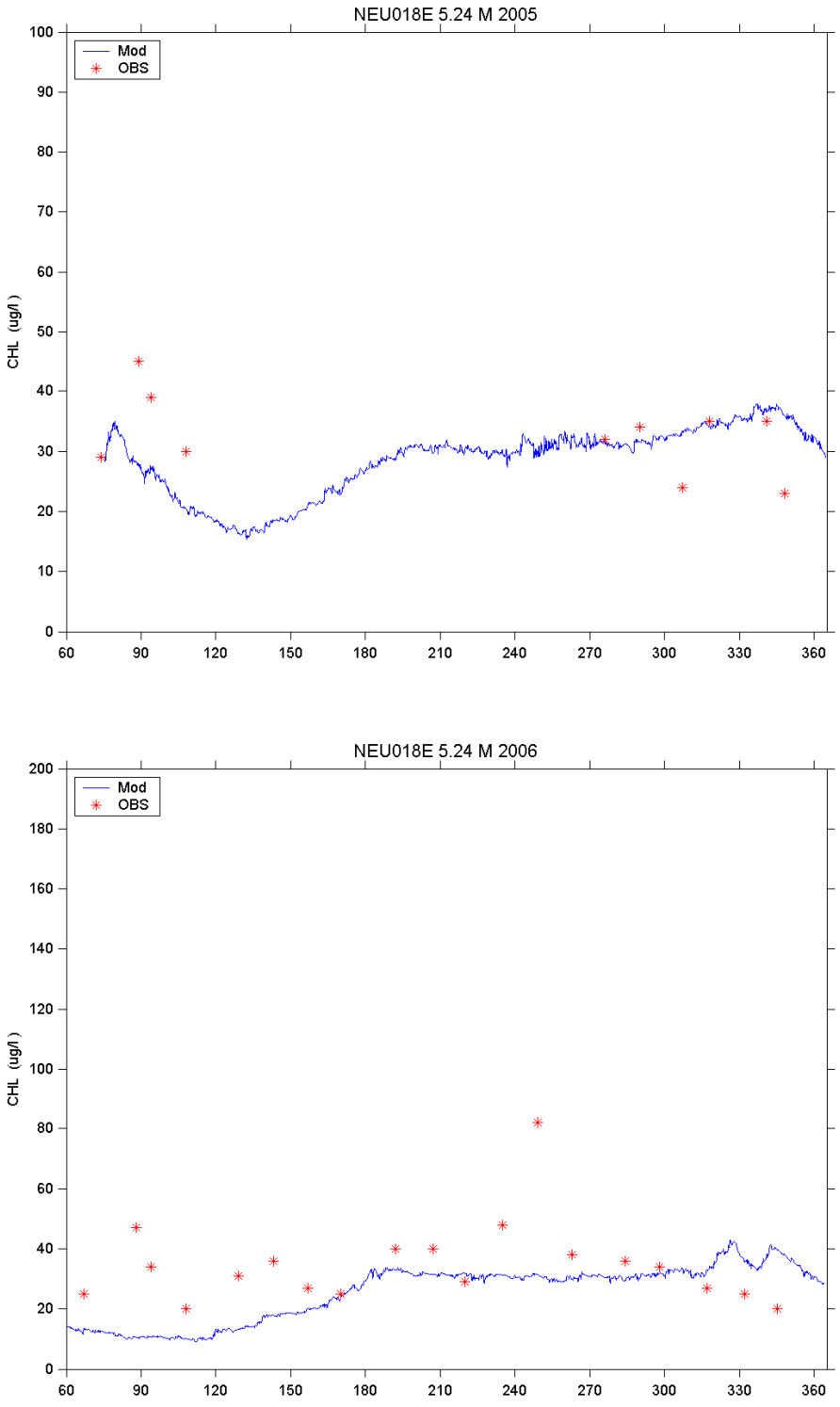

Fig. III-10. Time series plots of model-simulated (lines) and observed (stars) chlorophyll-*a* concentrations at NEU018E in 2005 (upper panel) and 2006 (lower panel).

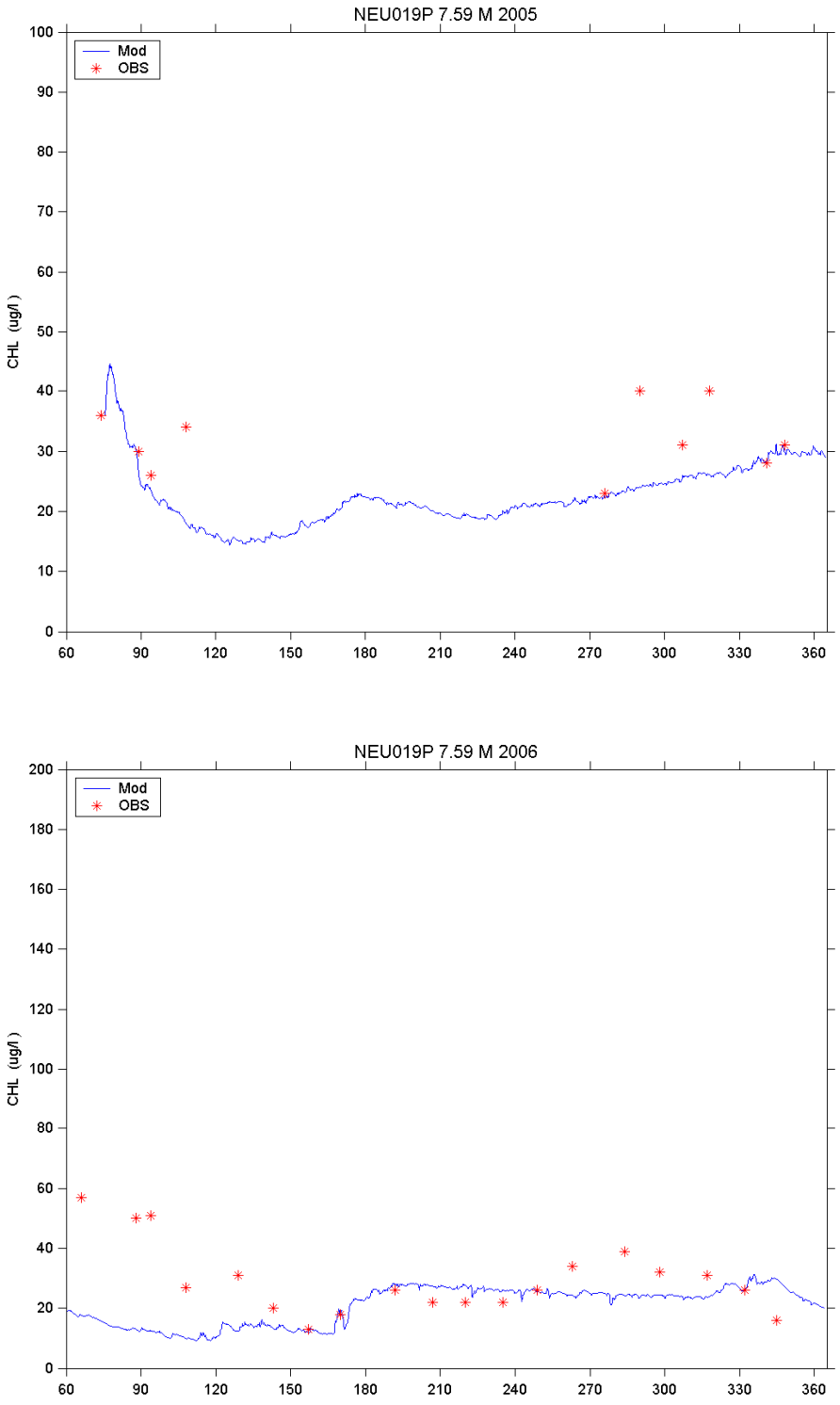

Fig. III-11. Time series plots of model-simulated (lines) and observed (stars) chlorophyll-*a* concentrations at NEU019P in 2005 (upper panel) and 2006 (lower panel).

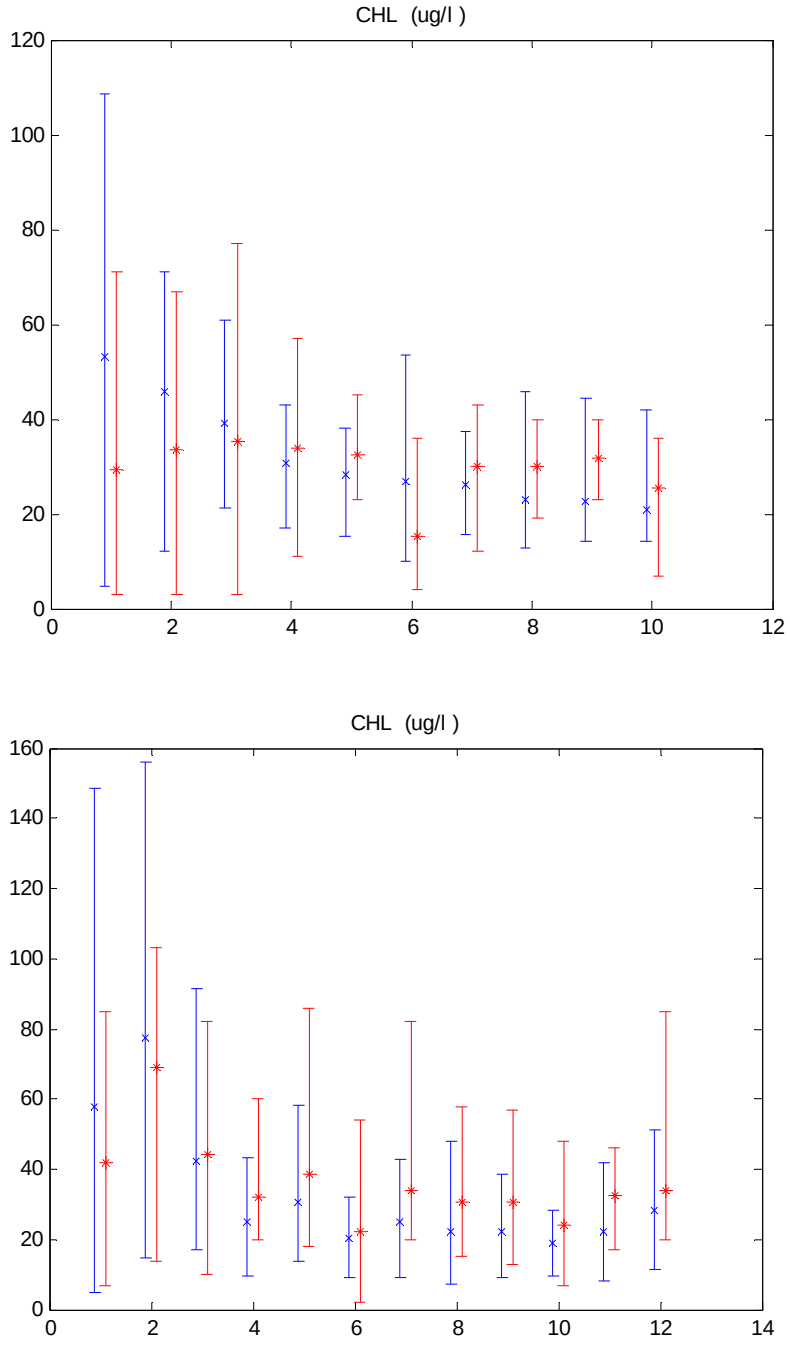

Fig. III-12. Comparisons between model-simulated (blue) and observed (red) yearly averaged chlorophyll-*a* concentrations (stars) and their ranges (lines) at the monitoring stations along the channel of the Falls Lake. The sequence of the stations are: NEU010, ELL10 (2006 only), NEU013, LC01(2006 only), NEU013B, NEU0171B, NEU018E, NEU019C, NEU019E, NEU019L, NEU019P, NEU020D. Upper panel 2005 and lower panel 2006.

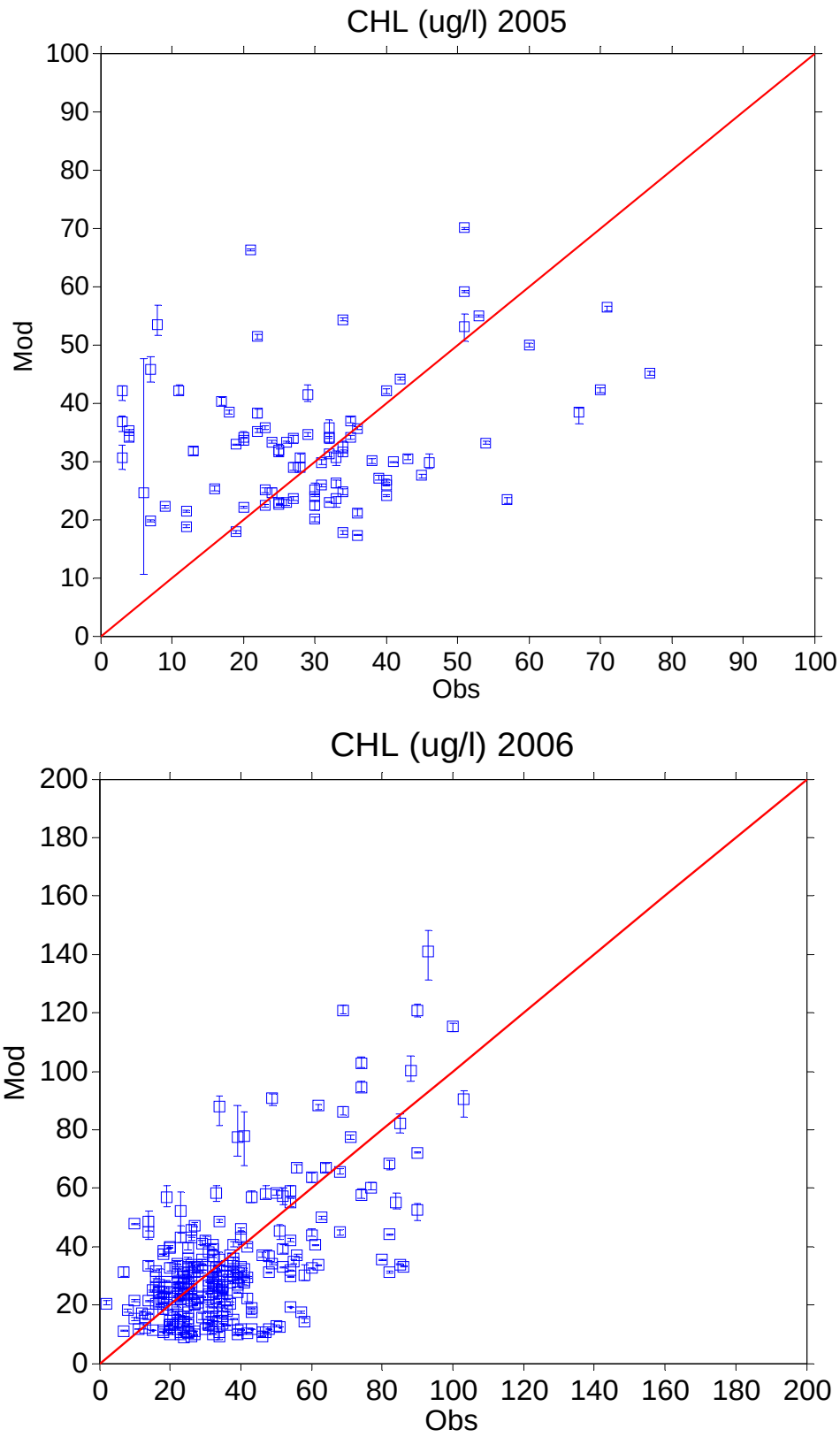

Fig. III-13. Scatter plots of model-simulated and observed chlorophyll-*a* variations at all stations in 2005 (upper panel) and 2006 (lower panel).

b. Total Organic Carbon (TOC)

Figures III-14 to III-16 show time series plots of model-predicted and observed TOC concentrations during 2005 and 2006 for stations NEU013B, NEU018E, and NEU019P, respectively. Both the observed and model-predicted TOC concentrations ranged from around 5 to 14 mg/l. Higher concentrations existed near the upper portion of Falls Lake and lower values existed (both from the observations and from the model) in the lower portions of the lake. The model slightly under-predicted DOC for 2006. Averaged errors of the predicted TOC were below 1.3 mg/l (less than the corresponding SD_{obs}) for both years.

Table III-5. Statistics for 2005 and 2006 TOC simulation

	RE	AE	SD_{obs}	R^2	RMSE	$RMSE/SD_{obs}$	CE	pBias
2005	-0.07	-0.54	1.41	0.37	1.25	0.89	0.22	-7.13%
2006	-0.15	-1.23	1.52	0.36	1.83	1.21	-0.46	-14.55%

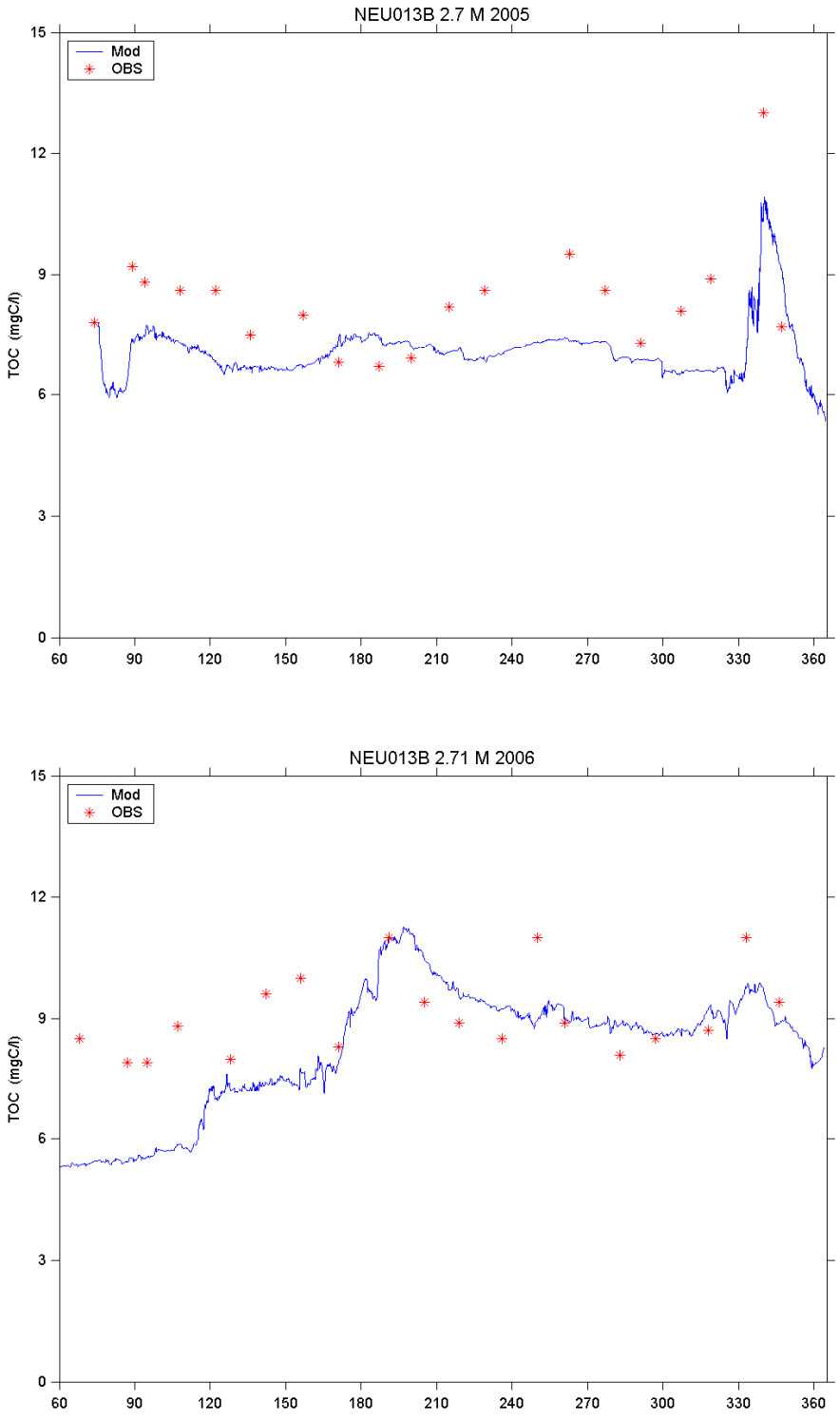

Fig. III-14. Time series plots of model-simulated (lines) and observed (stars) TOC concentrations at NEU013B in 2005 (upper panel) and 2006 (lower panel).

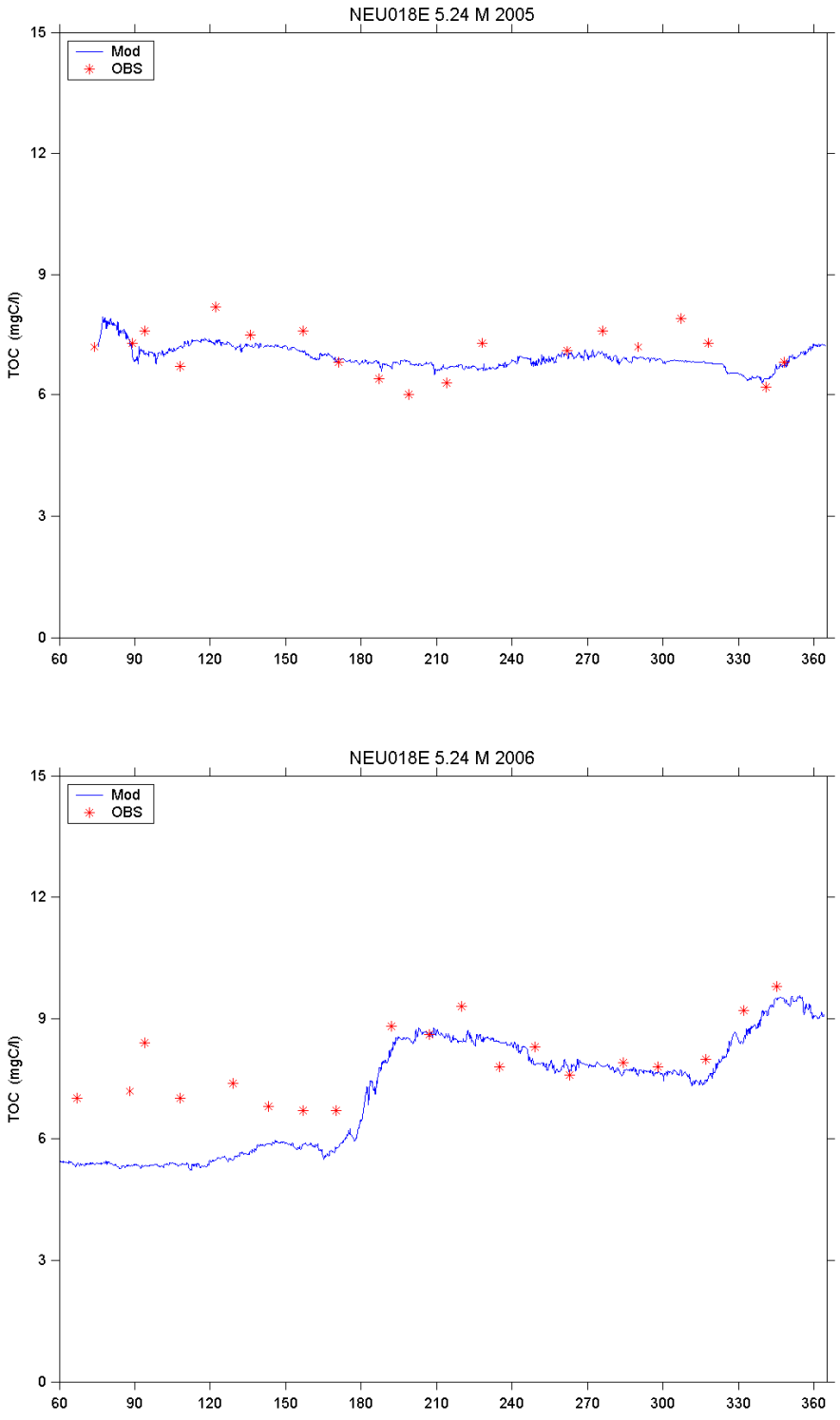

Fig. III-15. Time series plots of model-simulated (lines) and observed (stars) TOC concentrations at NEU018E in 2005 (upper panel) and 2006 (lower panel).

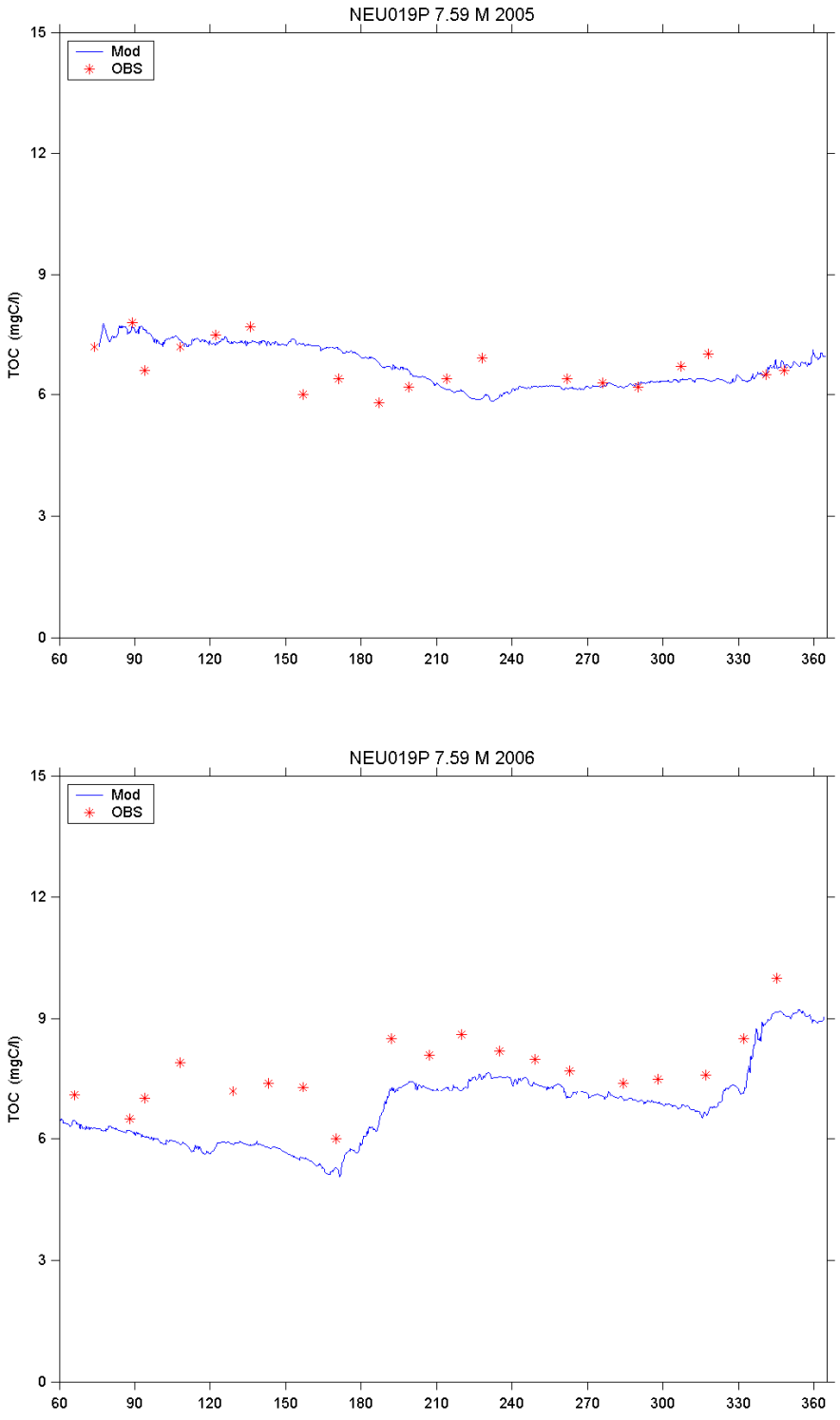

Fig. III-16. Time series plots of model-simulated (lines) and observed (stars) TOC concentrations at NEU019P in 2005 (upper panel) and 2006 (lower panel).

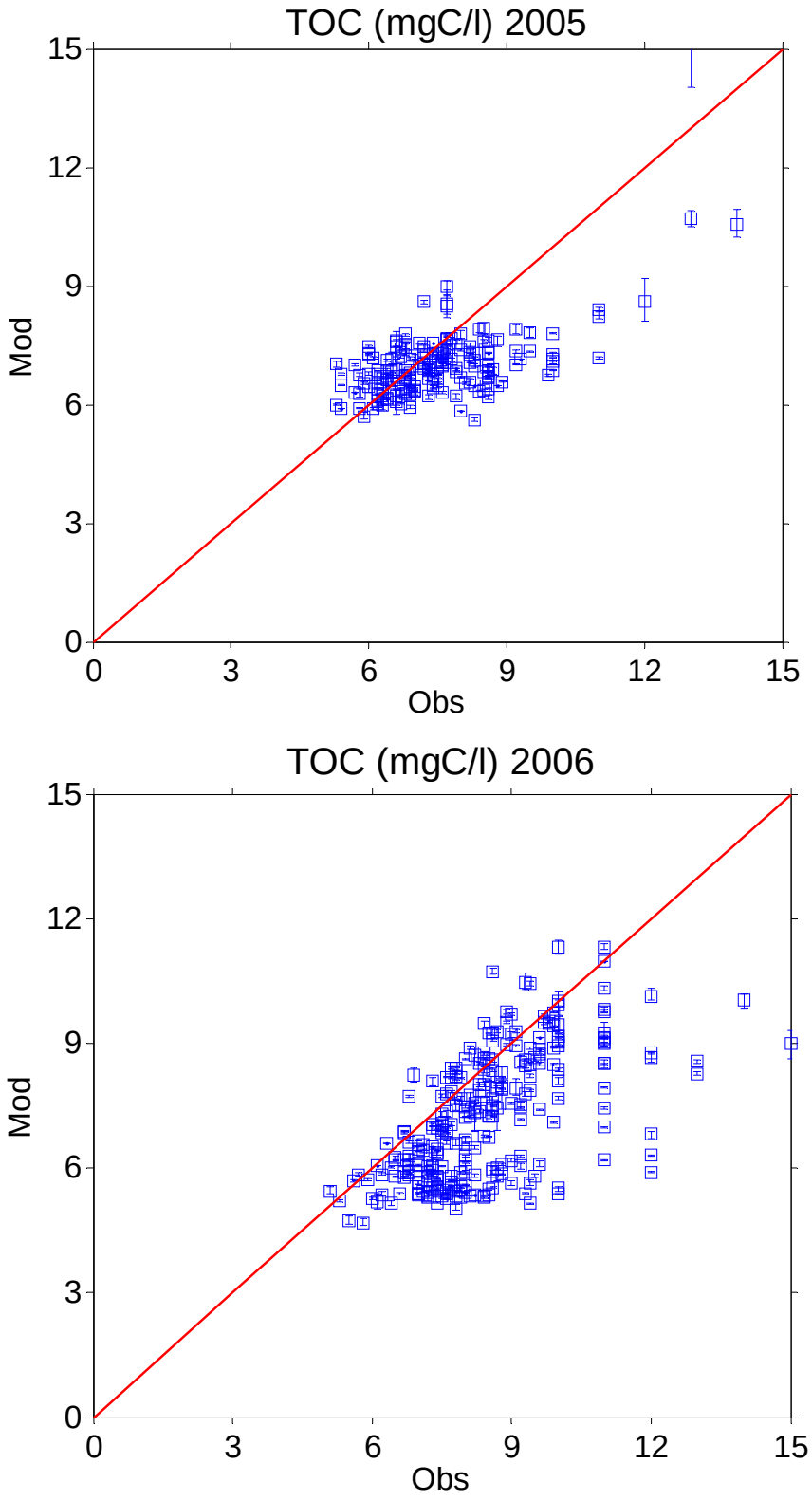

Fig. III-17. Scatter plots of model-simulated and observed TOC variations at all stations in 2005 (upper panel) and 2006 (lower panel).

c. Phosphorus

Time series plots are provided for both phosphate and total phosphorus at stations representing upper, middle, and lower portions of the lake. Statistics are provided only for TP because many of the phosphate observations were below detection limit. The model results agreed reasonably well with the observations.

Figures III-18 to III-20 show time series plots of model-predicted and observed phosphate concentrations during 2005 and 2006, respectively, at stations NEU013B, NEU018E, and NEU019P. The observed phosphate concentrations were often at detection limit, 0.02 mg P/l. The model-predicted phosphate concentrations in general agreed with the observations. The model slightly under-predicted TP concentrations overall, most likely due to under-prediction of high peak TP concentrations at the upper lake stations during drought conditions. Such under-prediction did not occur during 2006 when lake levels were close to normal (Figs. III-21 to III-24).

Table III-6. Statistics for 2005 and 2006 TP simulation

	RE	AE	SD_{obs}	R^2	RMSE	$RMSE/SD_{obs}$	CE	pBias
2005	-0.51	-0.04	0.07	0.01	0.09	1.29	-0.50	-51.14%
2006	-0.09	-0.01	0.04	0.32	0.04	1.00	-0.03	-9.31%

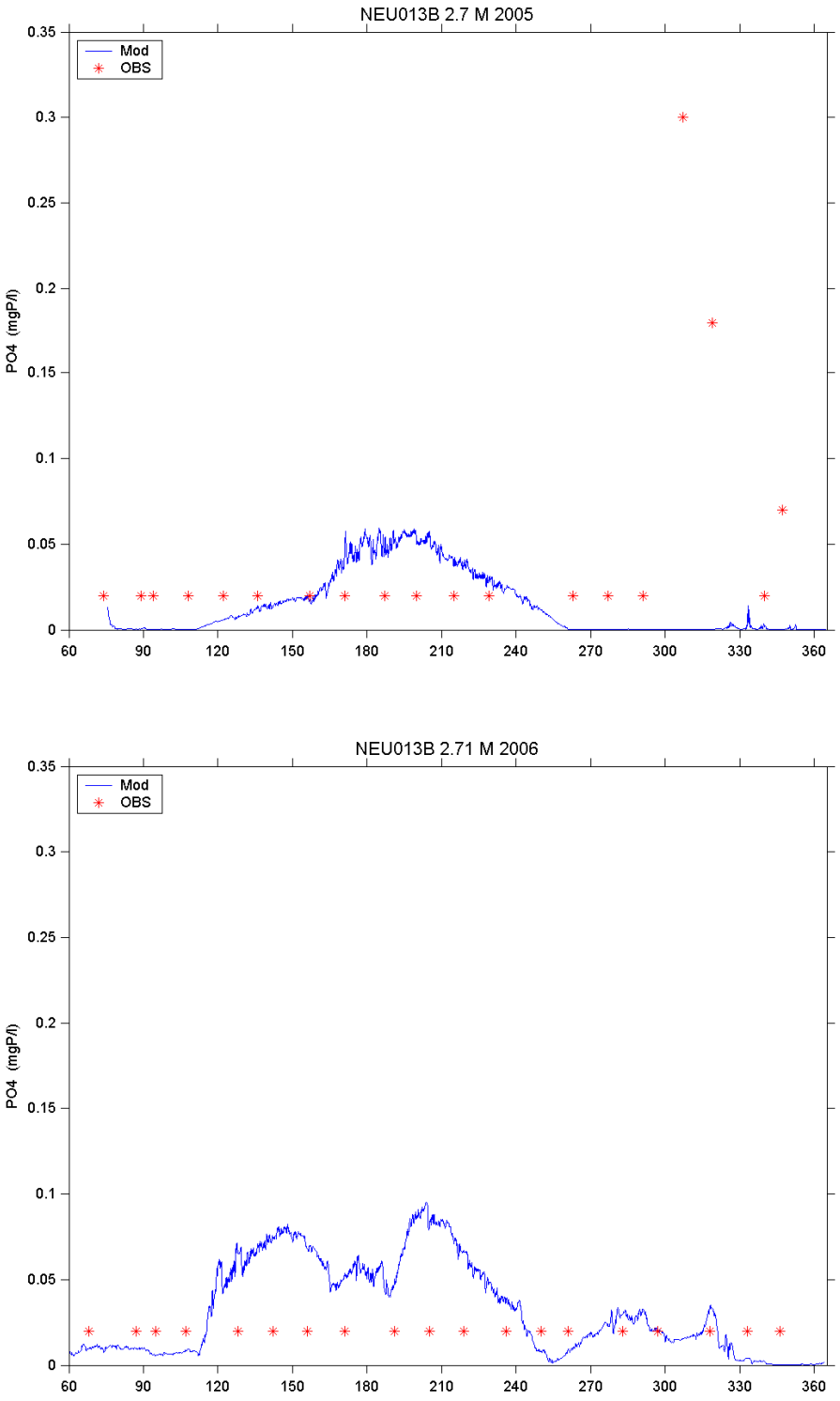

Fig. III-18. Time series plots of model-simulated (lines) and observed (stars) phosphate concentrations at NEU013B in 2005 (upper panel) and 2006 (lower panel).

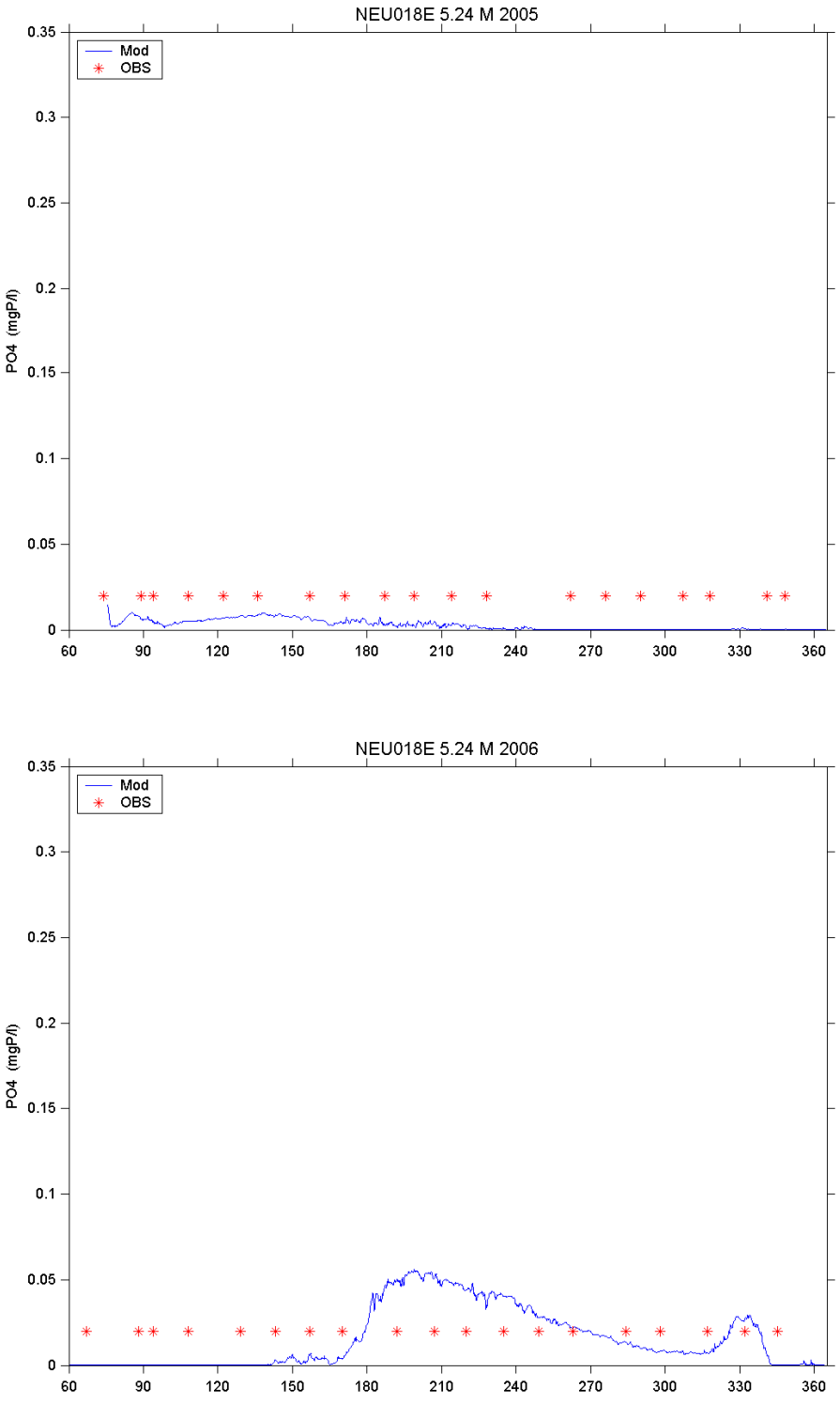

Fig. III-19. Time series plots of model-simulated (lines) and observed (stars) phosphate concentrations at NEU018E in 2005 (upper panel) and 2006 (lower panel).

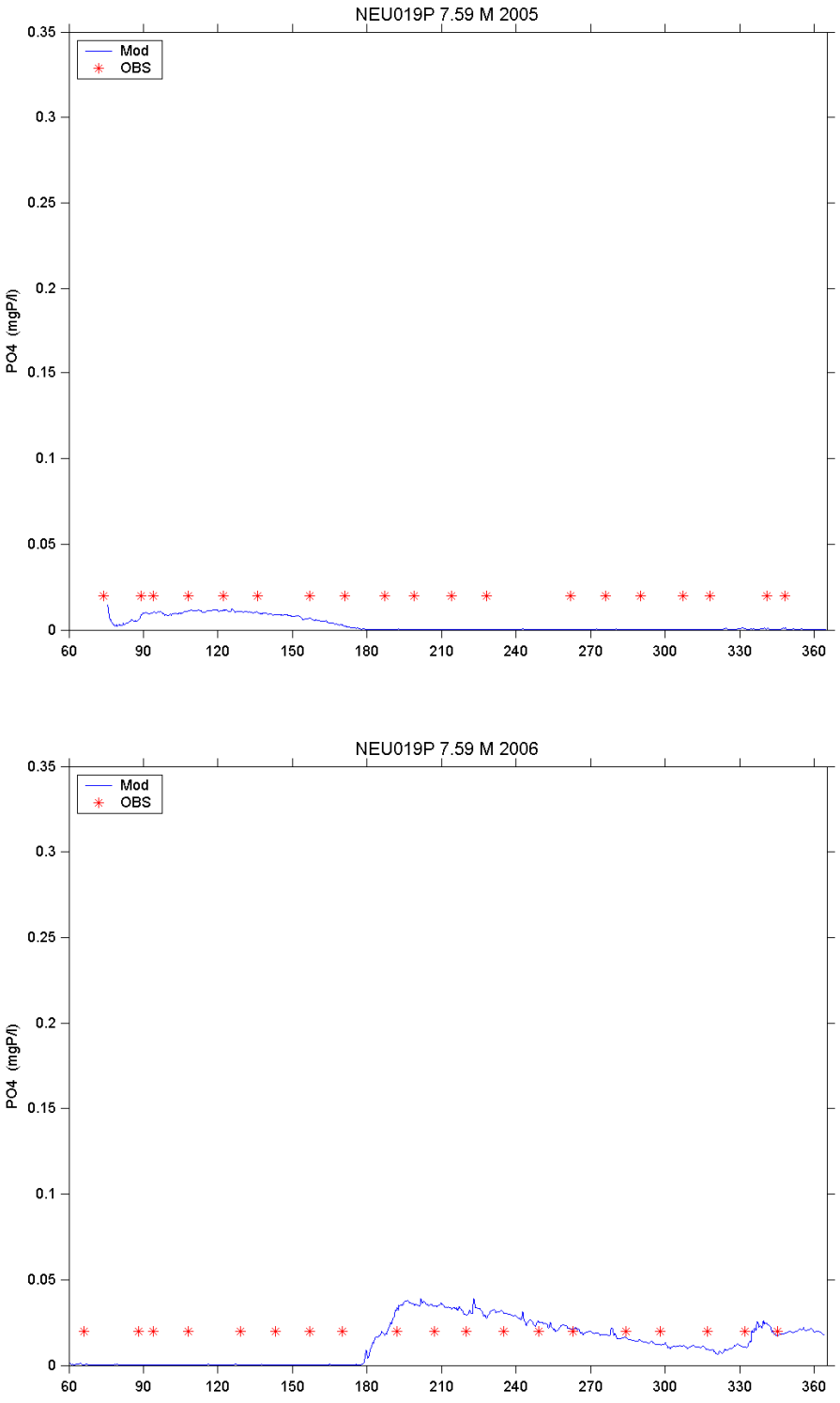

Fig. III-20. Time series plots of model-simulated (lines) and observed (stars) phosphate concentrations at NEU019P in 2005 (upper panel) and 2006 (lower panel).

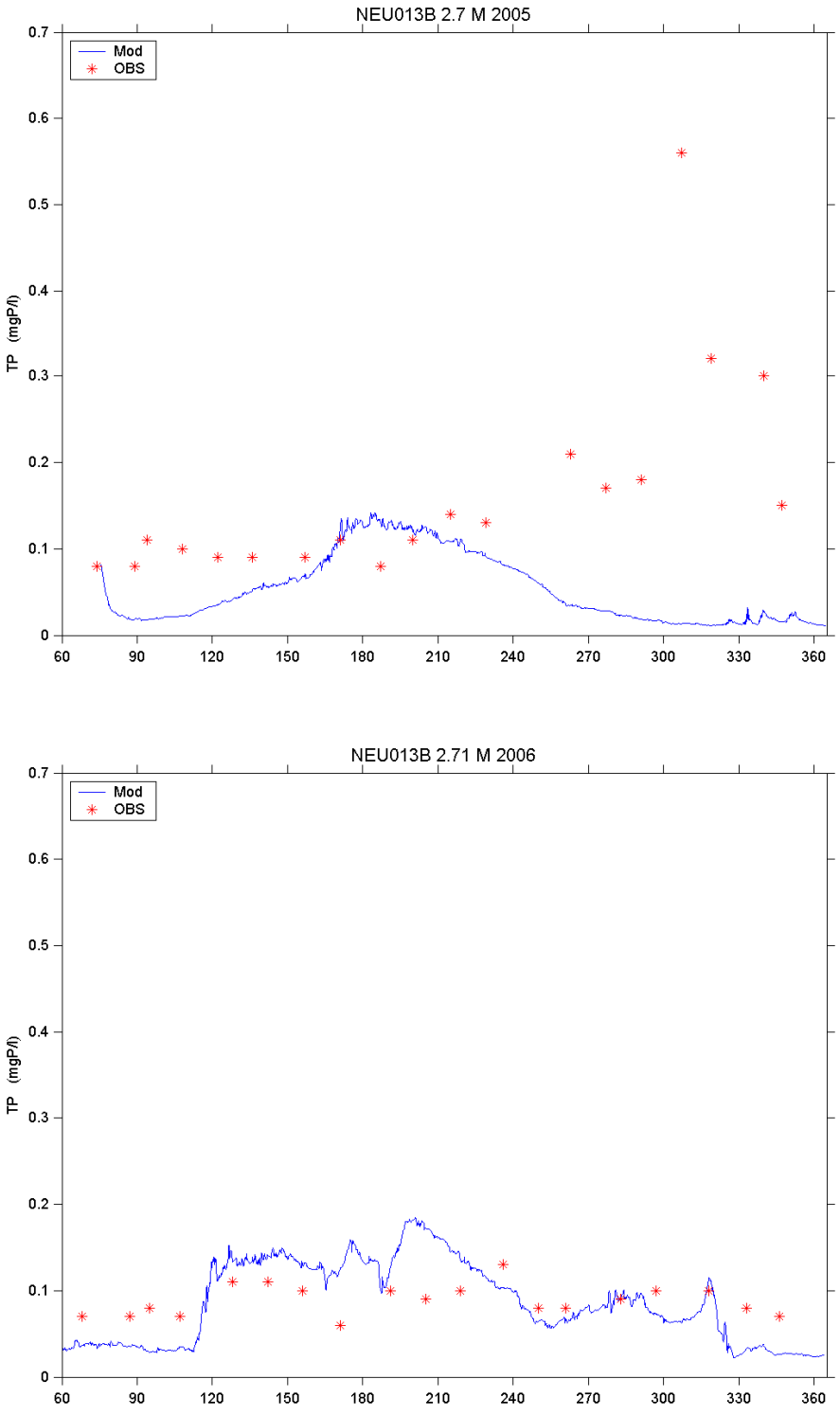

Fig. III-21. Time series plots of model-simulated (lines) and observed (stars) TP concentrations at NEU013B in 2005 (upper panel) and 2006 (lower panel).

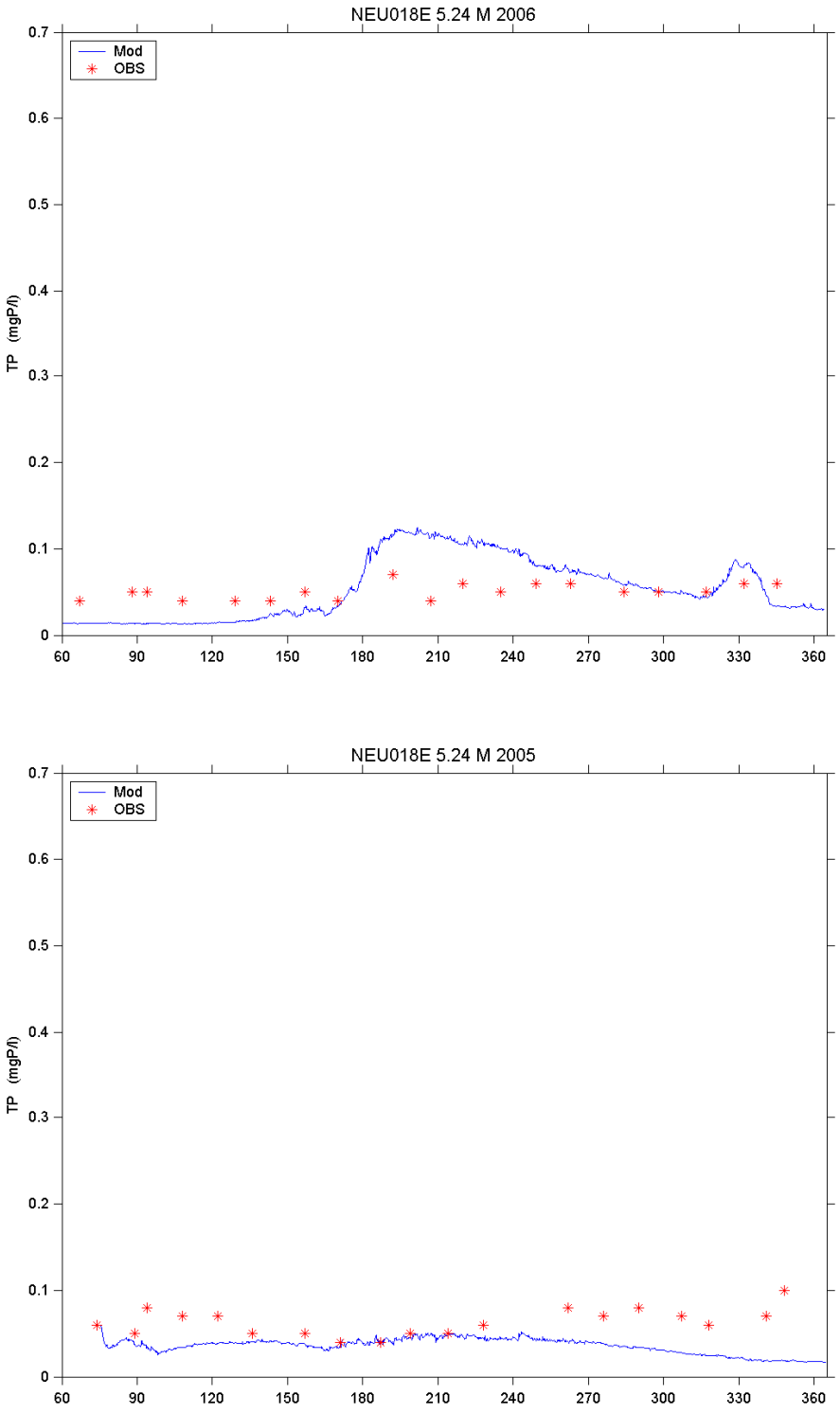

Fig. III-22. Time series plots of model-simulated (lines) and observed (stars) TP concentrations at NEU018E in 2005 (upper panel) and 2006 (lower panel).

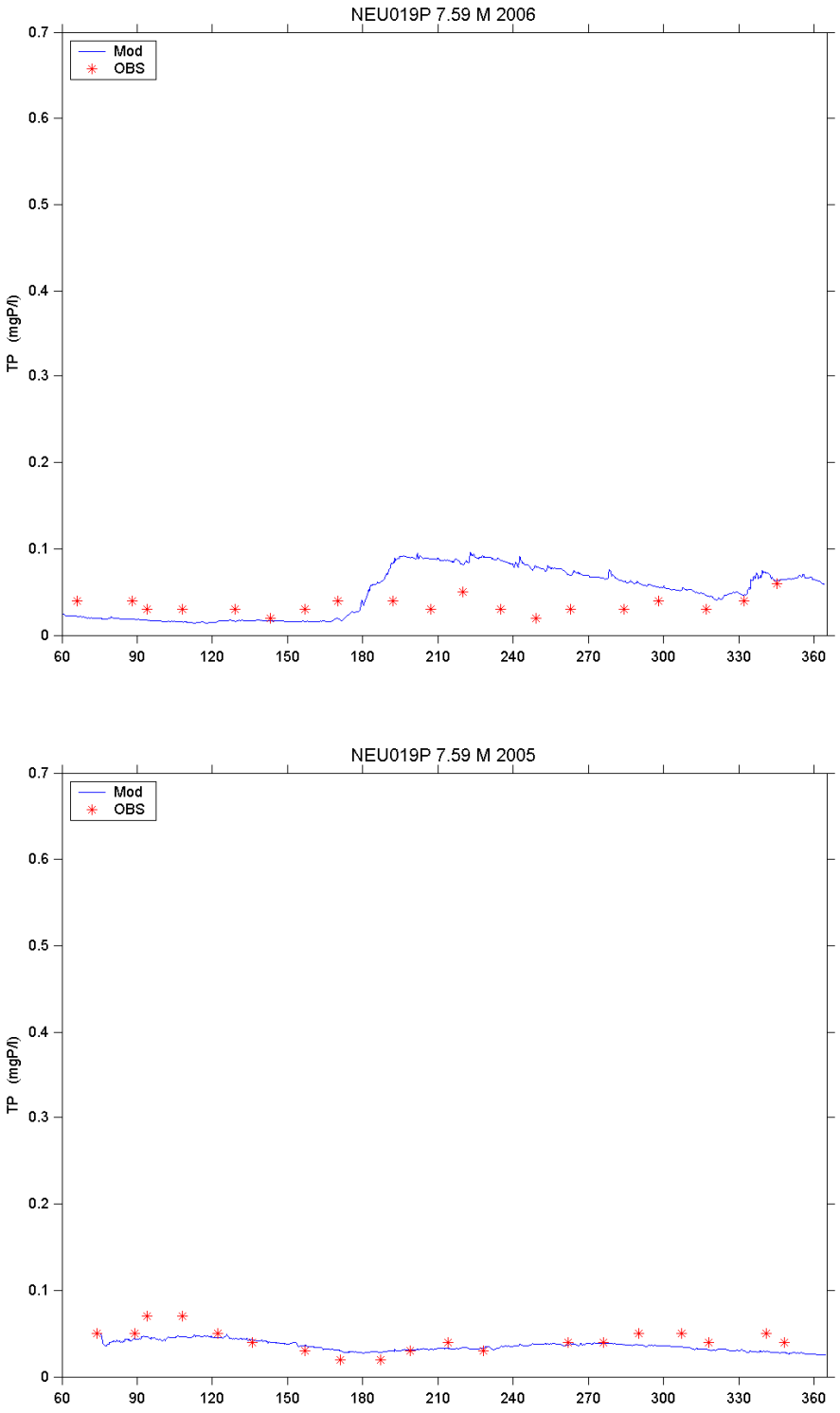

Fig. III-23. Time series plots of model-simulated (lines) and observed (stars) TP concentrations at NEU019P in 2005 (upper panel) and 2006 (lower panel).

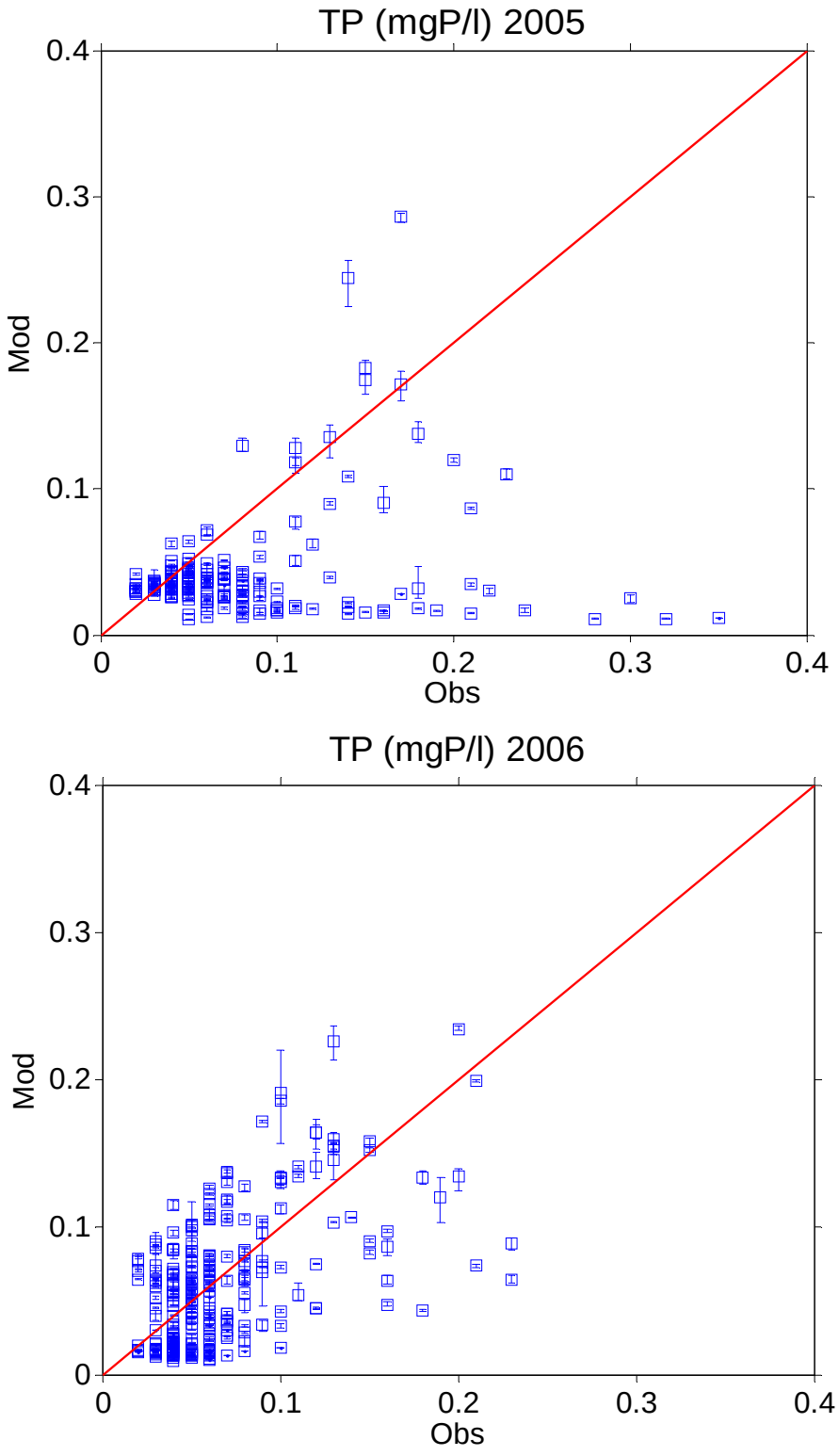

Fig. III-24. Scatter plots of model-simulated and observed TP variations at all stations in 2005 (upper panel) and 2006 (lower panel).

d. Nitrogen

Time series plots were generated for ammonia, nitrite/nitrate, and TKN concentrations at NEU013B, NEU018E, and NEU019P stations to represent the upper, middle, and lower portions of the lake, respectively (Figs. III-25 to III-33). The spatial and temporal variation patterns of ammonia, nitrite/nitrate, and TKN were generally represented well in the model. Ammonia and nitrite/nitrate concentrations were generally low except during winter to early spring. TKN concentrations ranged around 0.4 to 1.2 mg/l, with slightly higher values in the upper portion of the lake.

TN simulations generally agree with the observations, with average errors below 0.10 mg/l for both years (Fig. III-34, Table III-7). Similar to TP simulations, TN was slightly under-predicted at stations in the upper portion of the lake during 2005 when particularly dry conditions prevailed.

Statistics are provided for TN simulations in Table III-7. The absolute values of the average errors for model prediction are much less than the corresponding standard deviation for observations in both years, indicating a reasonable model representation of the observed TN conditions in the lake.

Table III-7. Statistics for 2005 and 2006 TN simulation

	RE	AE	SD_{obs}	R^2	RMSE	$RMSE/SD_{obs}$	CE	pBias
2005	-0.10	-0.09	0.40	0.35	0.33	0.83	0.30	-10.00%
2006	-0.12	-0.10	0.21	0.27	0.22	1.05	-0.12	-12.07%

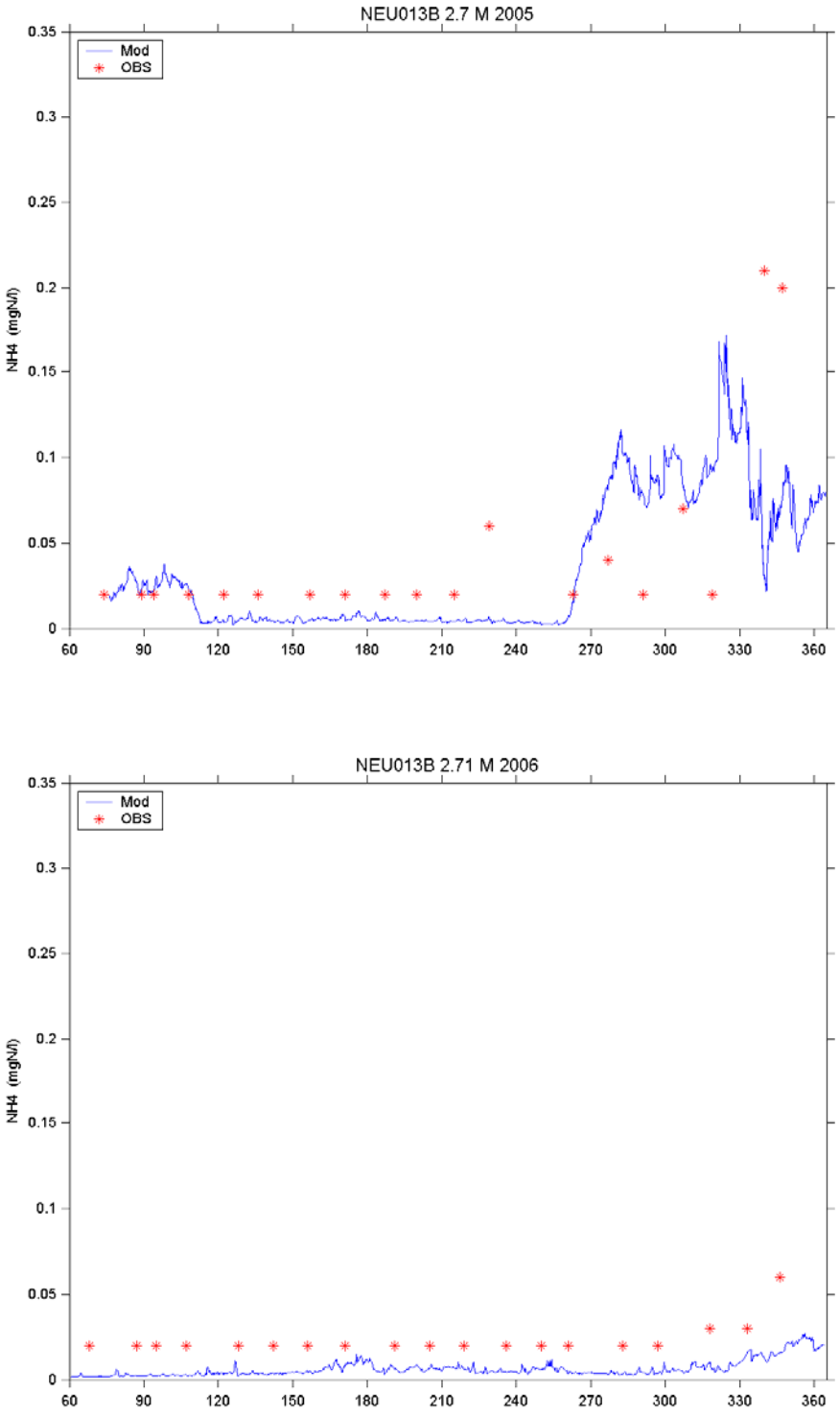

Fig. III-25. Time series plots of model-simulated (lines) and observed (stars) ammonia concentrations at NEU013B in 2005 (upper panel) and 2006 (lower panel).

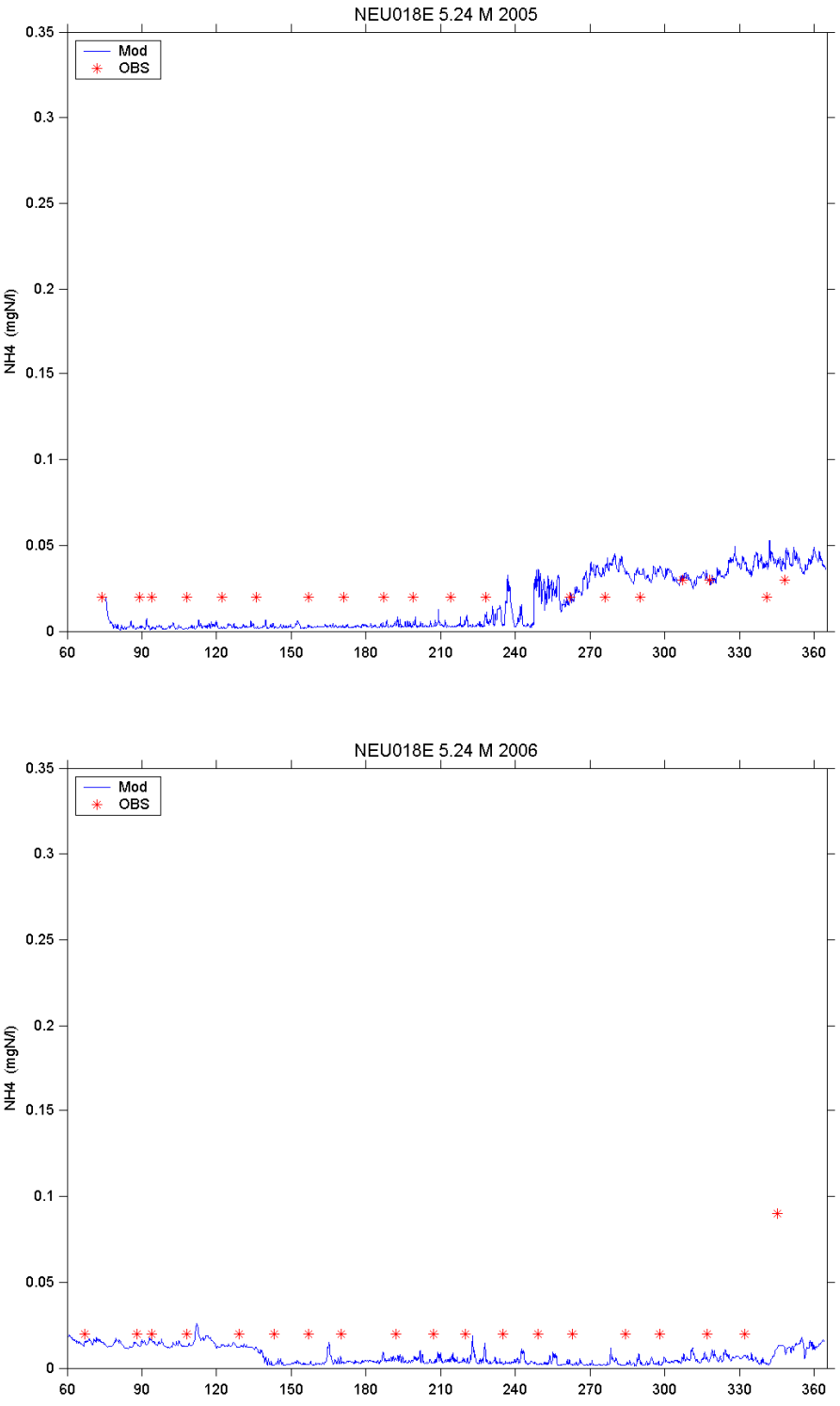

Fig. III-26. Time series plots of model-simulated (lines) and observed (stars) ammonia concentrations at NEU018E in 2005 (upper panel) and 2006 (lower panel).

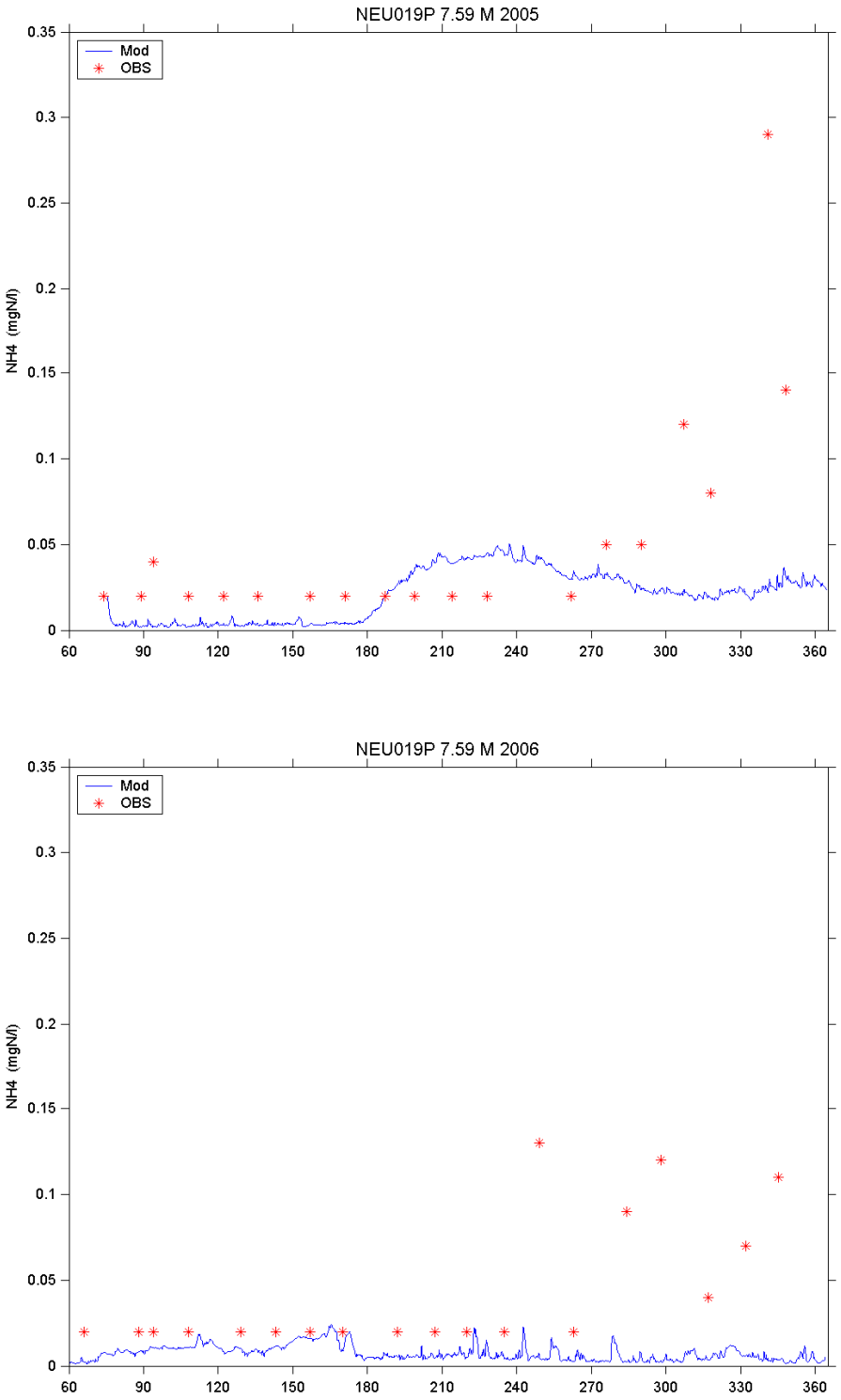

Fig. III-27. Time series plots of model-simulated (lines) and observed (stars) ammonia concentrations at NEU019P in 2005 (upper panel) and 2006 (lower panel).

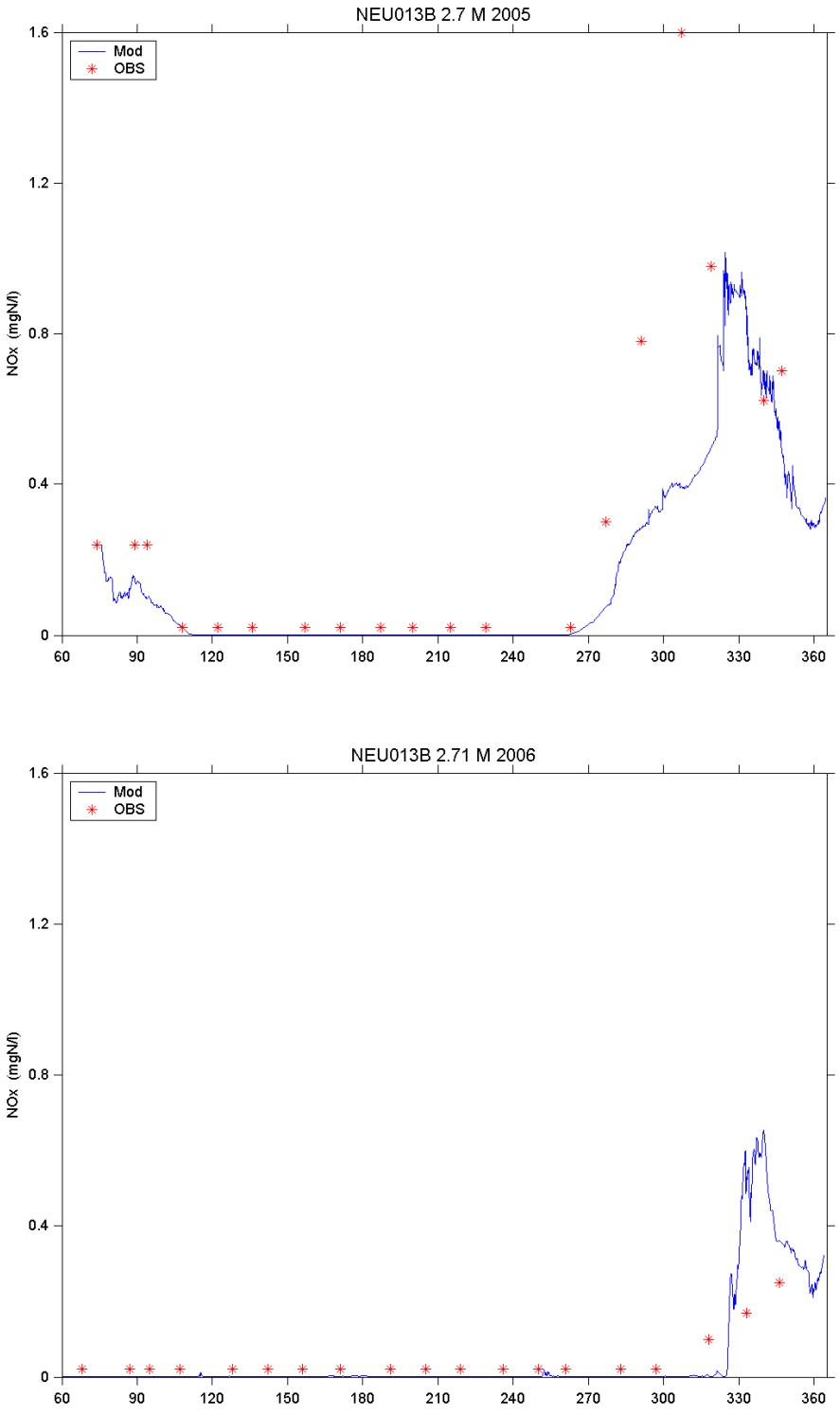

Fig. III-28. Time series plots of model-simulated (lines) and observed (stars) NOx concentrations at NEU013B in 2005 (upper panel) and 2006 (lower panel).

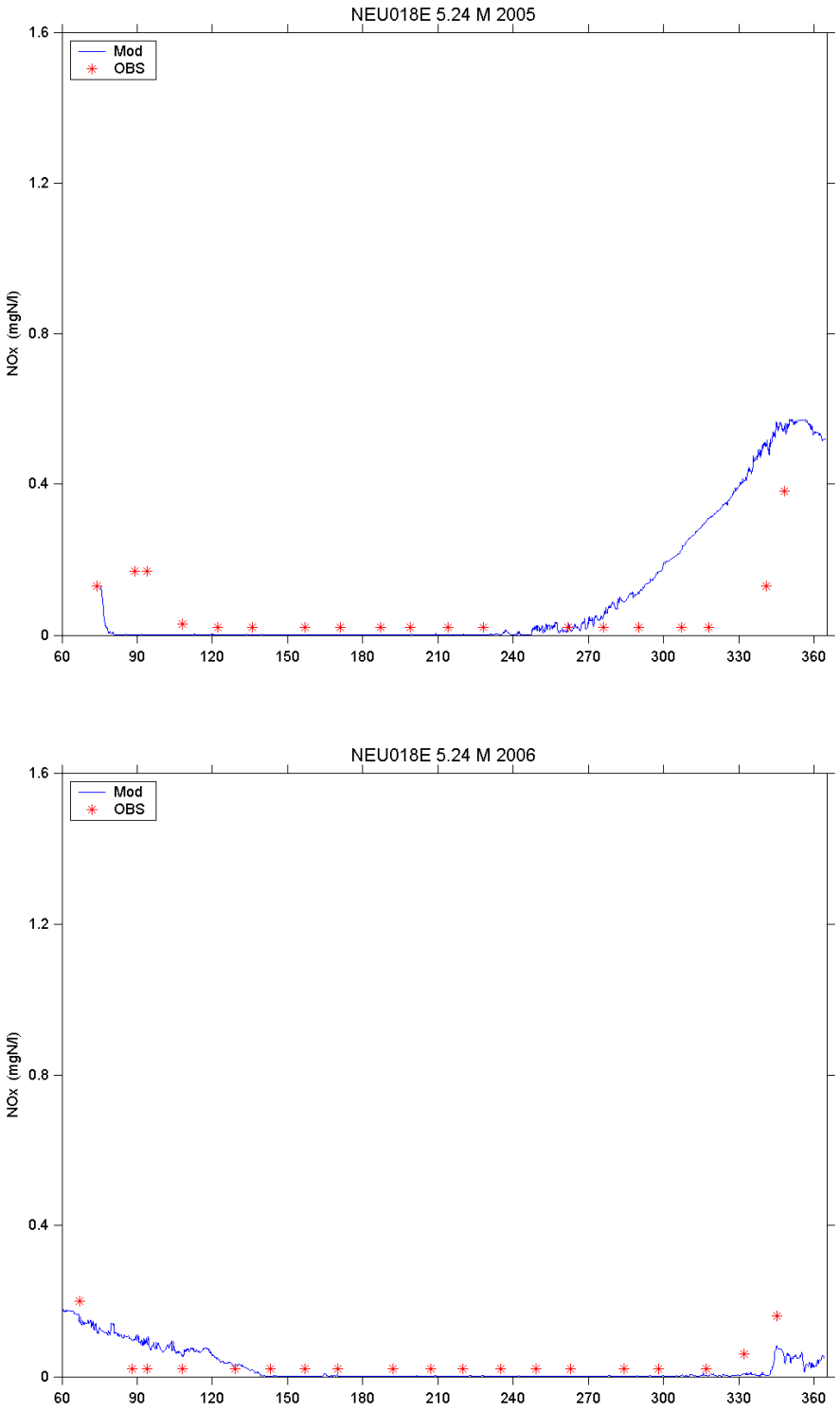

Fig. III-29. Time series plots of model-simulated (lines) and observed (stars) NOx concentrations at NEU018E in 2005 (upper panel) and 2006 (lower panel).

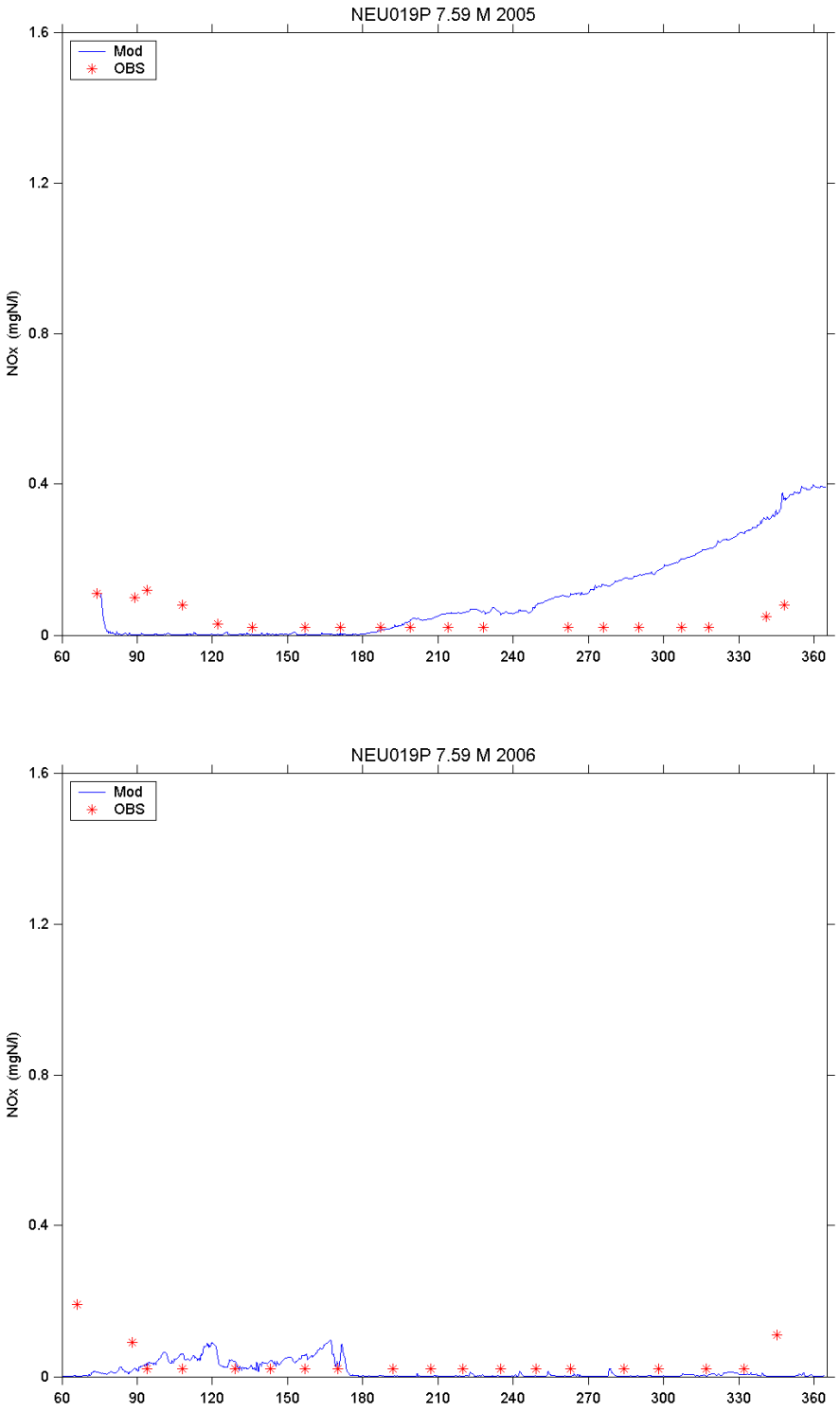

Fig. III-30. Time series plots of model-simulated (lines) and observed (stars) NOx concentrations at NEU019P in 2005 (upper panel) and 2006 (lower panel).

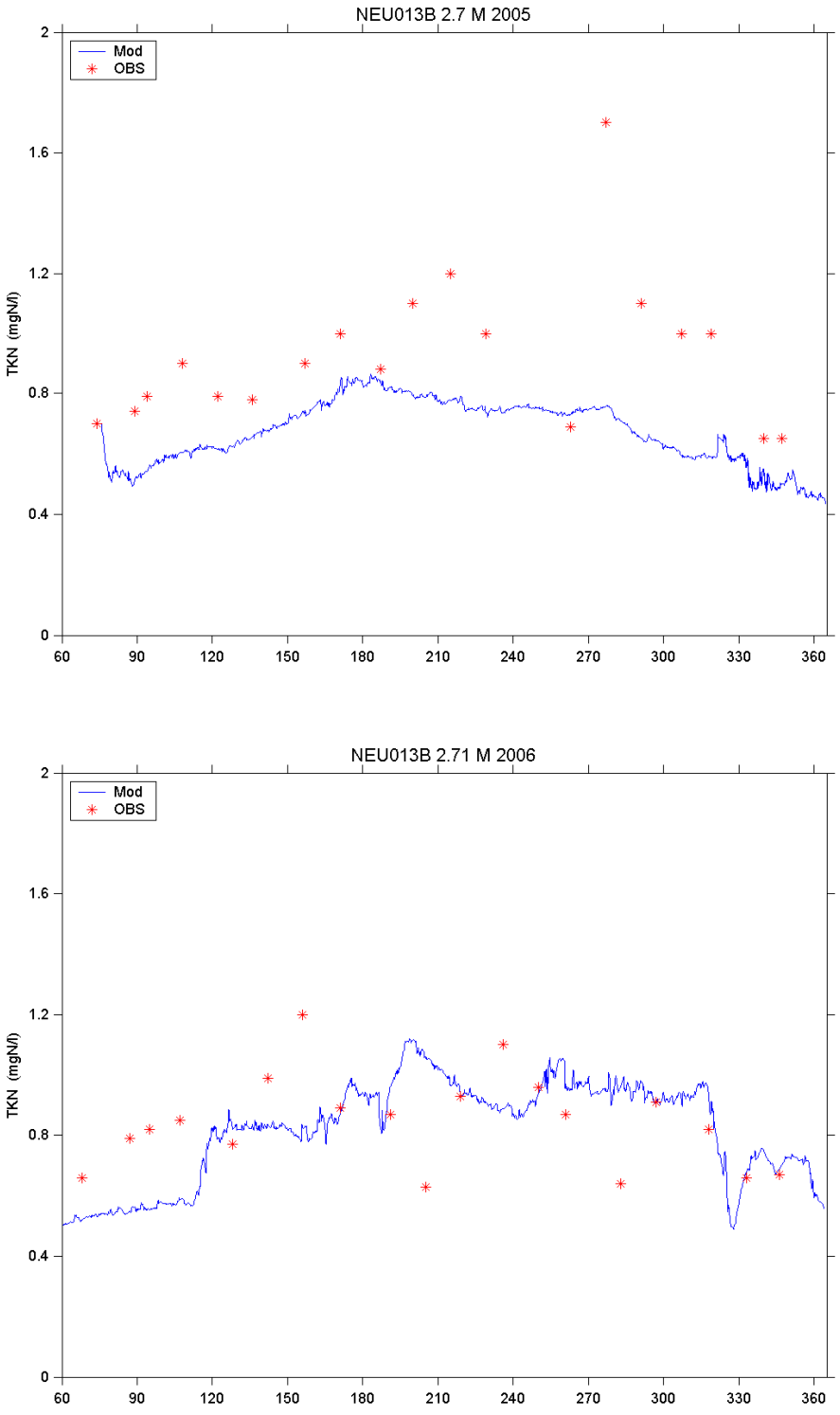

Fig. III-31. Time series plots of model-simulated (lines) and observed (stars) TKN concentrations at NEU013B in 2005 (upper panel) and 2006 (lower panel).

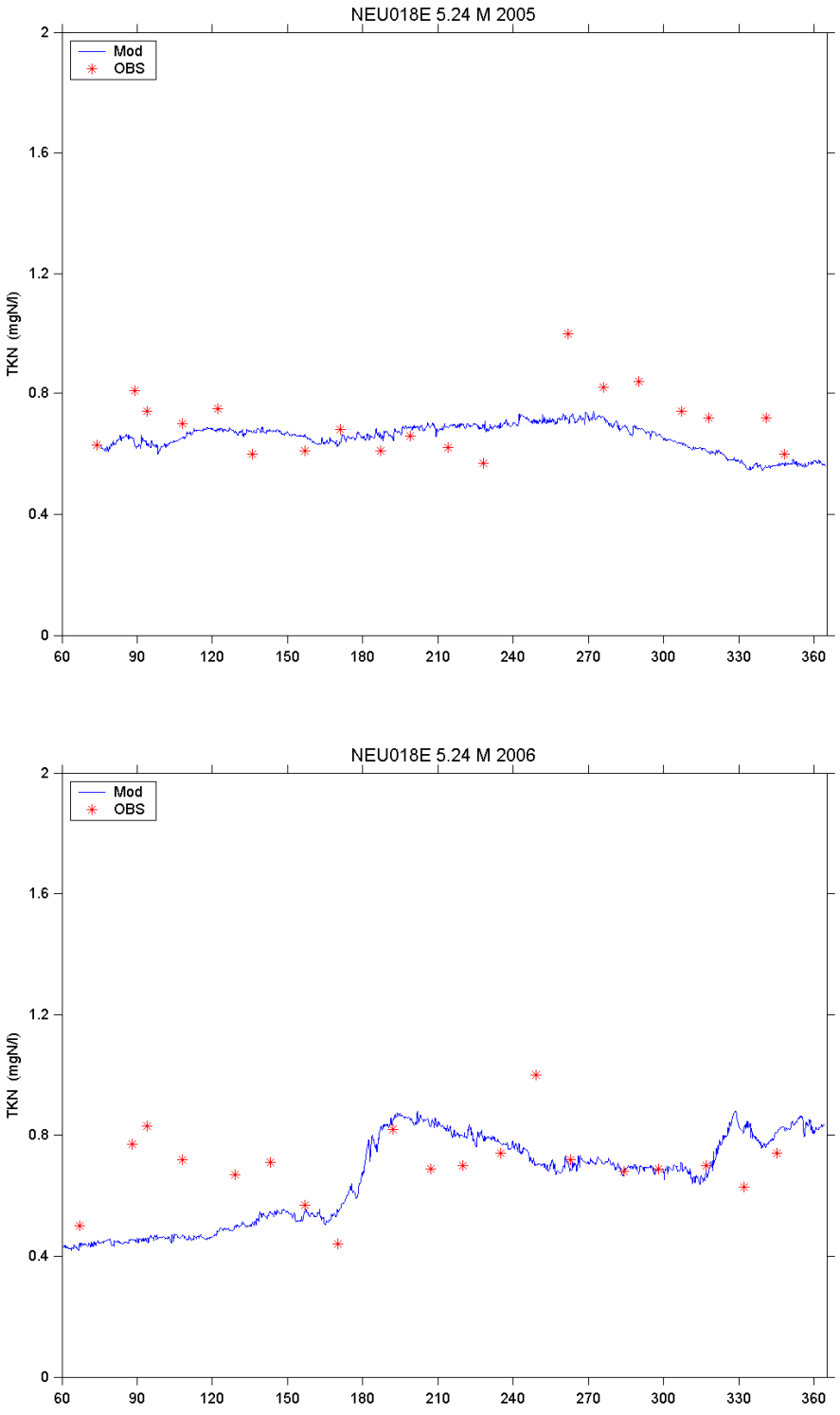

Fig. III-32. Time series plots of model-simulated (lines) and observed (stars) TKN concentrations at NEU018E in 2005 (upper panel) and 2006 (lower panel).

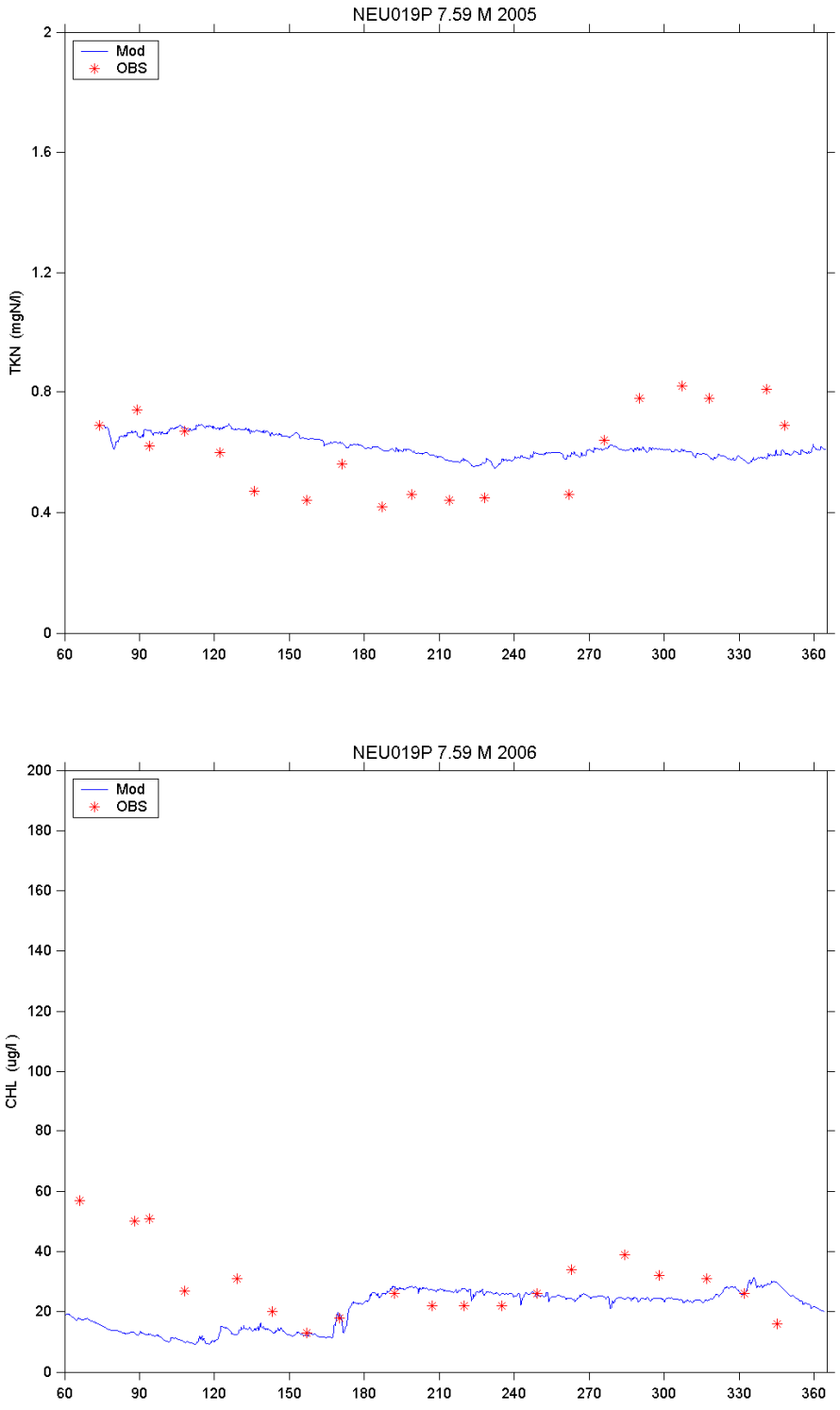

Fig. III-33. Time series plots of model-simulated (lines) and observed (stars) TKN concentrations at NEU019P in 2005 (upper panel) and 2006 (lower panel).

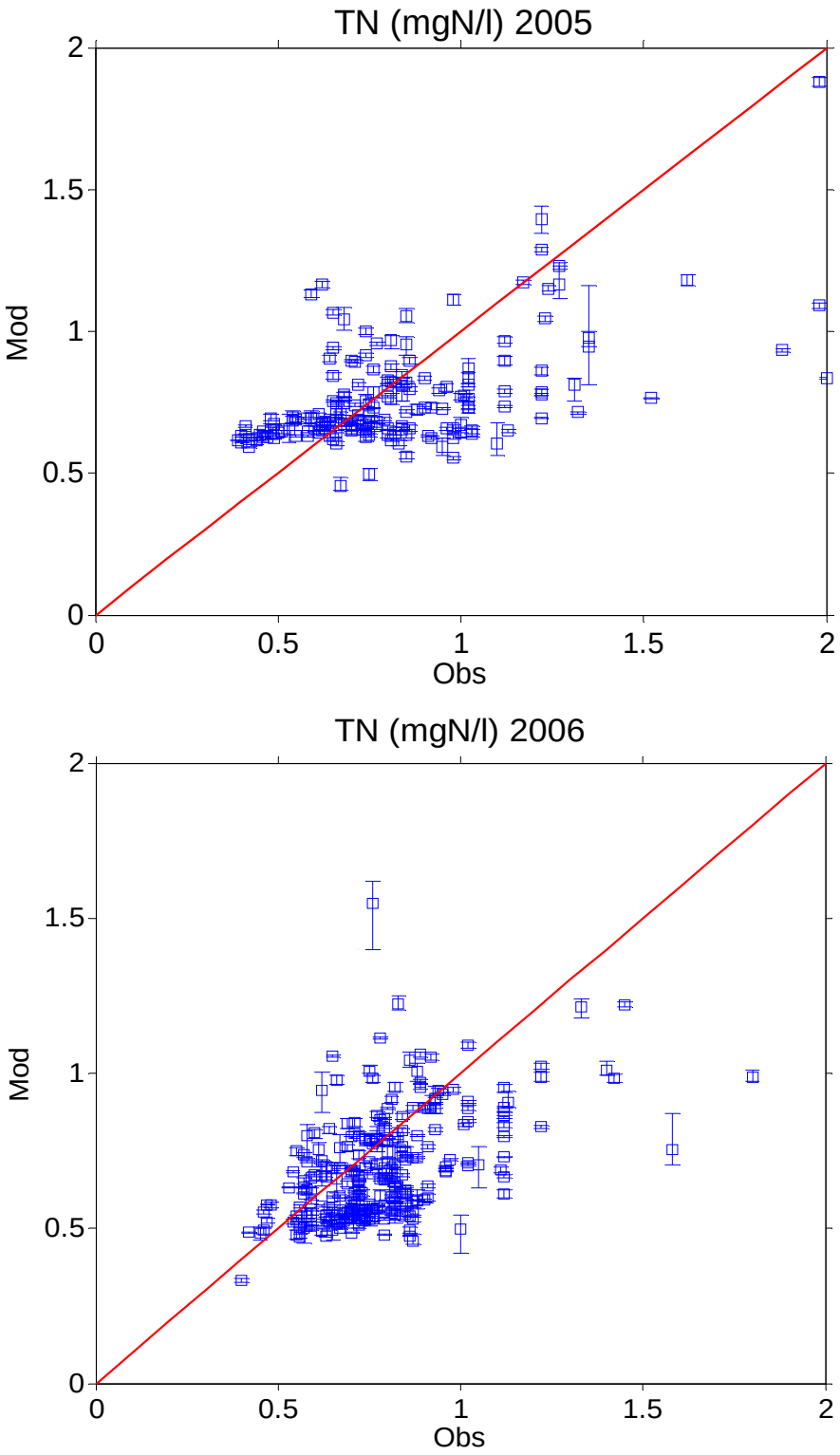

Fig. III-34. Scatter plots of model-simulated and observed TN variations at all stations in 2005 (upper panel) and 2006 (lower panel).

e. Dissolved oxygen

Time series plots show that the model predicted the spatial and temporal variations of dissolved oxygen well throughout the lake (Figs. III-35 to III-37). In the lower portions of the lake, where deep channels exist, the onset of stratification occurred during late spring to early autumn. The thermocline simulated by the model appeared to be slightly deeper than indicated by observations. The slight over-prediction of DO at layer 2 and 3 at the station NEU019P was most likely due to the slightly deeper thermocline simulated by the model.

Table III-8. Statistics for 2005 and 2006 DO simulation

	RE	AE	SD_{obs}	R^2	RMSE	$RMSE/SD_{obs}$	CE	pBias
2005	0.20	1.24	2.63	0.72	1.87	0.71	0.49	19.76%
2006	0.13	0.90	2.96	0.62	2.04	0.69	0.52	12.69%

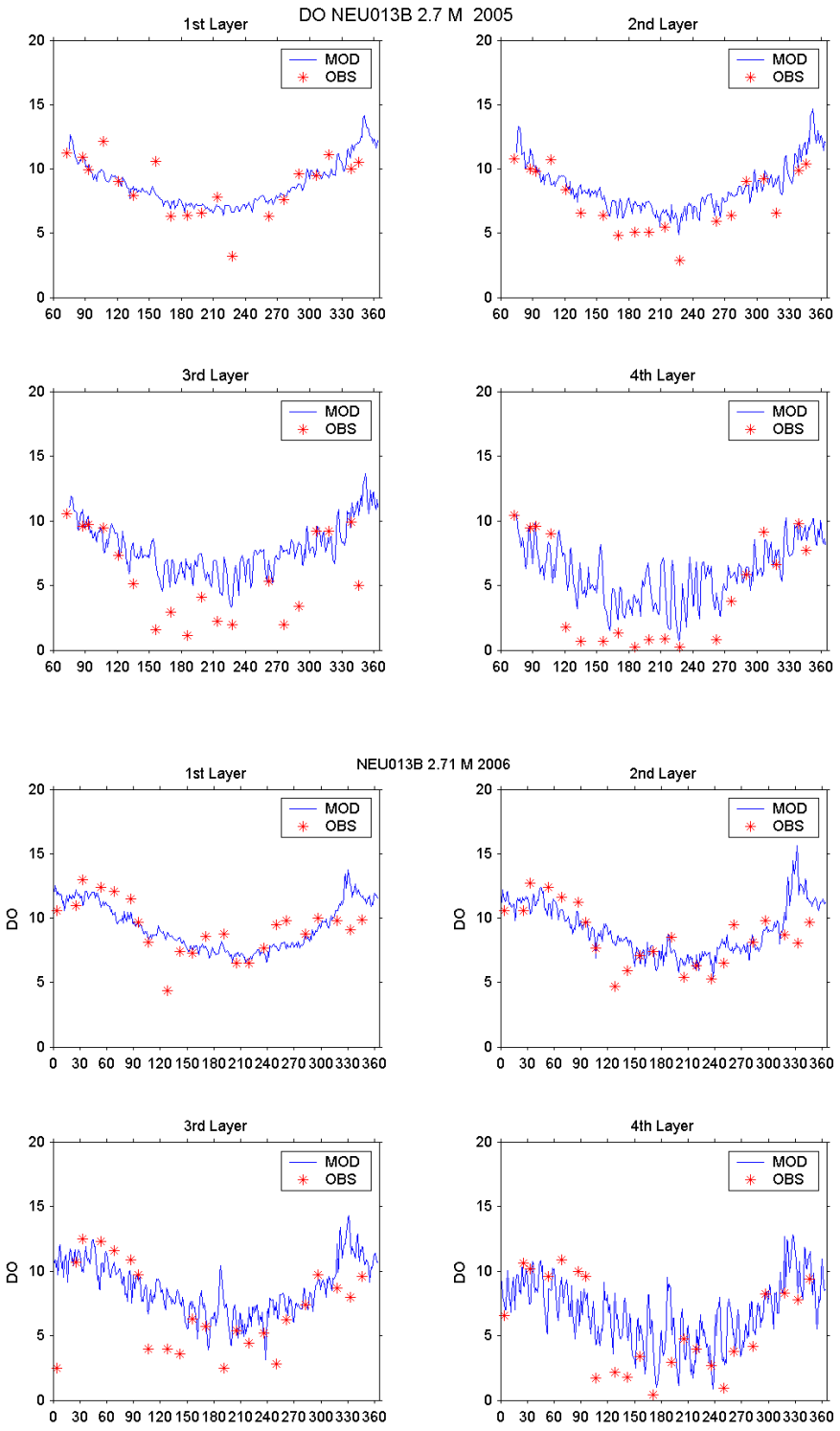

Fig. III-35. Time series plots of model-simulated (lines) and observed (stars) DO concentrations at NEU013B in 2005 (upper panel) and 2006 (lower panel).

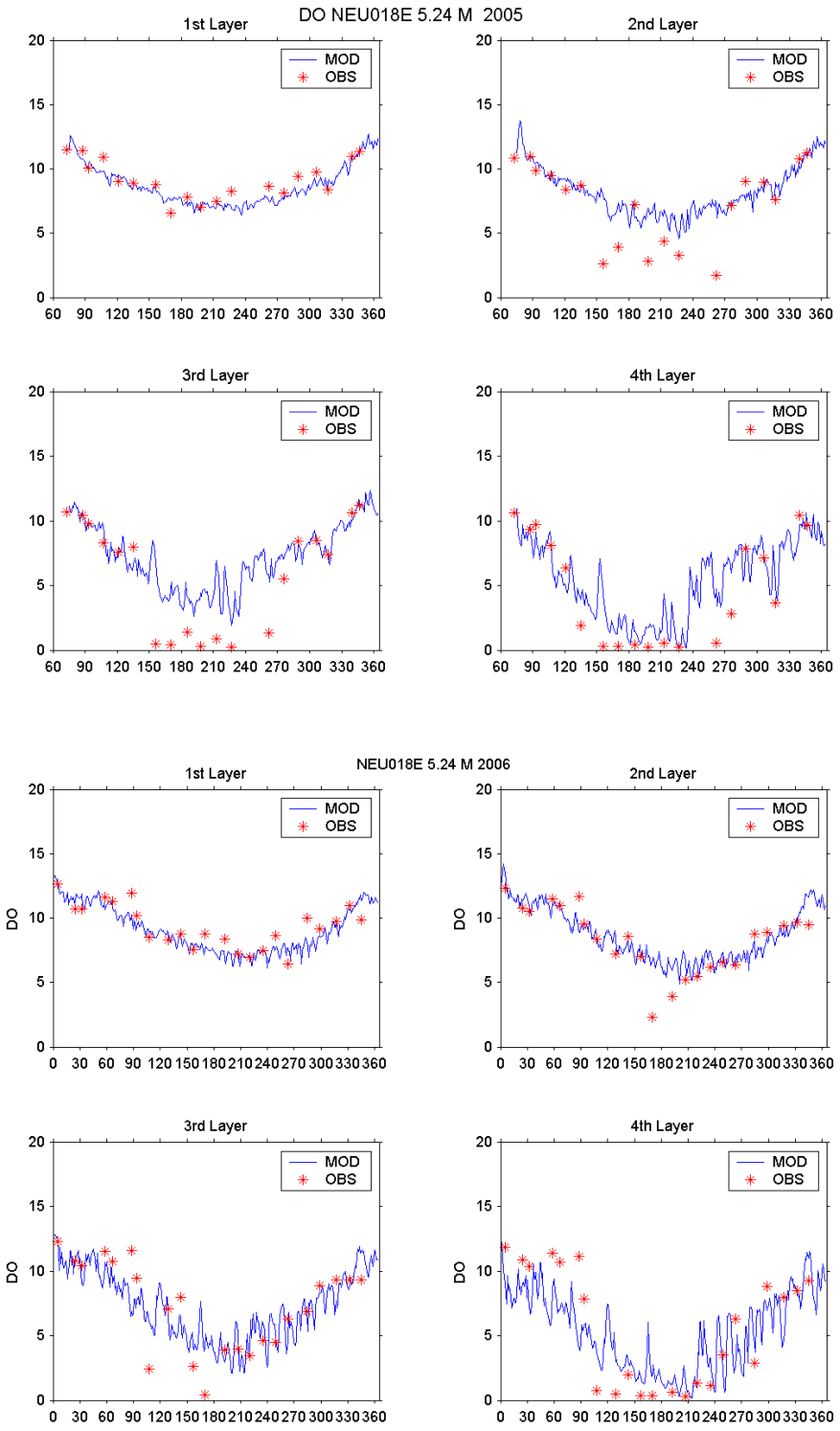

Fig. III-36. Time series plots of model-simulated (lines) and observed (stars) DO concentrations at NEU018E in 2005 (upper panel) and 2006 (lower panel).

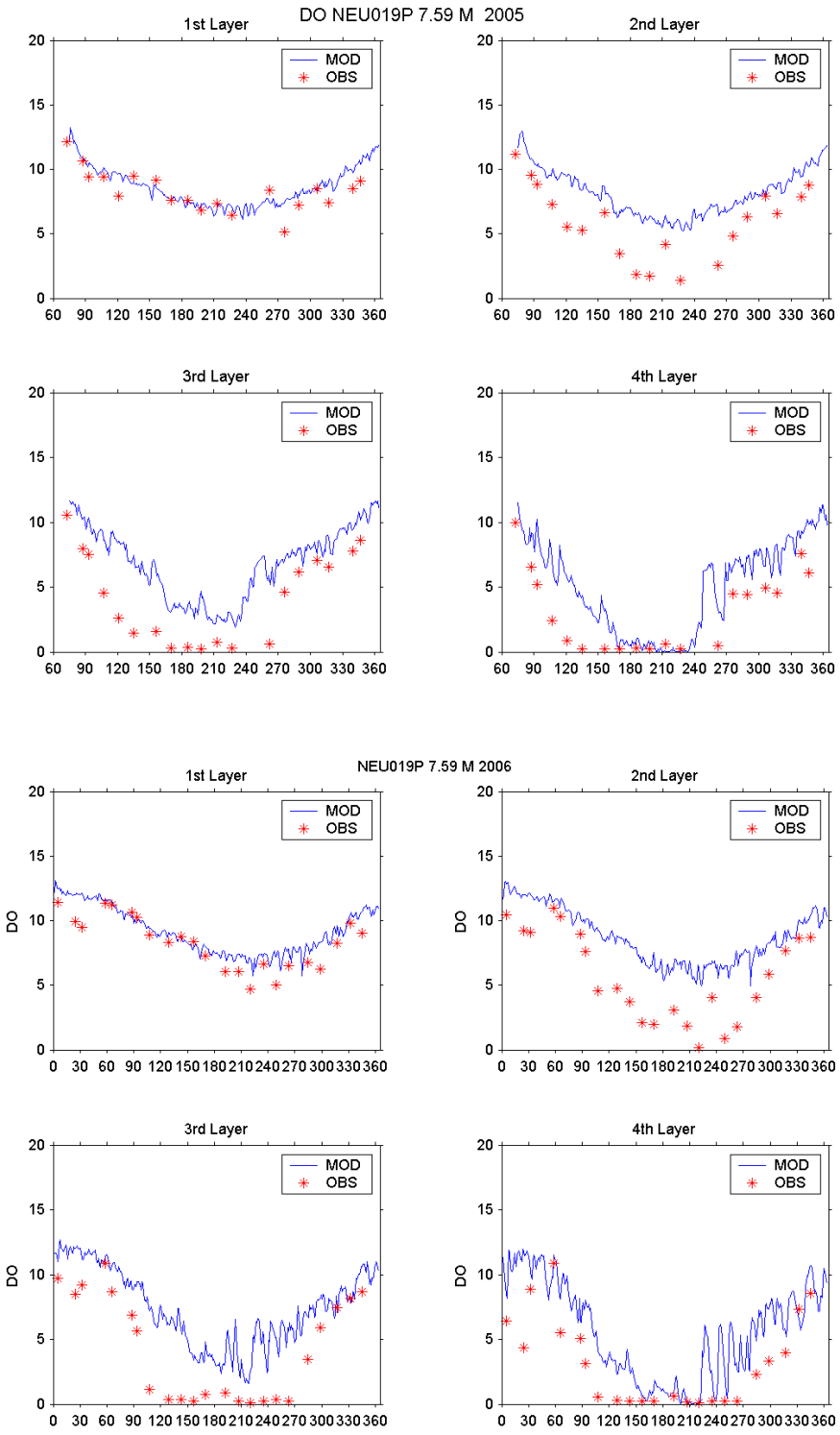

Fig. III-37. Time series plots of model-simulated (lines) and observed (stars) DO concentrations at NEU019P in 2005 (upper panel) and 2006 (lower panel).

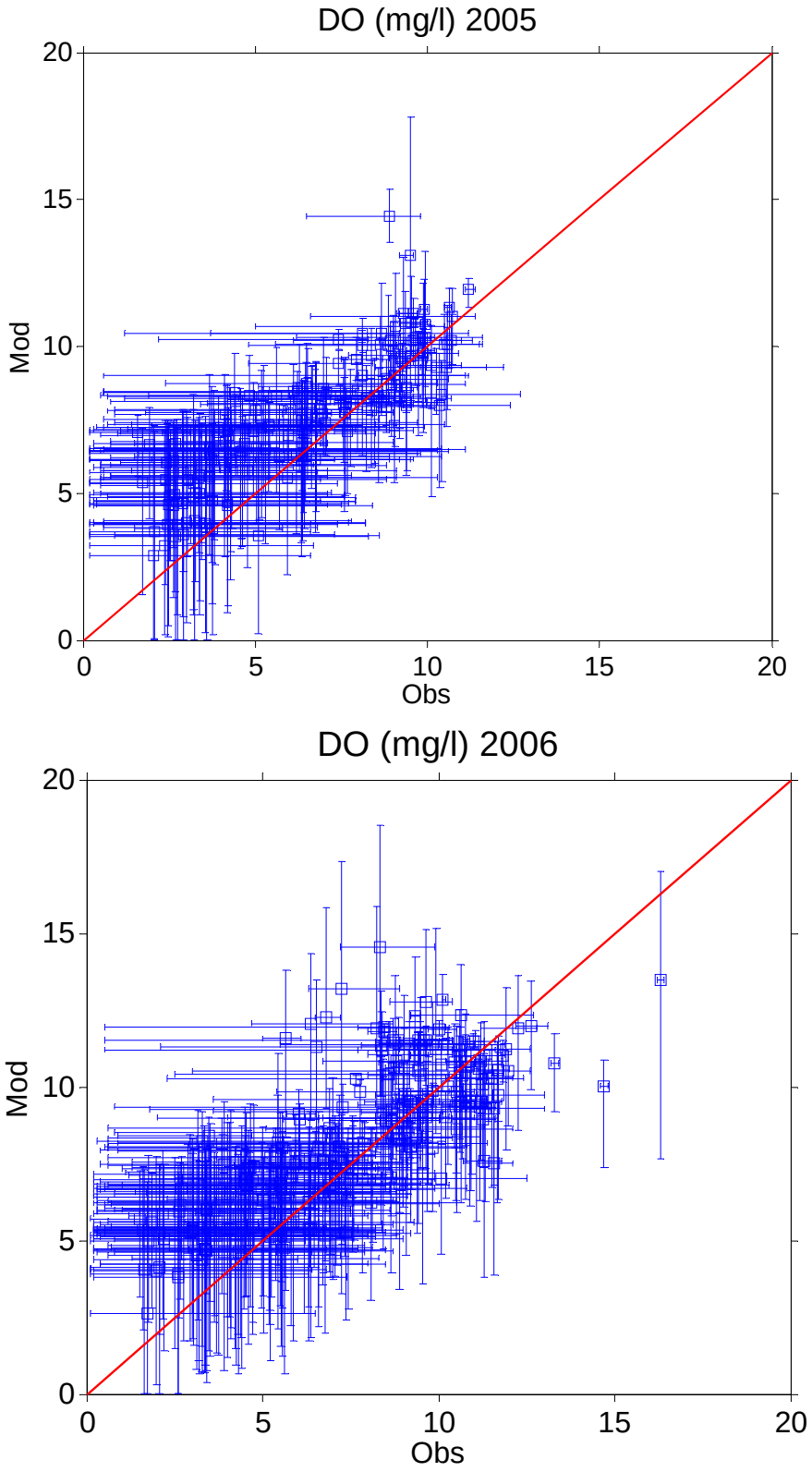

Fig. III-38. Scatter plots of model-simulated and observed DO variations at all stations in 2005 (upper panel) and 2006 (lower panel).

IV. Model Validation

Validation is the process of determining the degree to which a model, simulation, or federation of models and simulations, and their associated data are accurate representations of the real world from the perspective of the intended use(s) (http://en.wikipedia.org/wiki/Verification_and_Validation_(software)).

In this project, model validation was conducted by keeping all model parameters from the 2005 calibration, running the model with 2007 forcing functions, and comparing the model results with field data collected during 2007.

The choice of using the parameter set generated from the 2005 model calibration was made because both 2005 and 2007 are considered dry years. The lake hydrodynamics and the biogeochemical functions in the lake were assumed to be similar during 2005 and 2007.

As shown in the following figures (Fig. IV-1 to IV-39), the model has an overall reasonable representation of the observations during the validation period. The average errors associated with model prediction are much less than the standard deviation from the observations, and the RMSE associated with the model prediction is less than or equivalent to one standard deviation of the observations (Table IV-1). The overall fit for 2007 is not as good as in 2005-2006. The field data show that the thermocline during 2007 appeared to be more significant in deep regions of Falls Lake than during 2005-2006. By adopting all model parameters from 2005, the 2007 model moderately over-predicted water temperature at the third and fourth model layers during summer months at the deeper regions of the lake (Fig. IV-3 to IV-6).

Table IV-1. Statistics for 2007 model validation results

	RE	AE	SD_{obs}	R^2	RMSE	$RMSE/SD_{obs}$	CE	pBias
Water level	-0.003	-0.20	0.71	0.97	0.24	0.34	0.88	-0.27%
Temperature	0.09	1.72	7.96	0.95	2.98	0.37	0.86	9.34%
TSS	-0.48	-7.75	17.27	0.07	22.50	1.27	-0.70	-47.60%
Chl-*a*	-0.18	-7.50	29.52	0.33	25.47	0.86	0.26	-18.43%
TOC	-0.06	-0.49	1.50	0.08	1.60	1.06	-0.14	-5.64%
TN	-0.20	-0.20	0.72	0.35	0.66	0.92	0.15	-20.24%
TP	-0.45	-0.04	0.11	0.01	0.12	1.09	-0.16	-44.6%
DO	0.06	0.43	3.26	0.73	1.79	0.55	0.70	6.00%

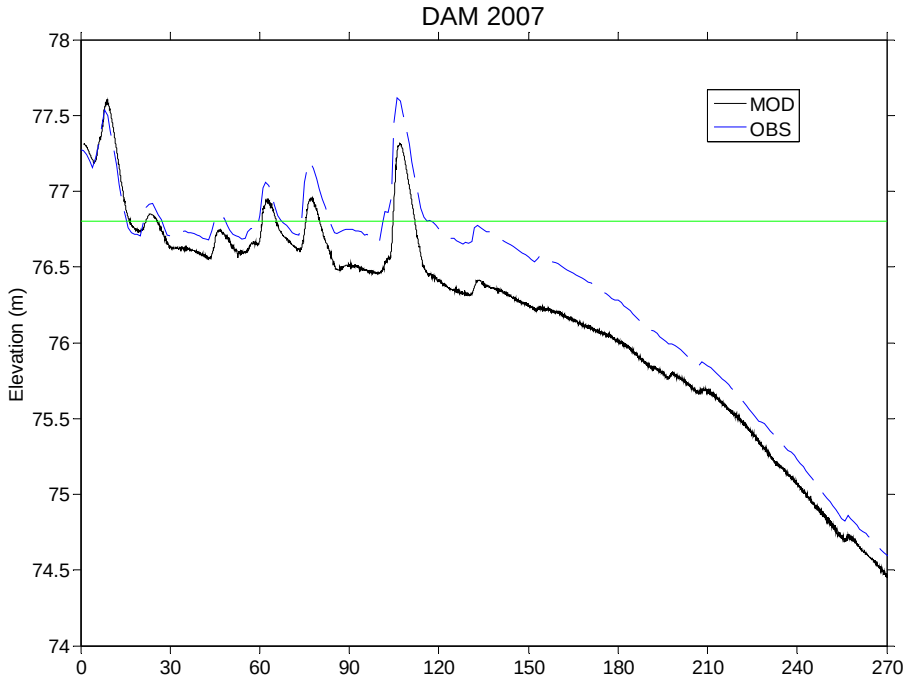

Fig. IV-1. Time series plot of modeled and observed water level variation during 2007.

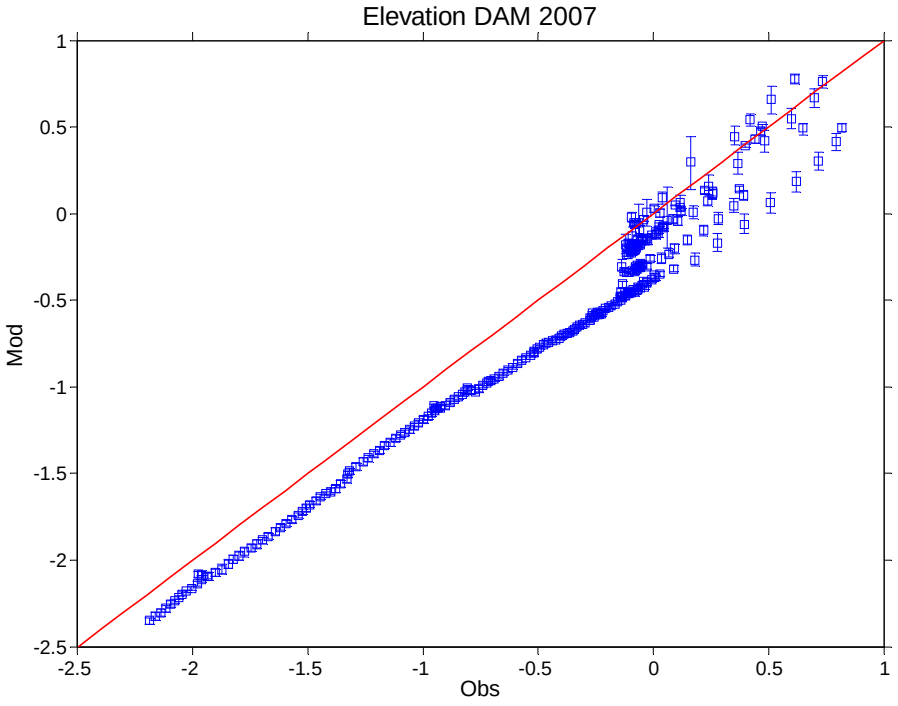

Fig. IV-2. Scatter plot of modeled and observed water level variation during 2007.

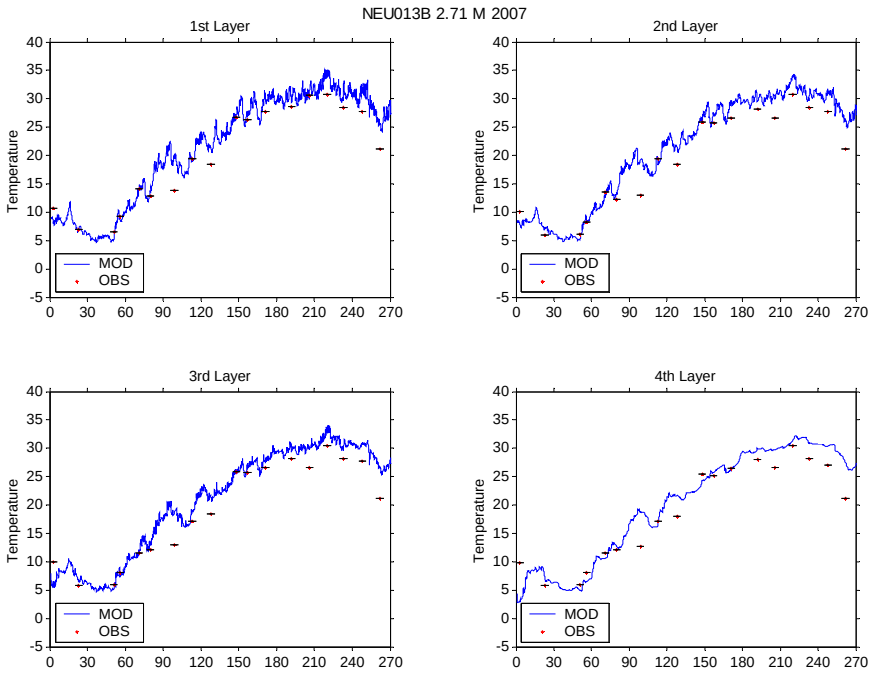

Fig. IV-3. Time series plot of modeled and observed water temperature variation at NEU 013B during 2007.

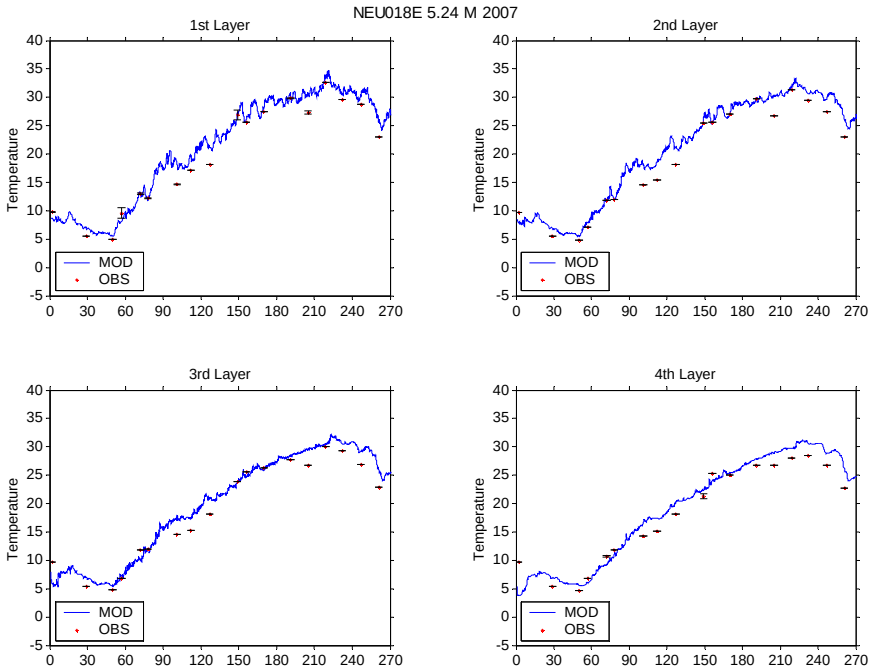

Fig. IV-4. Time series plot of modeled and observed water temperature variation at NEU 018E during 2007.

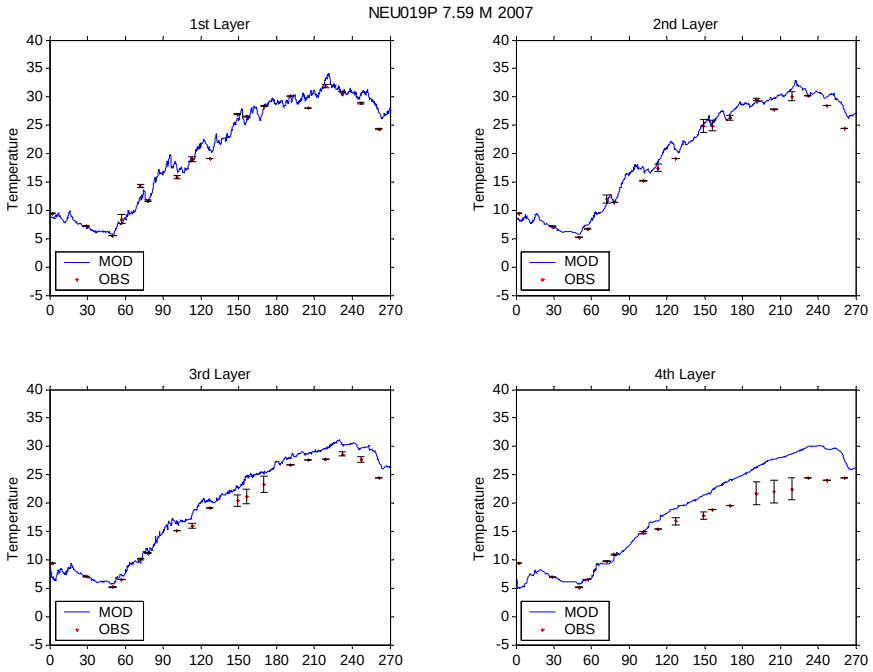

Fig. IV-5. Time series plot of modeled and observed water temperature variation at NEU 019P during 2007.

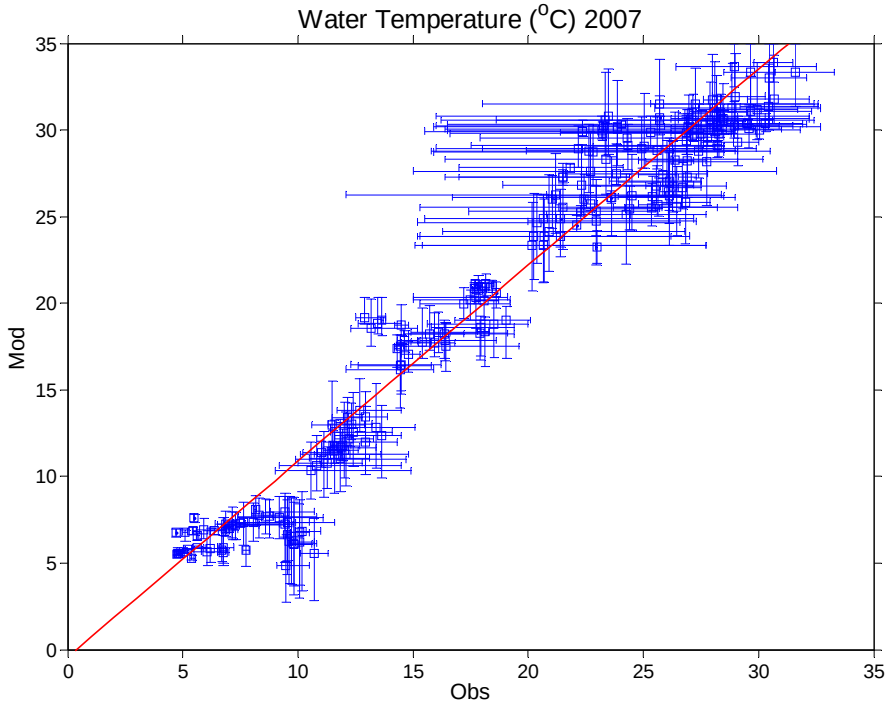

Fig. IV-6. Scatter plot of modeled and observed water temperature variation at all stations during 2007.

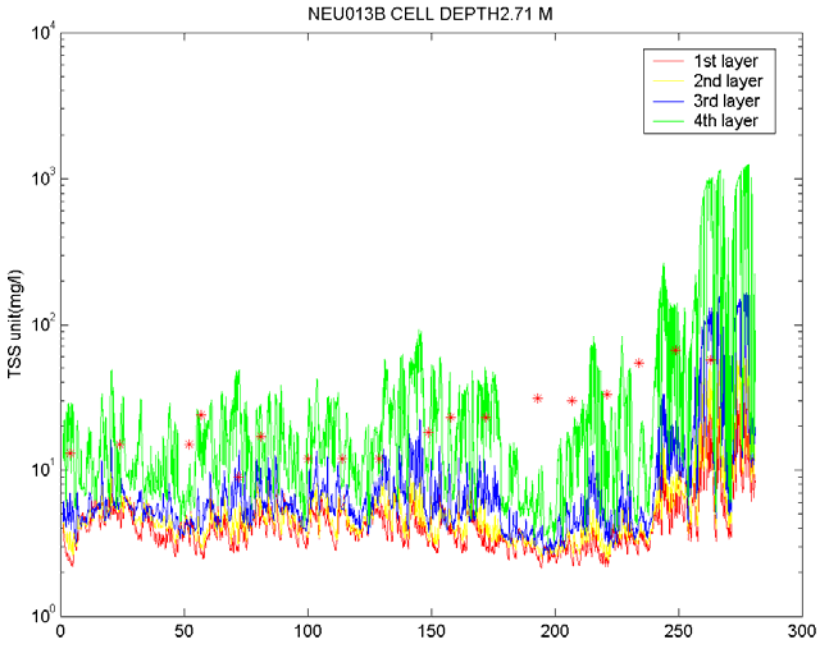

Fig. IV-7. Time series plot of modeled and observed TSS variation at NEU 013B during 2007.

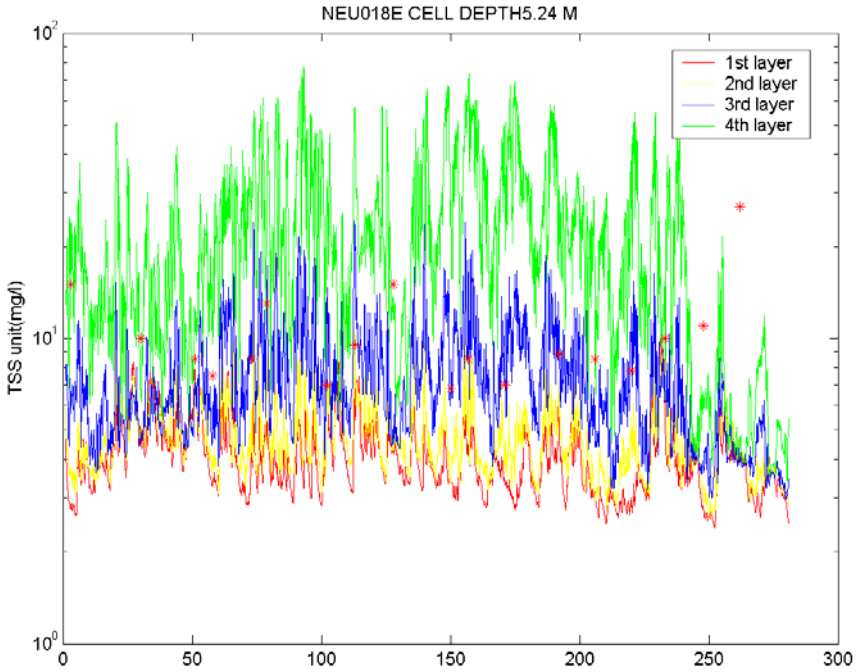

Fig. IV-8. Time series plot of modeled and observed TSS variation at NEU 018E during 2007.

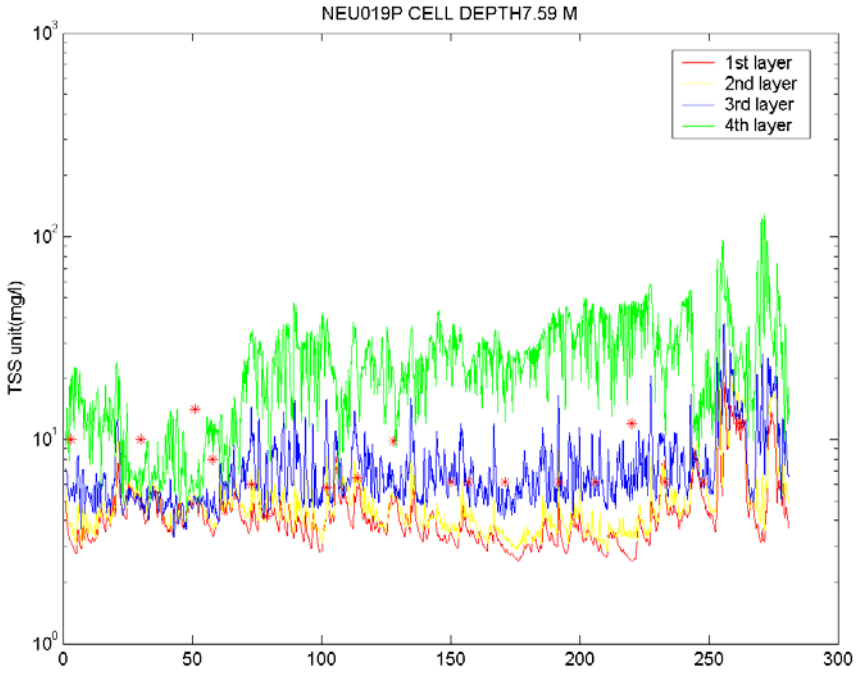

Fig. IV-9. Time series plot of modeled and observed TSS variation at NEU 019P during 2007.

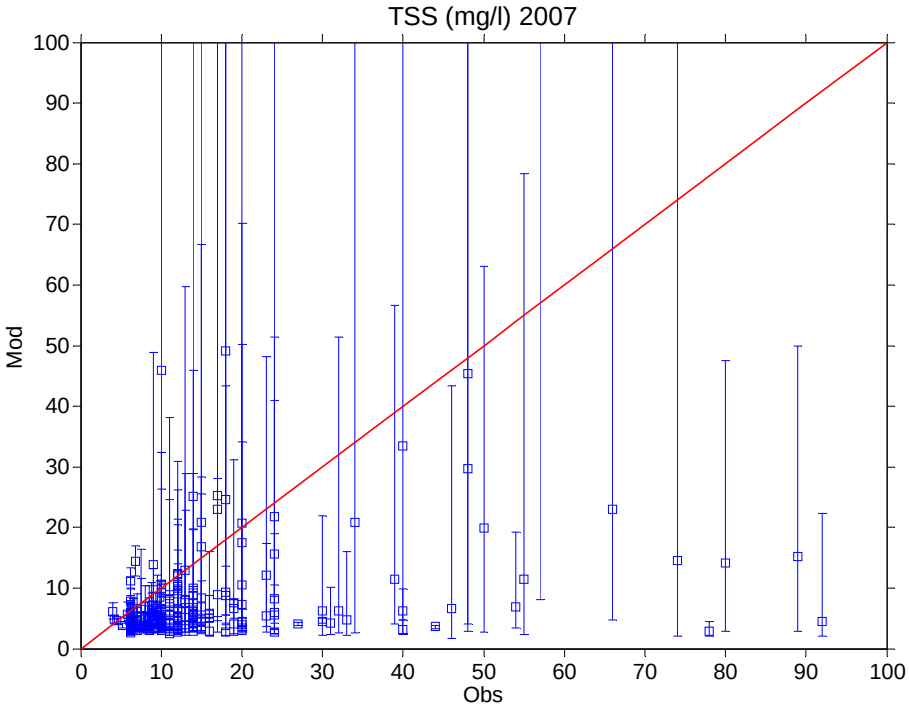

Fig. IV-10. Scatter plot of modeled and observed TSS variation at all stations during 2007.

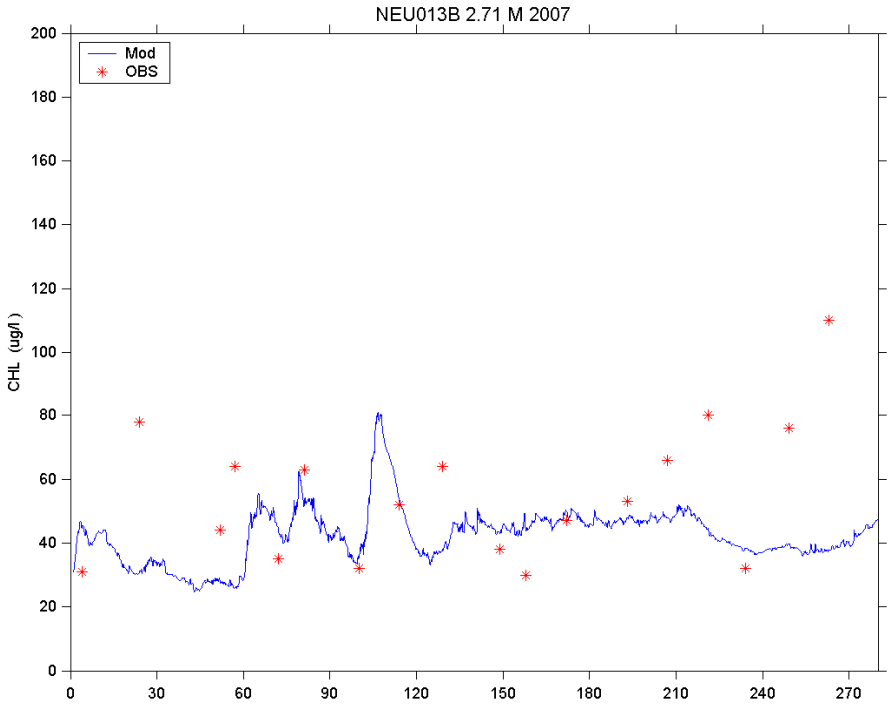

Fig. IV-11. Time series plot of modeled and observed chl-*a* variation at NEU 013B during 2007.

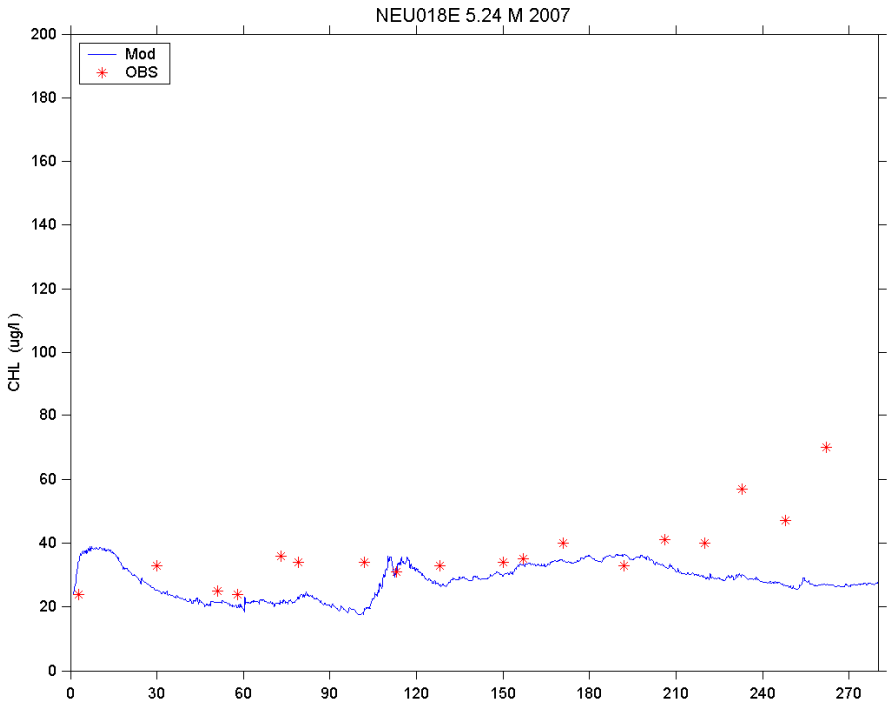

Fig. IV-12. Time series plot of modeled and observed chl-*a* variation at NEU 018E during 2007.

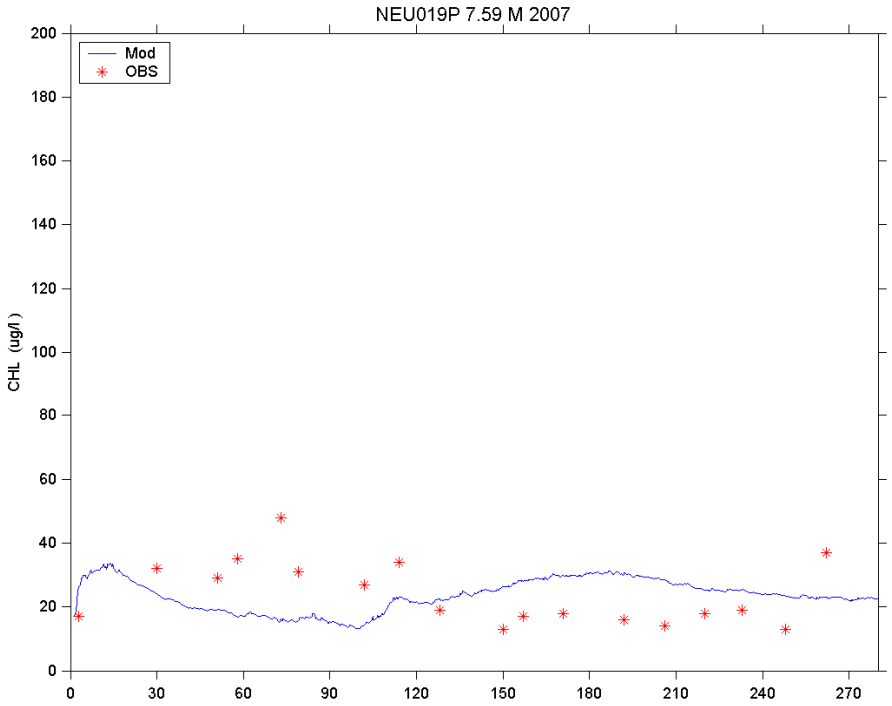

Fig. IV-13. Time series plot of modeled and observed chl-*a* variation at NEU 019P during 2007.

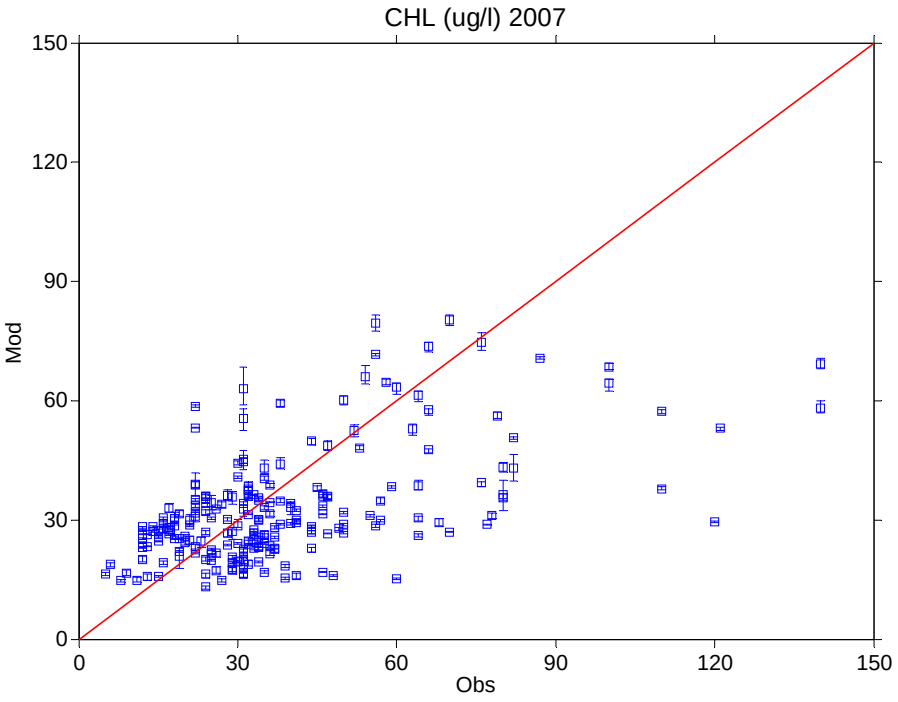

Fig. IV-14. Scatter plot of modeled and observed chl-*a* variation at all stations during 2007.

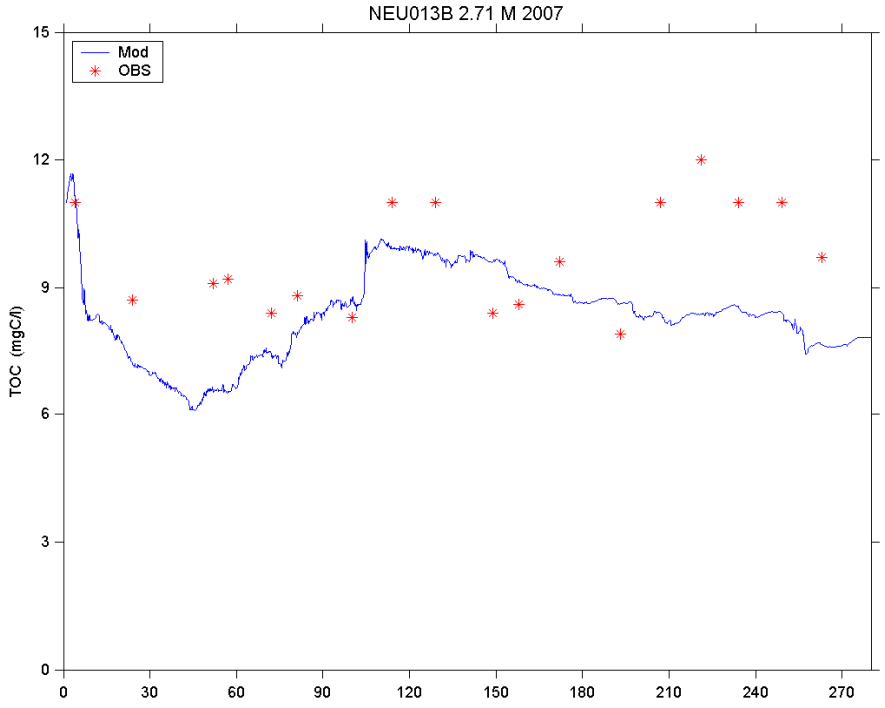

Fig. IV-15. Time series plot of modeled and observed TOC variation at NEU013B during 2007.

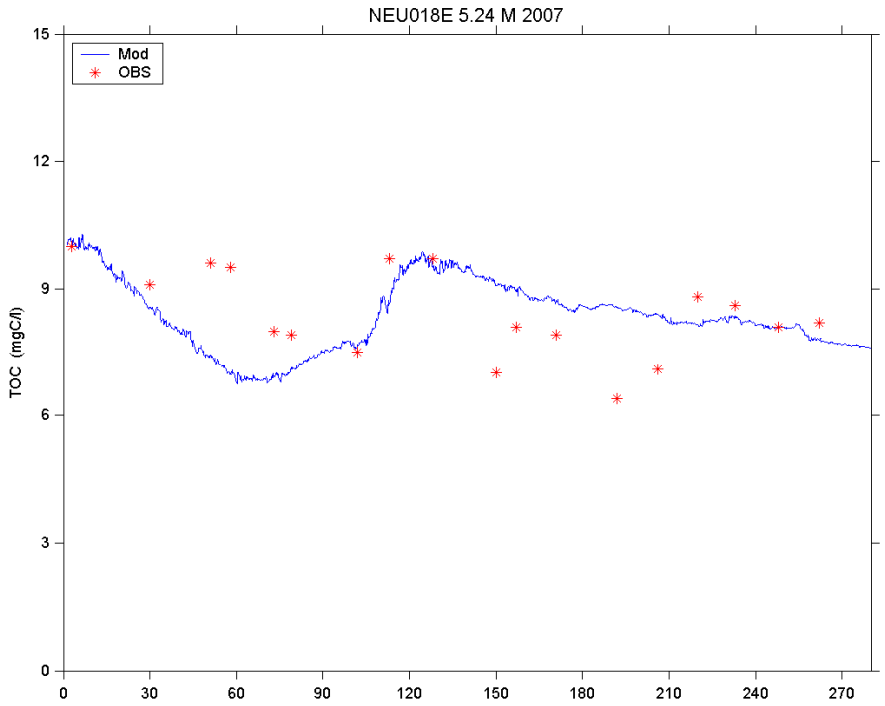

Fig. IV-16. Time series plot of modeled and observed TOC variation at NEU018E during 2007.

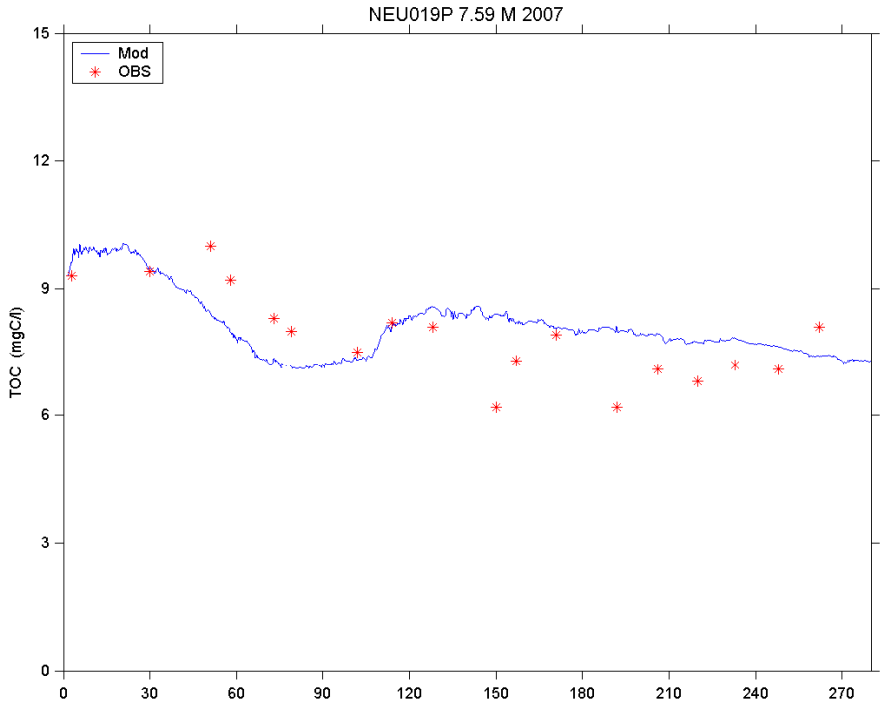

Fig. IV-17. Time series plot of modeled and observed TOC variation at NEU019P during 2007.

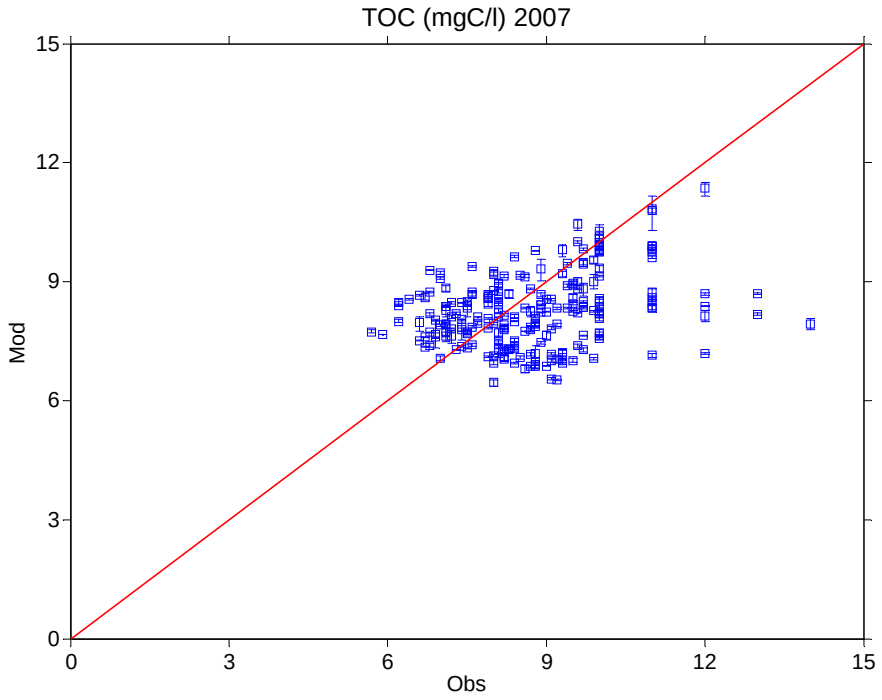

Fig. IV-18. Scatter plot of modeled and observed TOC variation at all stations during 2007.

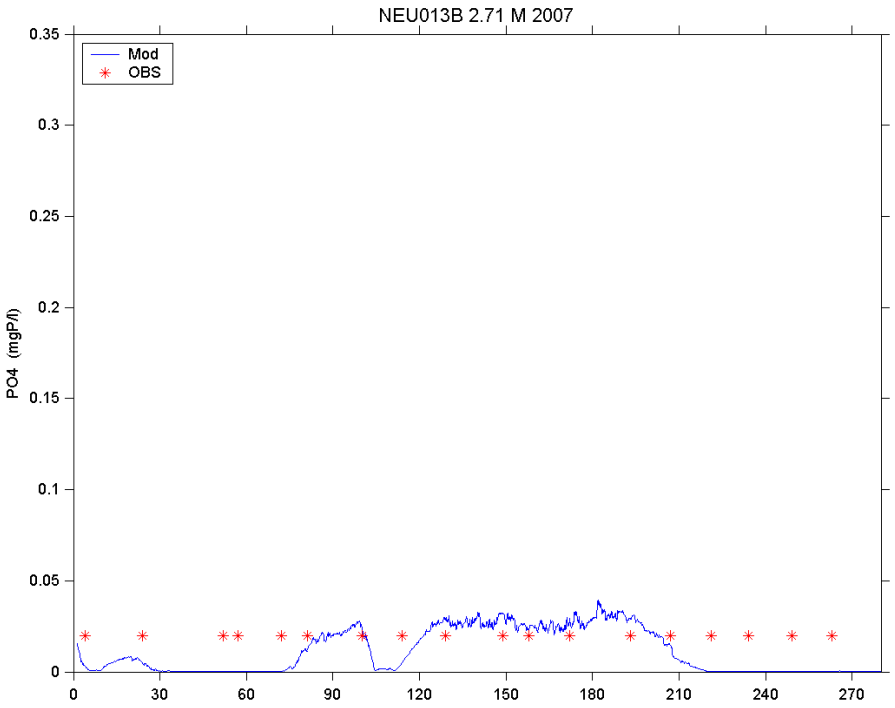

Fig. IV-19. Time series plot of modeled and observed PO_4 variation at NEU013B during 2007.

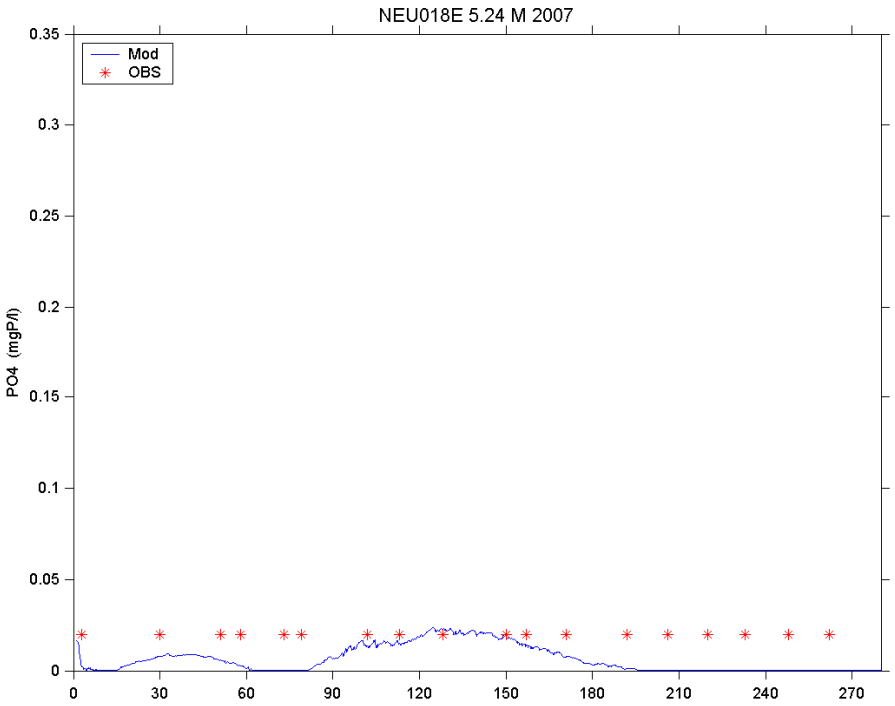

Fig. IV-20. Time series plot of modeled and observed PO_4 variation at NEU018E during 2007.

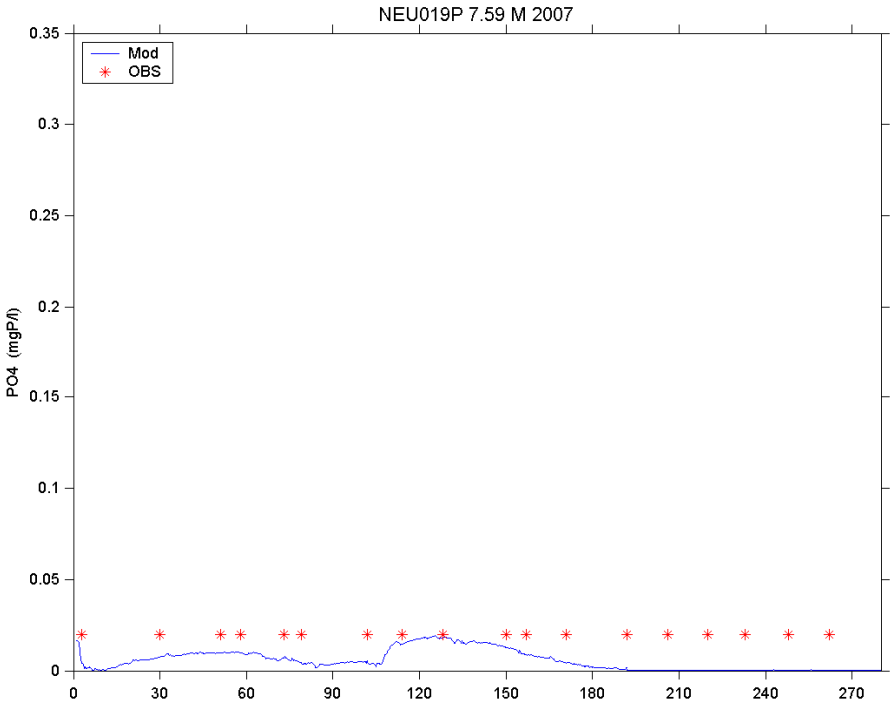

Fig. IV-21. Time series plot of modeled and observed PO_4 variation at NEU019P during 2007.

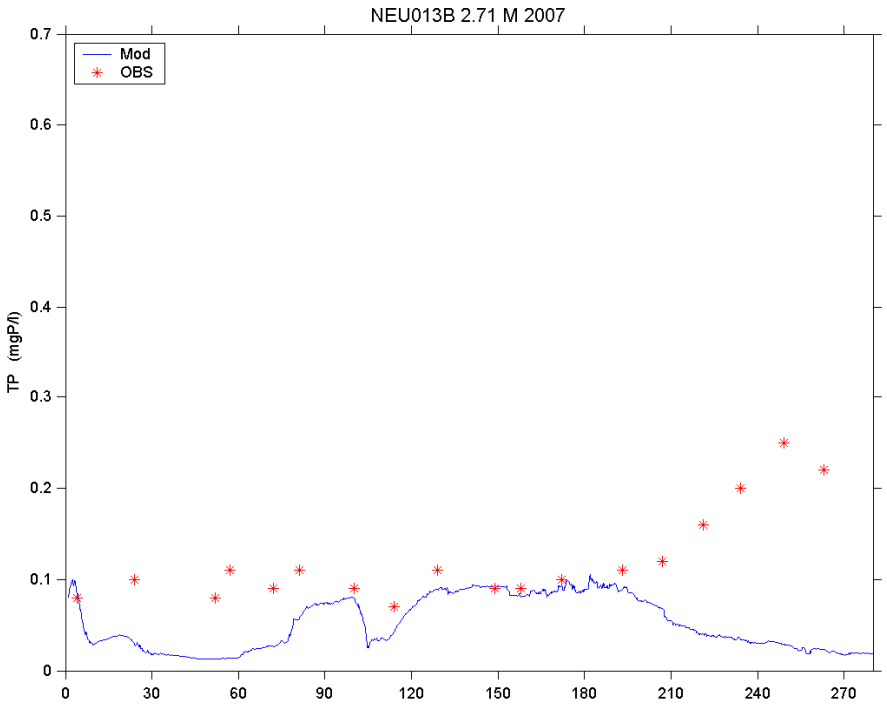

Fig. IV-22. Time series plot of modeled and observed TP variation at NEU013B during 2007.

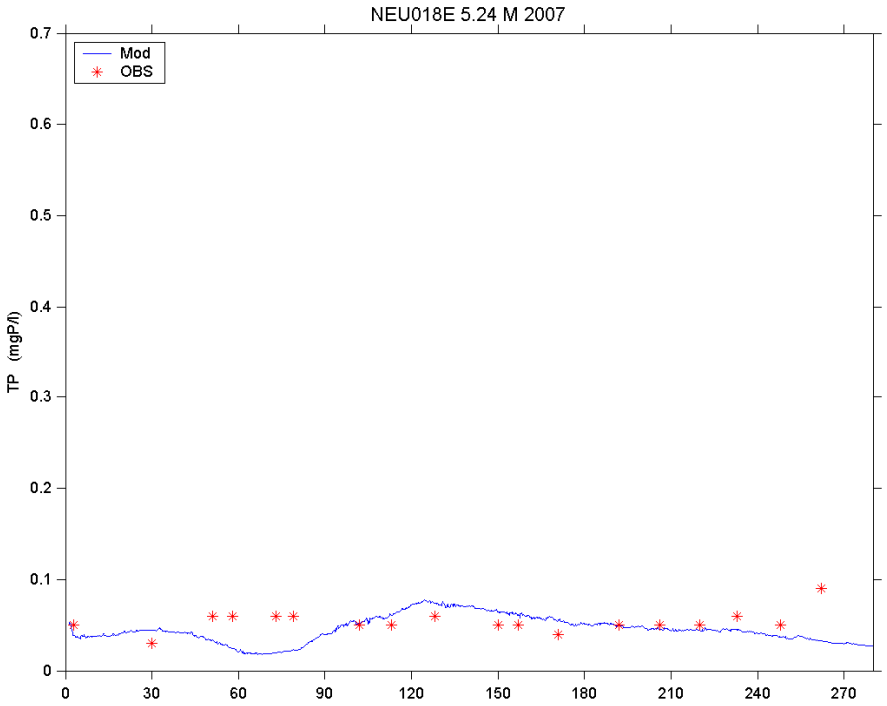

Fig. IV-23. Time series plot of modeled and observed TP variation at NEU018E during 2007.

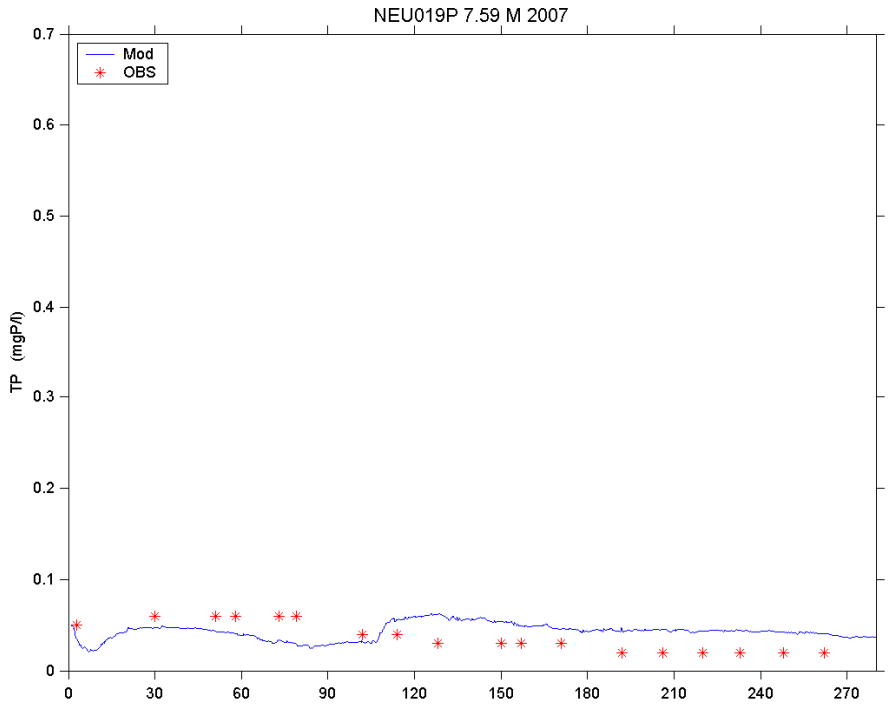

Fig. IV-24. Time series plot of modeled and observed TP variation at NEU019P during 2007.

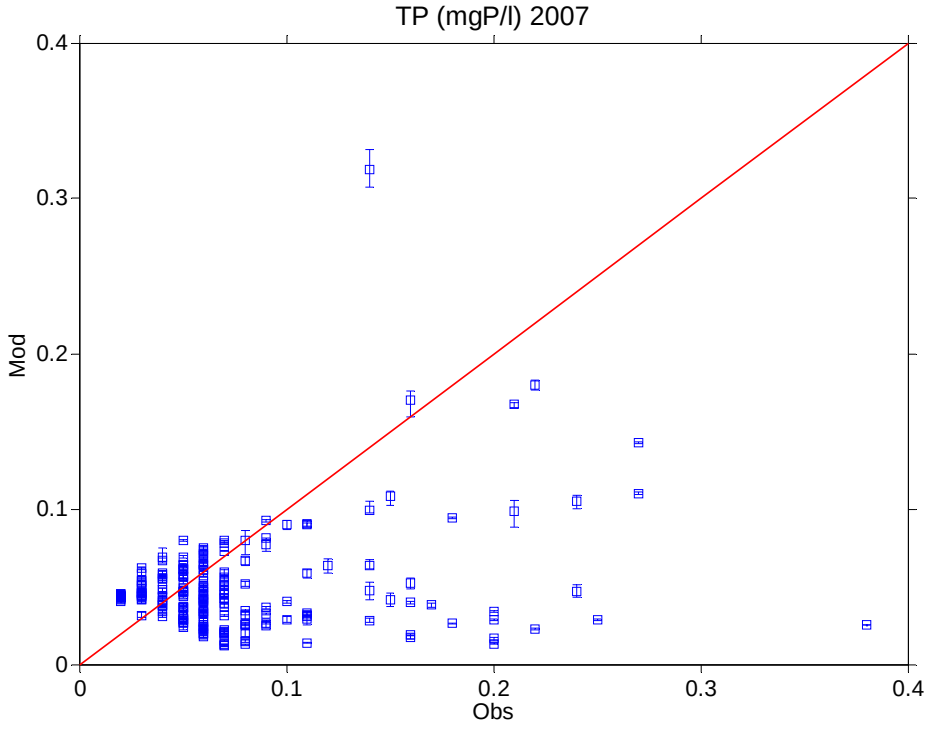

Fig. IV-25. Scatter plot of modeled and observed TP variation at all stations during 2007.

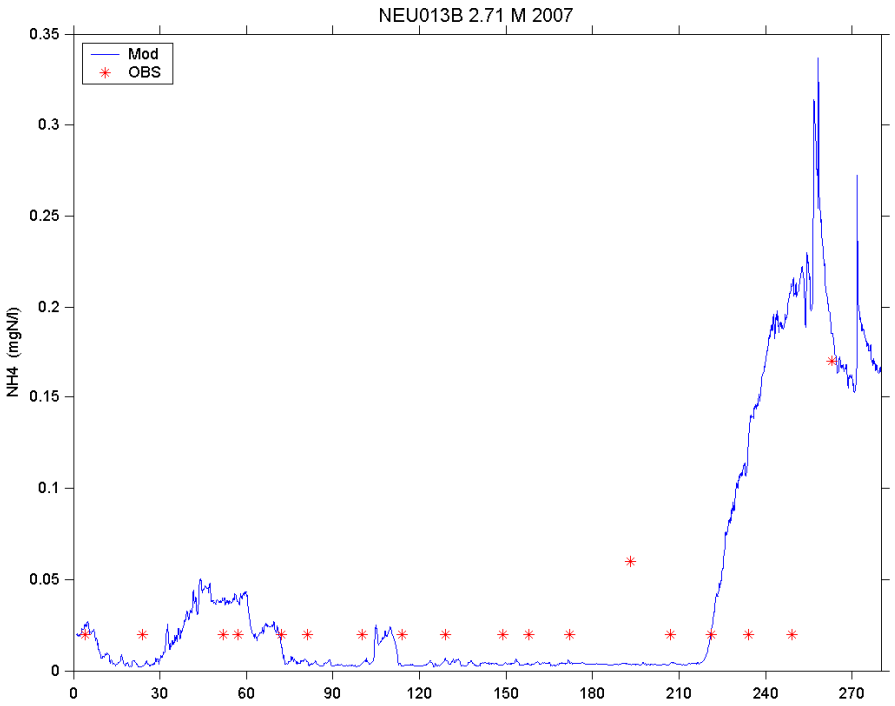

Fig. IV-26. Time series plot of modeled and observed NH_4 variation at NEU013B during 2007.

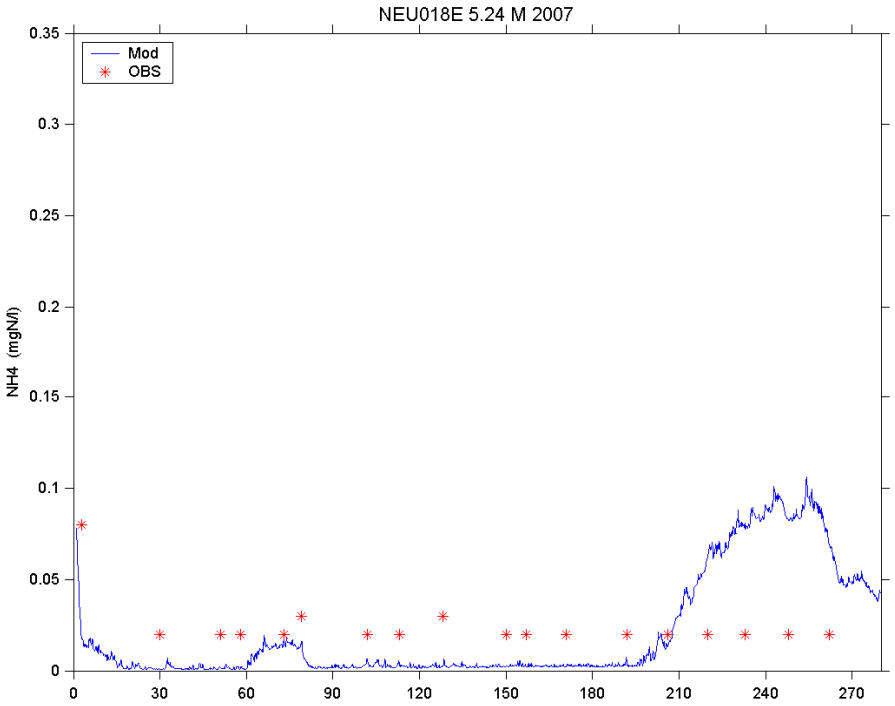

Fig. IV-27. Time series plot of modeled and observed NH_4 variation at NEU018E during 2007.

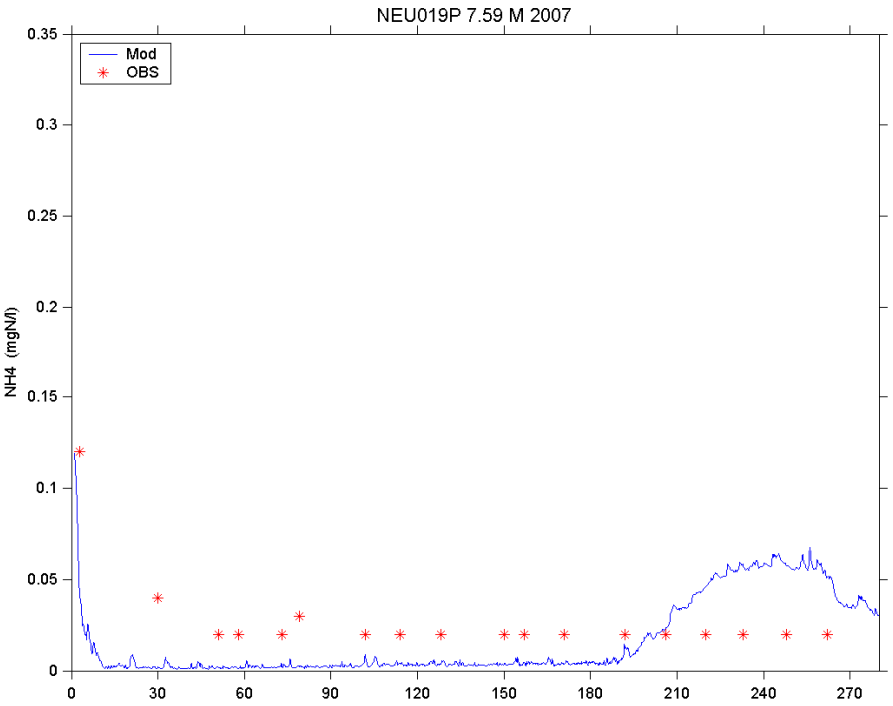

Fig. IV-28. Time series plot of modeled and observed NH_4 variation at NEU019P during 2007.

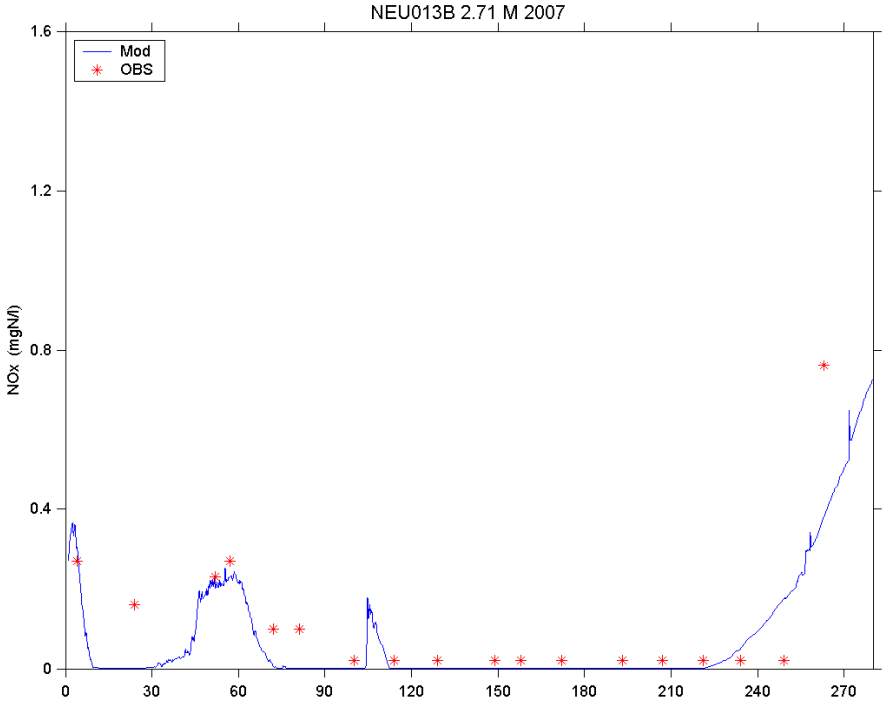

Fig. IV-29. Time series plot of modeled and observed NO_x variation at NEU013B during 2007.

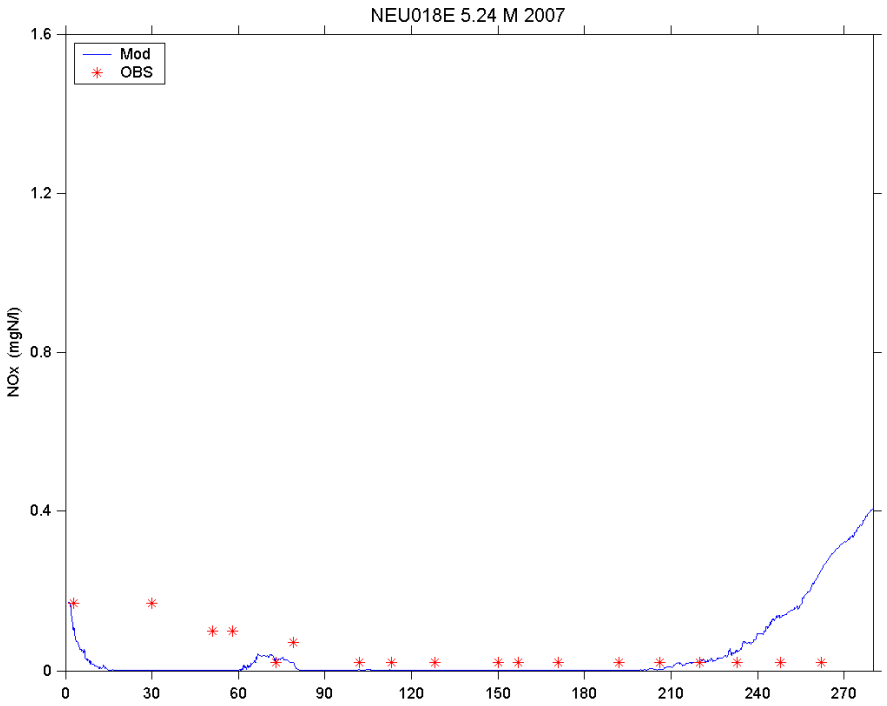

Fig. IV-30. Time series plot of modeled and observed NO_x variation at NEU018E during 2007.

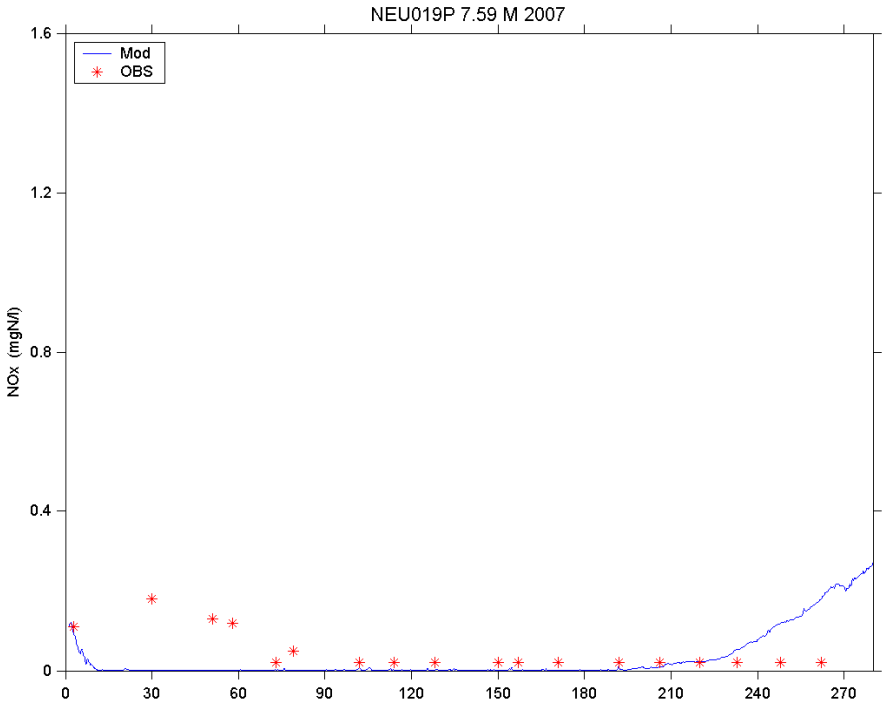

Fig. IV-31. Time series plot of modeled and observed NO_x variation at NEU019P during 2007.

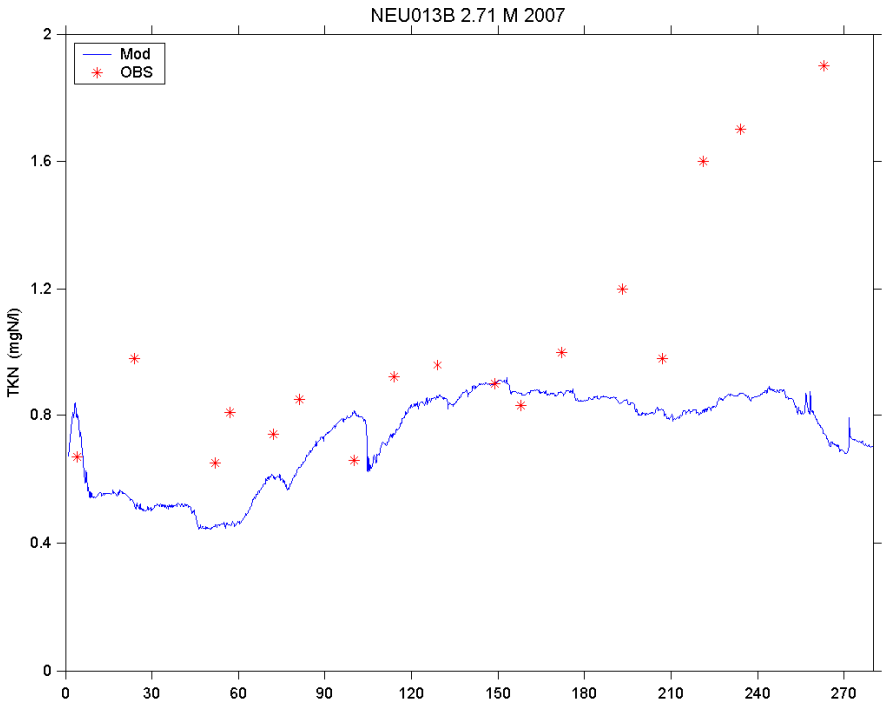

Fig. IV-32. Time series plot of modeled and observed TKN variation at NEU013B during 2007.

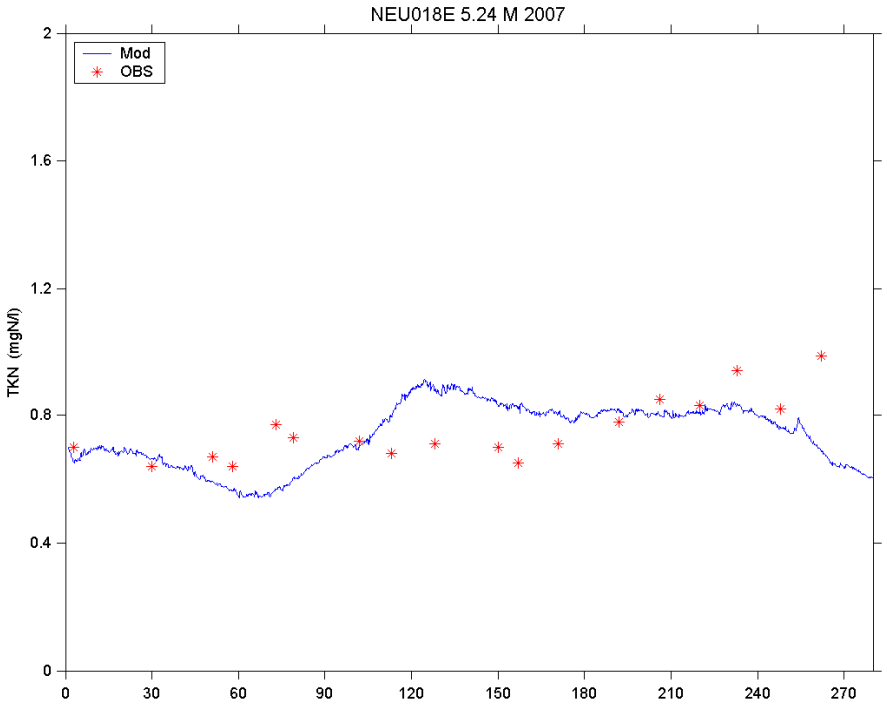

Fig. IV-33. Time series plot of modeled and observed TKN variation at NEU018E during 2007.

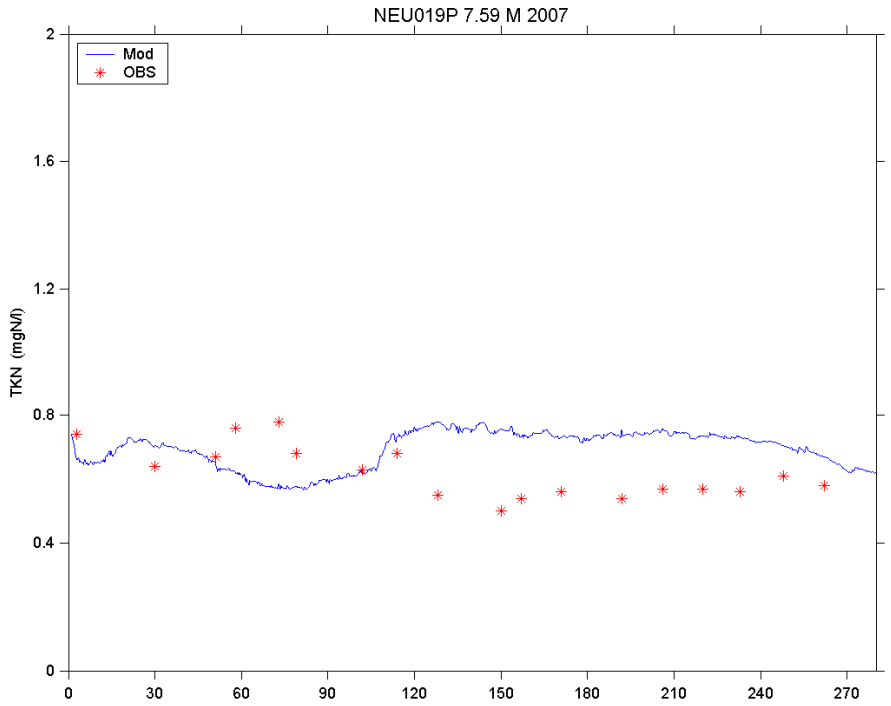

Fig. IV-34. Time series plot of modeled and observed TKN variation at NEU019P during 2007.

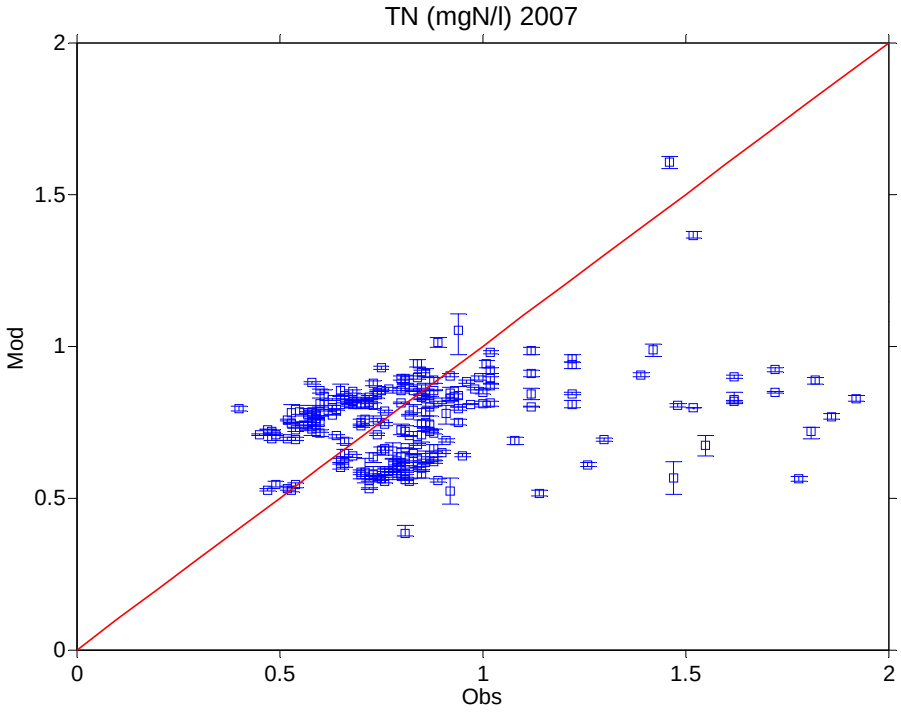

Fig. IV-35. Scatter plot of modeled and observed TN variation at all stations during 2007.

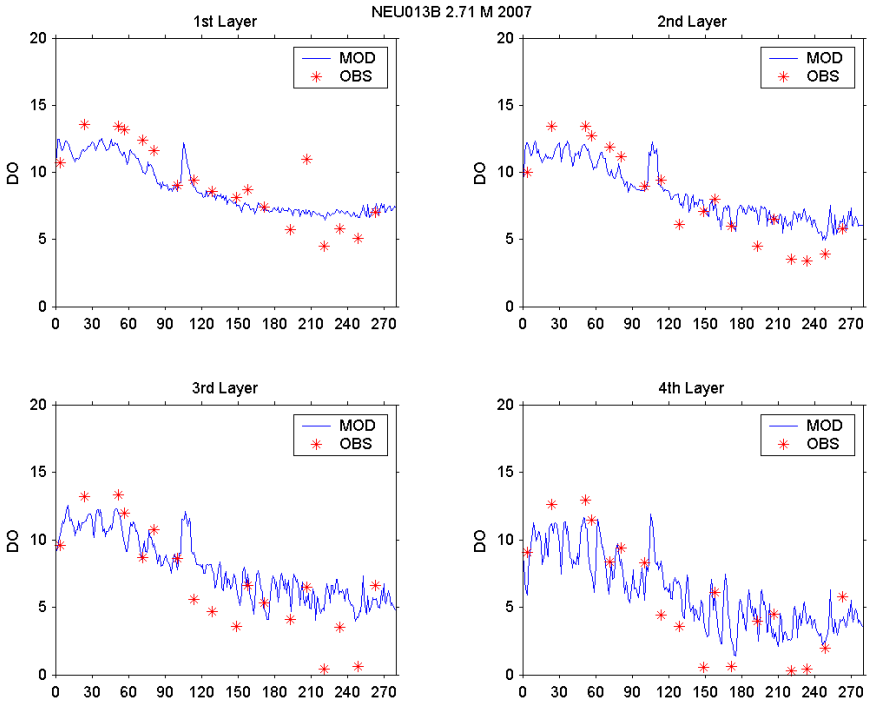

Fig. IV-36. Time series plot of modeled and observed DO variation at the 4 model layers at NEU013B during 2007.

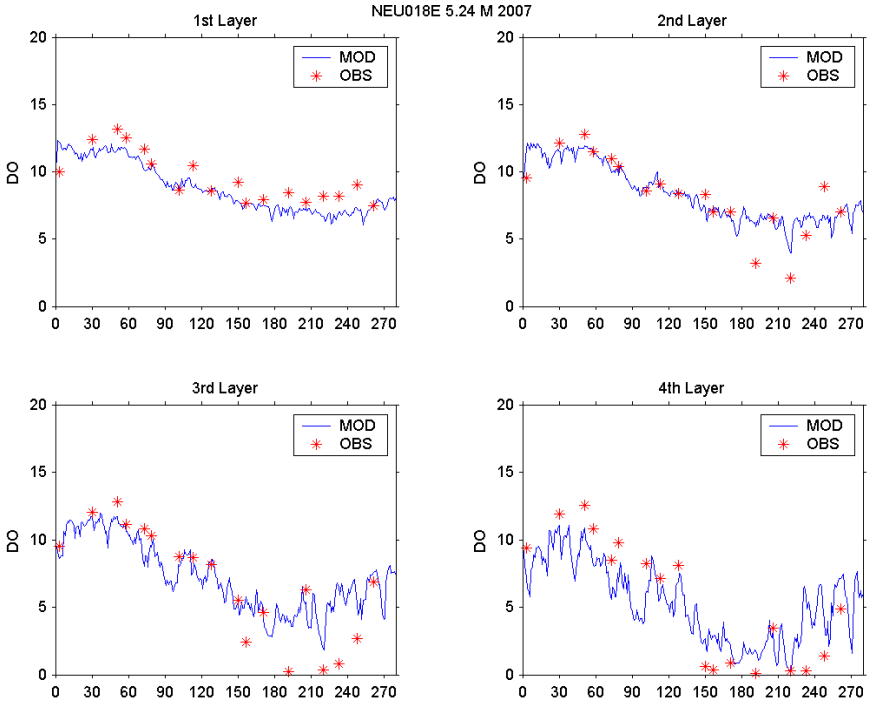

Fig. IV-37. Time series plot of modeled and observed DO variation at the 4 model layers at NEU018E during 2007.

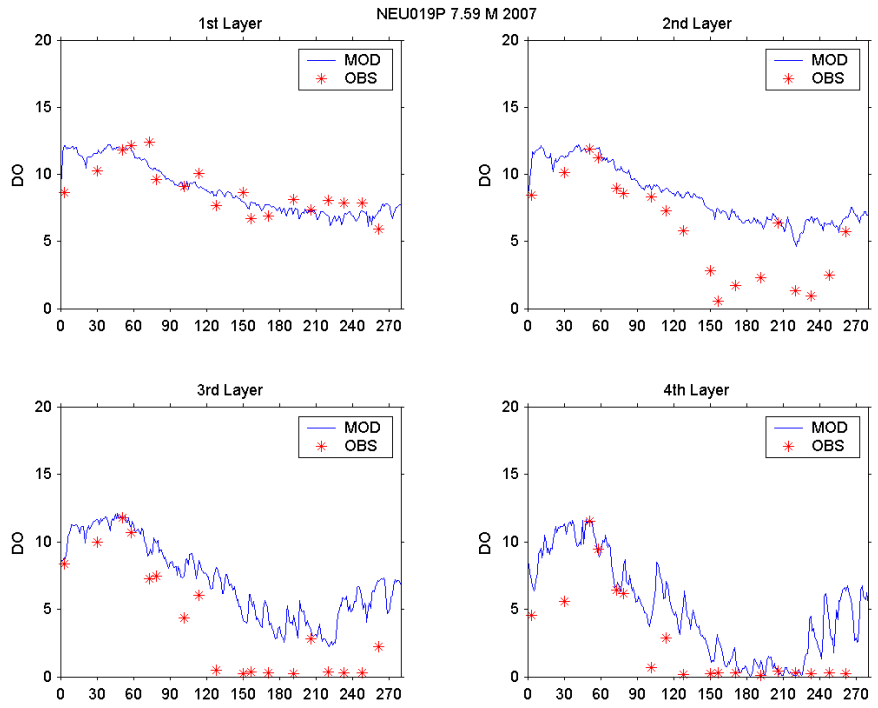

Fig. IV-38. Time series plot of modeled and observed DO variation at the 4 model layers at NEU019P during 2007.

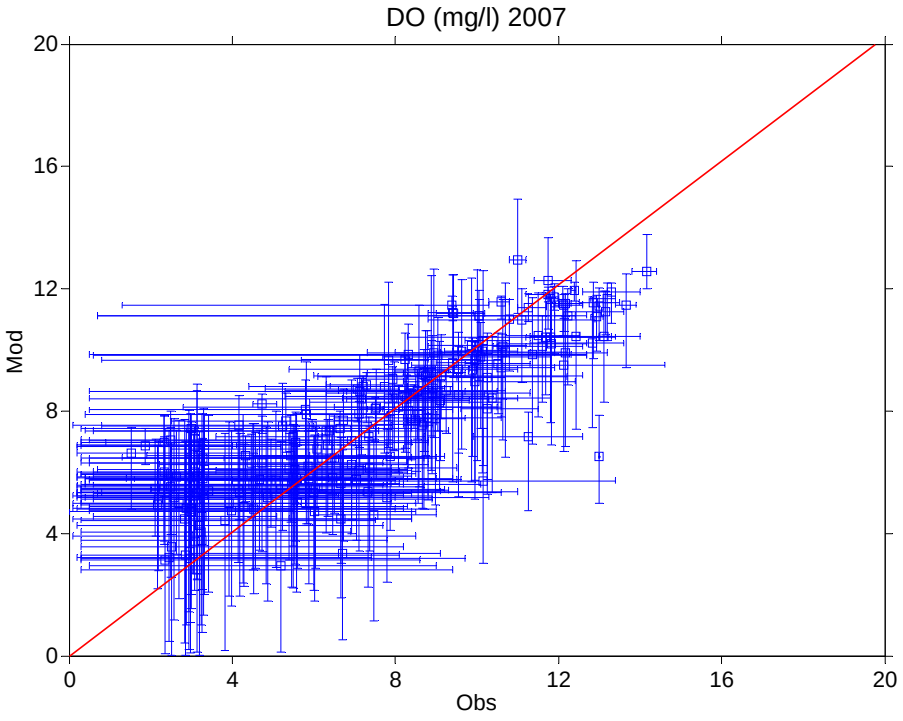

Fig. IV-39. Scatter plot of modeled and observed DO variation at all stations during 2007. Error bars indicate vertical variations.

V. Limitation Factors for Phytoplankton Growth

Multiple factors limit phytoplankton growth in lakes and estuaries. Phytoplankton growth (P) is represented in the model as the multiplication of maximum phytoplankton growth rate (PM, in day^{-1}), a nutrient limitation function ($f_1(N)$, $0 \leq f_1 \leq 1$), a light limitation function ($f_2(I)$, $0 \leq f_2 \leq 1$), and a temperature function ($f_3(T)$, $0 \leq f_3 \leq 1$):

$$P = PM \bullet f_1(N) \bullet f_2(I) \bullet f_3(T) \qquad \text{(V-1)}$$

a. Nutrient limitation

The effect of nutrient limitation on phytoplankton growth (silica is assumed to be abundant enough not to be a limiting factor for diatom growth in the model) is expressed in the model as:

$$f_1(N) = \min\left(\frac{NH_4 + NO_3}{KHN + NH_4 + NO_3}, \frac{PO_4d}{KHP + PO_4d}\right) = \min(f_{1N}, f_{1P}) \qquad \text{(V-2)}$$

where KHN is the half-saturation constant for nitrogen uptake, KHP is the half-saturation constant for phosphorus uptake, PO_4d is the dissolved portion of total phosphate, and f_{1N} and f_{1P} refer to the nitrogen and phosphorus limitation functions, respectively.

b. Light limitation

The effect of light on phytoplankton growth takes the form of a daily and vertically integrated version of Steele's equation (Steele, 1962):

$$f_2(I) = \frac{2.718 \bullet FD}{Kess \bullet \Delta z}(e^{-\alpha B} - e^{-\alpha T}) \qquad \text{(V-3)}$$

$$\alpha_B = \frac{I_0}{FD \bullet I_s} e^{-Kess(H_T + \Delta z)} \qquad \text{(V-4)}$$

$$\alpha_T = \frac{I_0}{FD \bullet I_s} e^{-Kess(H_T)} \qquad \text{(V-5)}$$

where FD is the fractional day length ($0 \leq FD \leq 1$), Kess (in m^{-1}) is the total light extinction coefficient, Δz is the model layer thickness, I_0 (in langleys day^{-1}) is the

daily total light intensity at water surface, I_s (in langleys day^{-1}) is the optimal light intensity for the simulated phytoplankton group, and H_T is depth from the free surface to the top of the model layer.

Light extinction in the water column was approximated with a four-component model including: light absorption by water itself, extinction due to suspended particles (Ke_{TSS}), and extinction due to light absorption by ambient chlorophyll:

$$Kess = Ke_b + Ke_{TSS} \bullet TSS + Ke_{Chl} \bullet Chl \qquad \text{(V-6)}$$

where Ke_b (in m^{-1}) is the background light extinction coefficient, Ke_{TSS} (in m^{-1} per g m^{-3}) is the light extinction coefficient for total suspended solids (TSS, in g m^{-3}), and Ke_{Chl} (in m^{-1} per mg Chl m^{-3}) is the light extinction coefficient for chl-*a* (Chl, in mg Chl m^{-3}).

c. Temperature Limitation

A Gaussian probability curve is used to represent the temperature dependency of phytoplankton growth (Park et al., 1995b; Cerco and Cole, 1994):

$$f_3(T) = \begin{cases} e^{-KTG1(T-TM1)^2} & T \le TM \\ e^{-KTG2(TM2-T)^2} & T > TM \end{cases} \qquad \text{(V-7)}$$

where T is the water temperature and TM1 (20ºC is used) and TM2 (26ºC is used) are the lower and upper bounds of optimal temperature for phytoplankton growth, respectively. KTG1 (0.005) and KTG2 (0.005) are constants relating to the effect of water temperature below TM1 and above TM2, respectively.

For the three algal species (blue-green algae, diatoms, and other) simulated in the model, parameters related with nutrient and light limitations were kept the same. Parameters related with temperature dependency (TM1 and TM2) were specified at different values for different algal species. Therefore, nutrient and light dependency functions (f_1(N) and f_2(I)) were the same for the three algal groups and the values of f_3(T) were different.

Figure V-1 shows the model-simulated limitation functions as "Nutrient" (minimum of f_{1N} and f_{1P}), "Light" ($f_2(I)$), and "Temperature" ($f_3(T)$ for "other algal species") at the monitoring stations in Falls Lake during 2006.

The model results suggest that nutrients severely limited phytoplankton growth, especially at the surface waters. This finding confirms that water-quality conditions in Falls Lake are nutrient sensitive. The effective nutrient limitation function was between 0-0.2 for most of the time throughout the surface waters of the entire Falls Lake. The lower the value the limitation function is, the more stringent the limitation. In the bottom waters, nutrient limitation was alleviated especially at the downstream portion of the lake, where stratification may have blocked the nutrient from being mixed into surface waters.

N and P limitations were alternately predicted (Fig. V-2). At the upper portion of Falls Lake during 2006, nitrogen limits phytoplankton growth the majority of the time. In contrast, at the lower portion of the lake, algal growth was limited by nitrogen and phosphorus at a similar frequency.

Light limitation ranged from 0.2 to 0.8 in the surface waters of the monitoring stations. The more severe light limitation at the upstream of Falls Lake probably is due to higher concentrations of TSS and chl-*a* there. In contrast, in the bottom waters, light limitation was more severe in the downstream part of the lake, where deeper channels exist.

Temperature dependency of phytoplankton growth rate follows a seasonal pattern, where growth rate was inhibited when water temperature is very low or very high. The model results suggest that the growth of blue-green algae (not shown) is more sensitive to water temperature (lower values were simulated for temperature limitation function). In contrast, diatoms appeared to be least sensitive to water temperature.

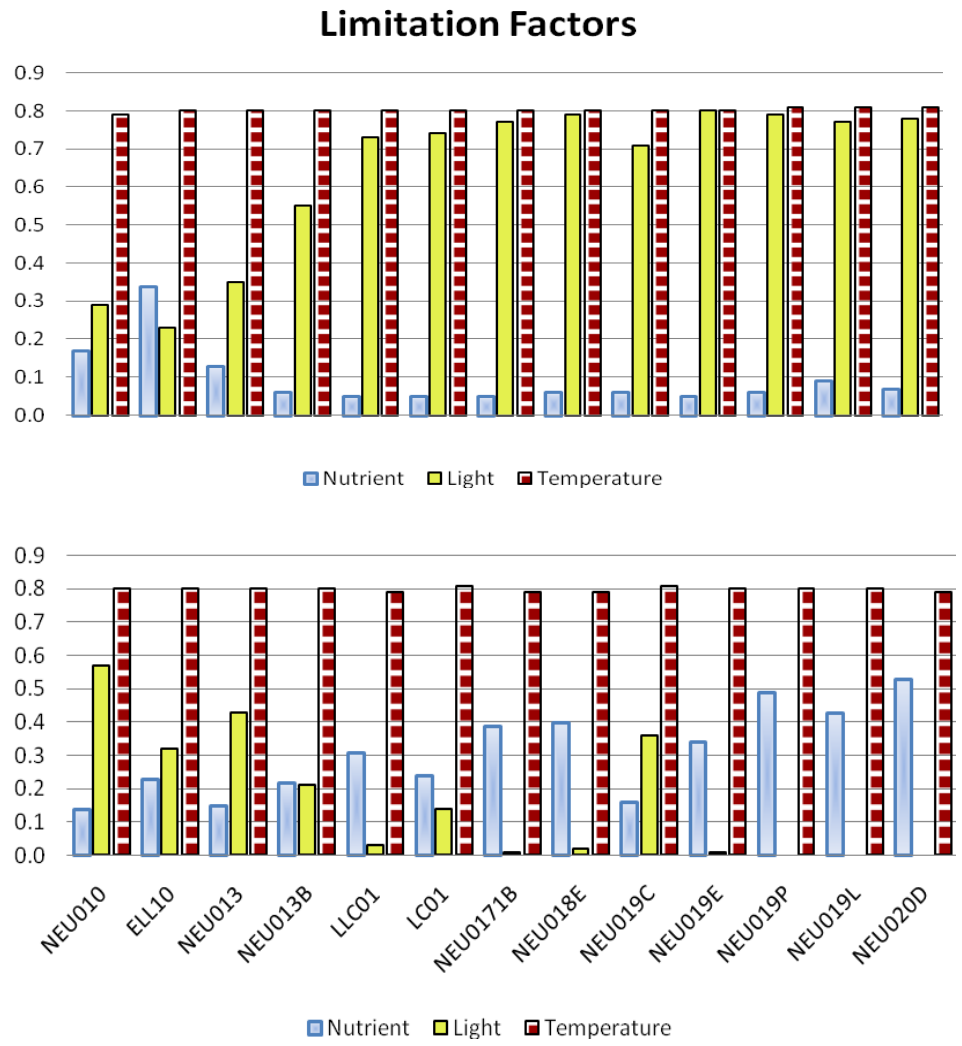

Fig. V-1. Model-simulated limitation functions at the surface (upper panel) and bottom (lower panel) layers of the monitoring stations in Falls Lake during 2006. The temperature limitation function shown here is for the 3rd algae group ("other algae," i.e., algae species besides blue-green algae and diatoms).

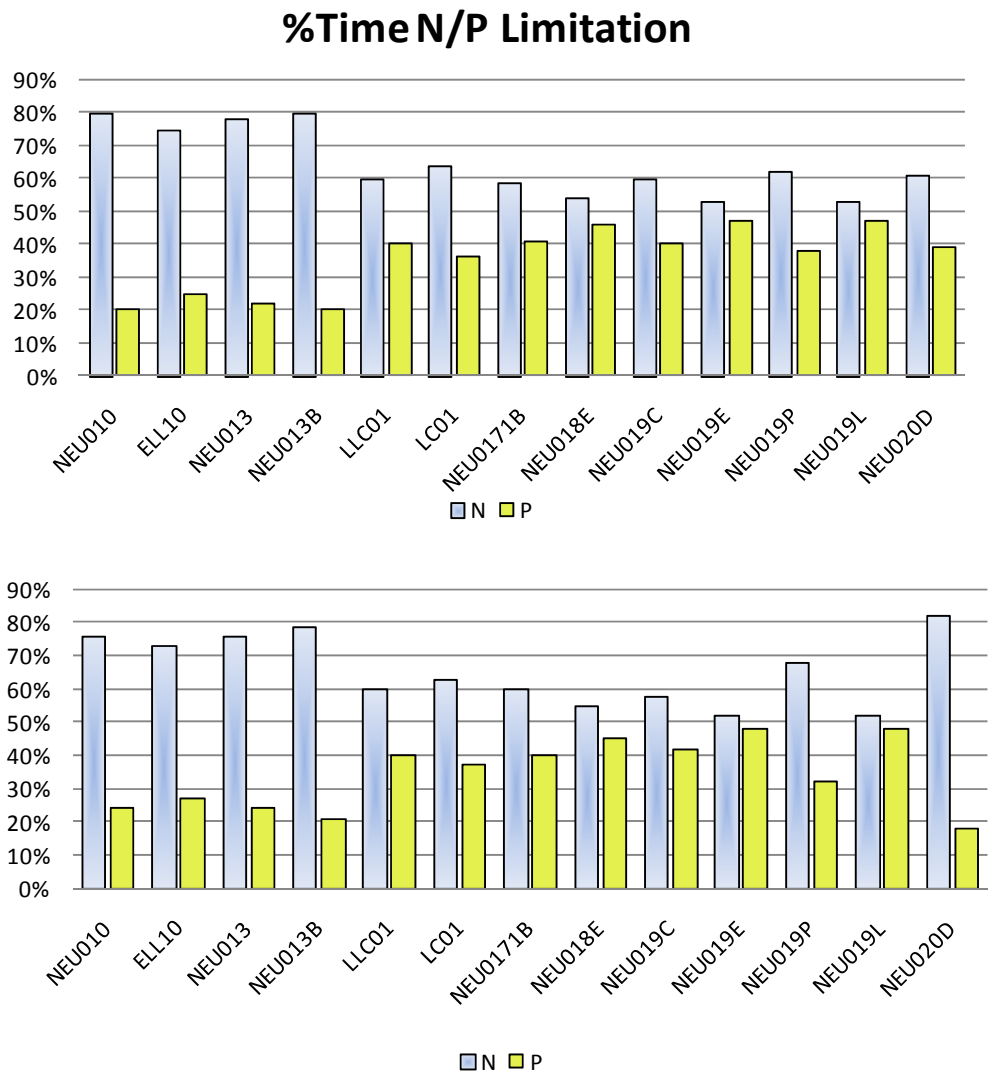

Fig. V-2. Model-simulated percent of time phytoplankton is N or P limited at the surface (upper panel) and bottom (lower panel) layers of the monitoring stations in Falls Lake during 2006.

VI. Nutrient Reduction Scenario

In order to examine the response of chlorophyll-*a* exceedance rate to various levels of nutrient input in Falls Lake, scenario model runs were made under the following conditions:

1. Nutrient reduction was applied to the five upper major tributaries: the Eno River, Little River, Flat River, Ellerbe Creek, and Knap of Reeds Creek.

   As shown by Fig. VI-1, the chlorophyll-*a* standard exceedance rates based on observations of 2005-2007 were highest at the upper part of the Falls Lake. In the middle part of the lake, the exceedance rate became much lower and at the lower part of the lake near the dam area, the exceedance rates were generally below 10%. Model results also suggest that high chlorophyll-*a* concentrations in the middle part of the lake were often found after high chlorophyll-*a* concentrations occur at the upper part of the lake. In addition, typically greater than 60% of the river discharge and greater than 70% of nutrient loading are from the five upper major tributaries to the lake.
2. 2006 model year was selected as the baseline year.

   In order to save computational time and as constrained by available field data for model calibration, the Falls Lake model was set up to run year by year. As discussed in section II-2e, 2006 was recognized as the most close-to-normal year, and hence more representative year, as compared to 2005 and 2007, according to rainfall and lake level observations.

   In addition, 2006 is also the year that more data is available, including discharge data provided by the newly added USGS gage station at both Ellerbe Creek and Knap of Reeds, chl-*a* data available for the entire year, and benthic nutrient flux data collected in April 2006. These extra data enable a better model representation of 2006 lake dynamics.
3. The model cell containing NEU013B was selected as the baseline area for the calculation of chlorophyll-*a* standard exceedance rate. Model-simulated

chlorophyll-*a* concentrations at the surface and subsurface layer were averaged to be consistent with composite field samples collected from water columns above twice the secchi disk depth.

NEU013B is located in the upper region of the lake where high chlorophyll-*a* concentrations were observed. Upstream and to the left of NEU013B, slightly higher chlorophyll-*a* standard exceedance rate was predicted by the model, and downstream and to the right side of NEU013B, a slightly lower chlorophyll-*a* standard exceedance rate was predicted by the model. Therefore, the model cell where NEU013B is within is also a good representation of its adjacent areas.

NEU013B is located just downstream of the conjunction of the five upper major tributaries. Chlorophyll-*a* concentrations at NEU013B are influenced by nutrient input from all of the five upper major tributaries.

In addition, the model predicted exceedance rate very well for chlorophyll-*a* concentrations at NEU013B (Fig. VI-2).

4. Nitrogen (N) reductions refer to reductions of total nitrogen (both organic and inorganic forms) and phosphorus (P) reductions refer to reductions of total phosphorus (both organic and inorganic forms).

Scenario model runs were made for a combination of a series of N and P reductions at 25%, 50%, 75%, and 100% of their original loadings. The model-predicted chlorophyll-*a* standard exceedance rates at NEU013B in response to different combinations of N and P reductions from the fiver upper major tributaries are summarized in Fig. VI-3. The 10% chlorophyll standard exceedance line is highlighted with a thick blue curve.

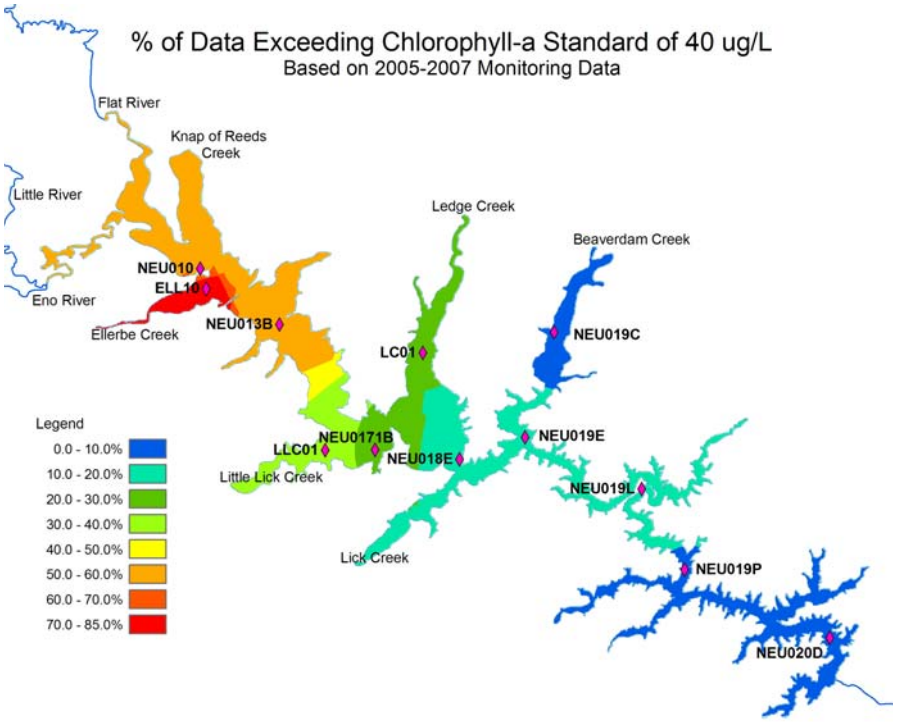

Fig. VI-1. Lake distributions of chlorophyll-*a* standard exceedance rates interpolated from 2005-2007 observations at the monitoring stations (indicated by red dots).

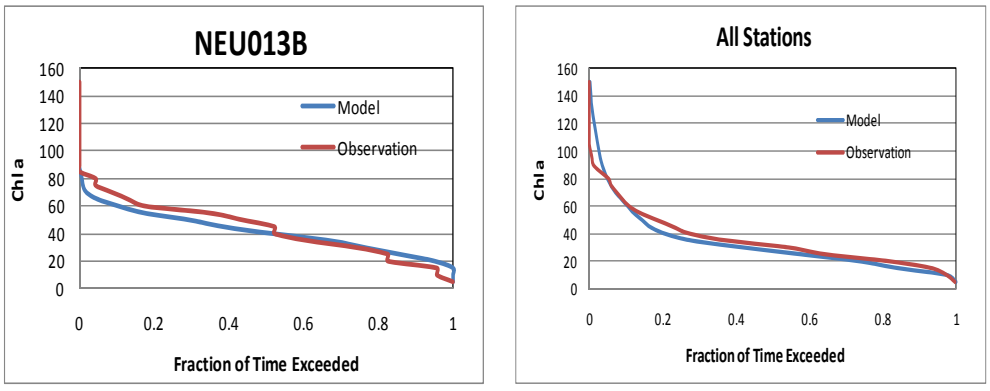

Fig. VI-2. The model-predicted and observed chlorophyll-*a* exceedance rates as a function of chlorophyll-*a* concentrations at NEU013B (left panel) and averaged at all monitoring stations (right panel).

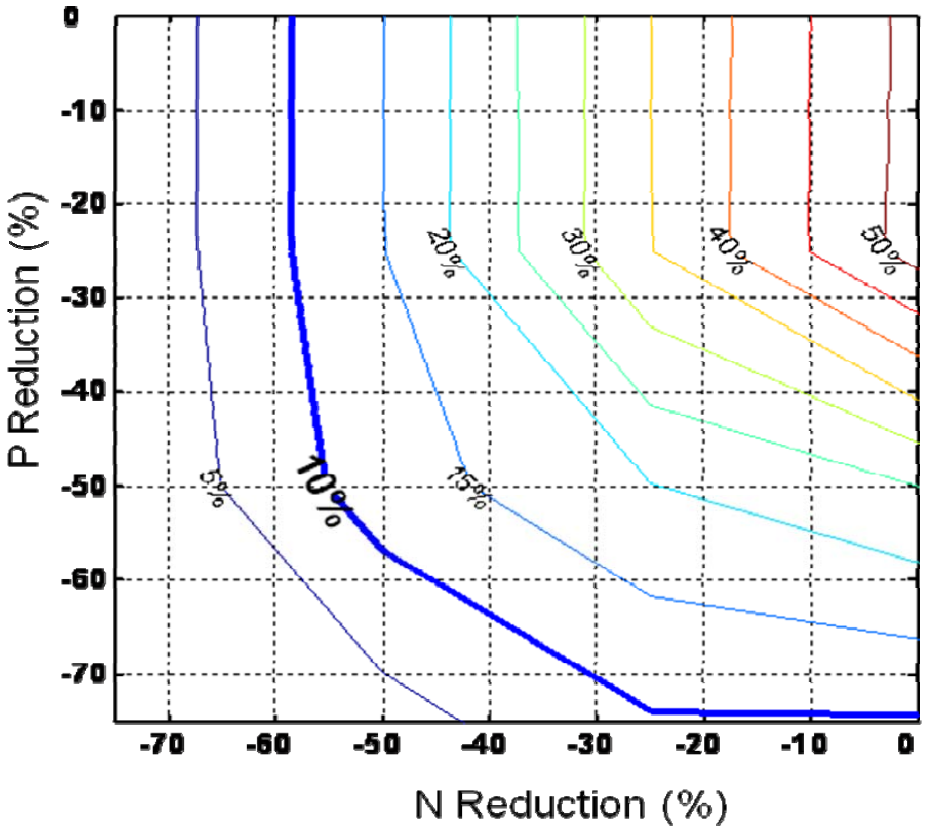

Fig. VI-3. The model-simulated P&N reduction curve.

VII. References

Cerco, C.F. and T.M. Cole (1993), Three-dimensional eutrophication model of Chesapeake Bay, Journal of Environmental Engineering, 119: 1006-25.

Cerco C.F. and T.M. Cole (1994), Three-dimensional eutrophication model of Chesapeake Bay: Volume 1, main report. Technical report EL-94-4, US Army Engineer Waterways Experiment Station, Vicksburg, MS.

Cerco, C.F. (1995), Simulation of long-term trends in Chesapeake Bay eutrophication. Journal of Environmental Engineering, 121 (4): 298-310.

Galperin, B., L.H. Kantha, S. Hassid, and A. Rosati (1988), A quasi-equilibrium turbulent energy model for geophysical flows. Journal of the Atmospheric Sciences 45: 55-62.

Hamrick, J.M. (1992), A three-dimensional environmental fluid dynamics computer code: theoretical and computational aspects. Special Report on Marine Science and Ocean Engineering No. 317, Virginia Institute of Marine Science/School of Marine Science, The College of William and Mary, Virginia.

Hamrick, J.M. (1996), User's manual for the environmental fluid dynamics computer code. Special Report in Applied Marine Science and Ocean Engineering No. 331, Virginia Institute of Marine Science/School of Marine Science, The College of William and Mary, Virginia.

Ji, Z.-G., M.R. Morton, and J.M. Hamrick (2001), Wetting and drying simulation of estuarine processes. Estuarine, Coastal and Shelf Science 53: 683-700.

Ji, ZhenGang, (2008), Hydrodynamics and Water Quality: Modeling Rivers, Lakes, and Estuaries, John Wiley & Sons Inc., Hoboken, New Jersey. 676pp.

Kim, S.-C., D.L. Wright, J.P.-Y. Maa, and J. Shen (1998), Morphodynamic responses to extratropical meteorological forcing on the inner shelf of the middle Atlantic Bight: wind wave, currents, and suspended sediment transport. In M.L. Spaulding (Eds.) Estuarine and Coastal Modeling VI, New York, pp. 238-249.

Kuo, A.Y., J. Shen, and J.M. Hamrick (1996), The effect of acceleration on bottom shear stress in tidal estuaries. ASCE Journal of Waterways, Ports, Costal and Ocean Engineering 122: 75-83.

Lung, W.-S. and H.W. Paerl (1988), Modeling blue-green algal blooms in the lower Neuse River. Water Research, 22 (7): 895-905.

Lin, J. and A.Y. Kuo (2003), A Model Study of Turbidity Maxima in the York River Estuary, Virginia, Estuaries 26(5): 1269-1280.

Lin, J., L. Xie, L.J. Pietrafesa, J.S. Ramus, H.W. Paerl, (2007), Water-Quality gradients across Albemarle-Pamlico Estuarine System: Seasonal Variations and Model Applications, Journal of Coastal Research 23(1): 213-229.

Lin J., L. Xie., L.J. Pietrafesa, H. Xu, W. Woods, M.A. Mallin, M.J. Durako, (2008), Water quality responses to simulated flow and nutrient reductions in the Cape Fear River Estuary and adjacent coastal region, North Carolina, Ecological Modeling 212: 200-217

Mallin, M.A., L.B. Cahoon, M.R. McIver, D.C. Parsons, and G.C. Shank (1999), Alteration of factors limiting phytoplankton production in the Cape Fear River Estuary, Estuaries 22(4): 825-836.

Mellor, G.L., and T. Yamada (1982), Development of a turbulence closure model for geophysical fluid problems. Reviews of Geophysics and Space Physics 20: 851-875.

Nakagawa, Y.; Sanford, L.P., and Halka, J.P., (2000), Effect of wind waves on distribution of muddy bottom sediments in Baltimore Harbor, USA. *Proceedings of the 27th International Conference on Coastal Engineering,* (Sydney, Australia), pp. 3516–3524.

NCDOT Highway Stormwater Program, (2008), Summary of atmospheric deposition data available for modeling nutrients in the Falls Lake, North Carolina, watershed, Draft Report, May 5, 2008.

ODEQ (Oklahoma Department of Environmental Quality), (2006), TMDL Development For Cobb Creek Watershed And Fort Cobb Lake, Final Report.

Park, K., A.Y. Kuo, and A.J. Butt (1995a), Application of a tidal prism water quality model to the Lynnhaven River, Virginia. A report to the Virginia Coastal Resources Management Program, Virginia Department of Environmental Quality, Special Report No. 329 in Applied Marine Science and Ocean Engineering, Virginia Institute of Marine Science/School of Marine Science, The College of William and Mary, Virginia.

Park, K., A.Y. Kuo, J. Shen, and J.M. Hamrick (1995b), A three-dimensional hydrodynamic-eutrophication model (HEM-3D): Description of water quality and sediment process submodels. Special Report in Applied Marine Science and Ocean Engineering No. 327, Virginia Institute of Marine Science/School of Marine Science, The College of William and Mary, Virginia.

Park, K., J. Shen, and A.Y. Kuo (1998), Application of a multi-step computation scheme to an intratidal estuarine water quality model. Ecological Modeling 110: 281-292.

Park, K., H.-S. Jung, H.-S. Kim, S.-M. Ahn, (2005), Three-dimensional hydrodynamic-eutrophication model (HEM-3D): application to Kwang-Yang Bay, Korea. Marine Environmental Research 60: 171-193.

Sanford, L.P.; Chao, S-Y.; Baker, J.E.; Chang, M.-L., and Nakagawa, Y., 1999. Development of a contaminant transport model for Baltimore Harbor. Baltimore, Maryland: *Draft Final Project Report* submitted to Maryland Department of the Environment, Technical and Regulatory Services Administration.

Shen, J., J.D. Boon, and A.Y. Kuo (1999), A modeling study of a tidal intrusion front and its impact on larval dispersion in the James River estuary, Virginia. Estuaries 22: 681-692.

Shen, J. and L. Haas (2004), Calculating age and residence time in the tidal York River using three-dimensional model experiments. Estuarine, Coastal and Shelf Science 61(3): 449-461.

Shore Protection Manual, 1984. Coastal Engineering Research Center. Vicksburg, Mississippi: Department of the Army, Waterways Experiment Station, Corps of Engineers.

Steele, J.H. (1962). Environmental control of photosynthesis in the sea. Limnology and Oceanography, 7(2): 137-150.

Tetra Tech (2007), The Environmental Fluid Dynamics Code Theory and Computation Volume 3: Water Quality Module, Fairfax VA.

US Environmental Protection Agency (US EPA), 1997. Compendium of tools for watershed assessment and TMDL development. EPA841-B-97-006, Office of Water, Washington, DC.

Xu, H.Z., J. Lin, and D.X. Wang (2008) Numerical study on salinity stratification in the Pamlico River Estuary, Estuarine, Coastal, and Shelf Science 80: 74-84.

Appendix A. Model Bathymetry Representation

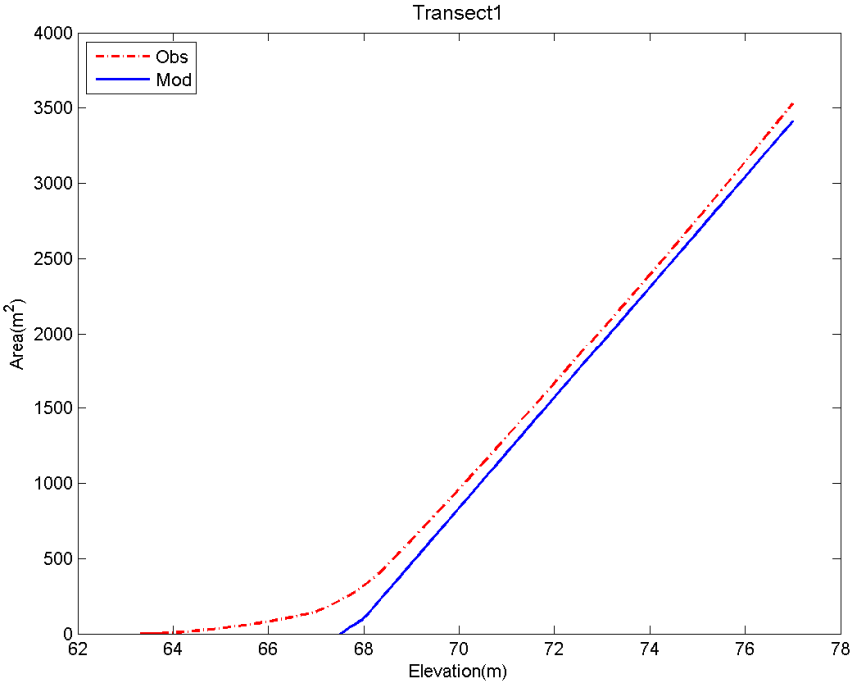

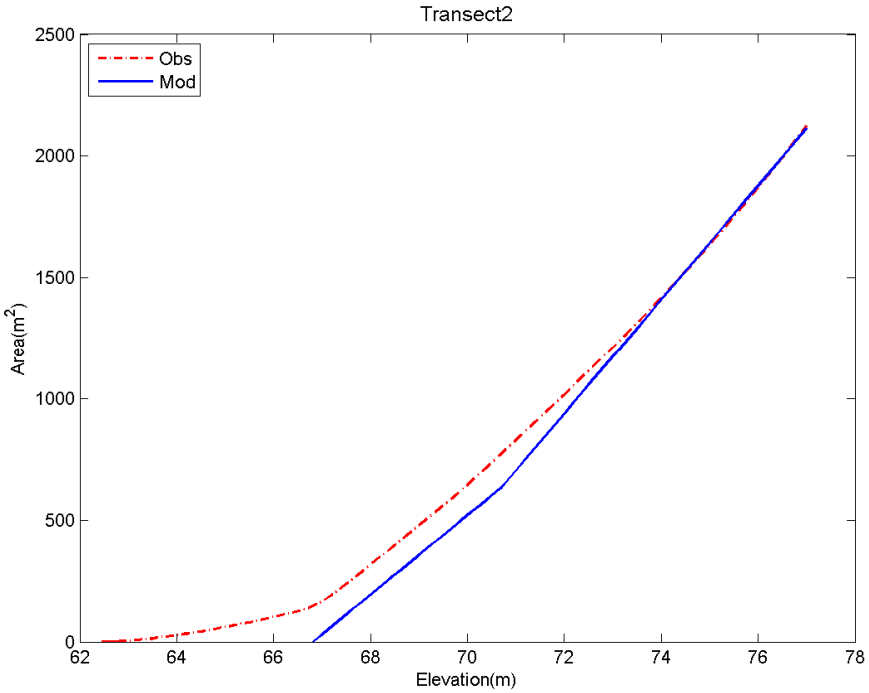

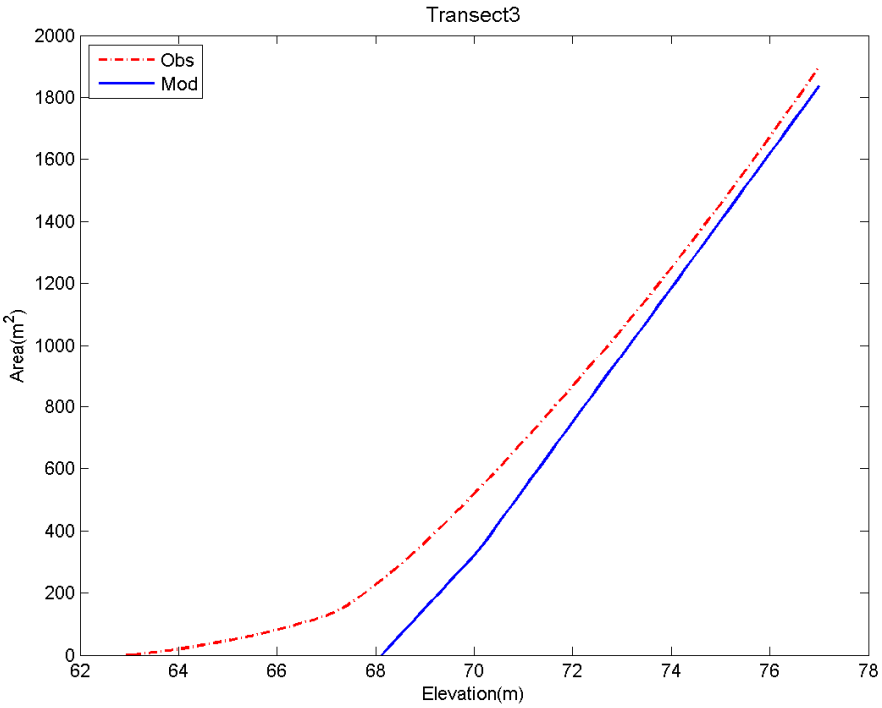
Transect3
Obs
Mod
Area(m2)
Elevation(m)
0
200
400
600
800
1000
1200
1400
1600
1800
2000
62
64
66
68
70
72
74
76
78

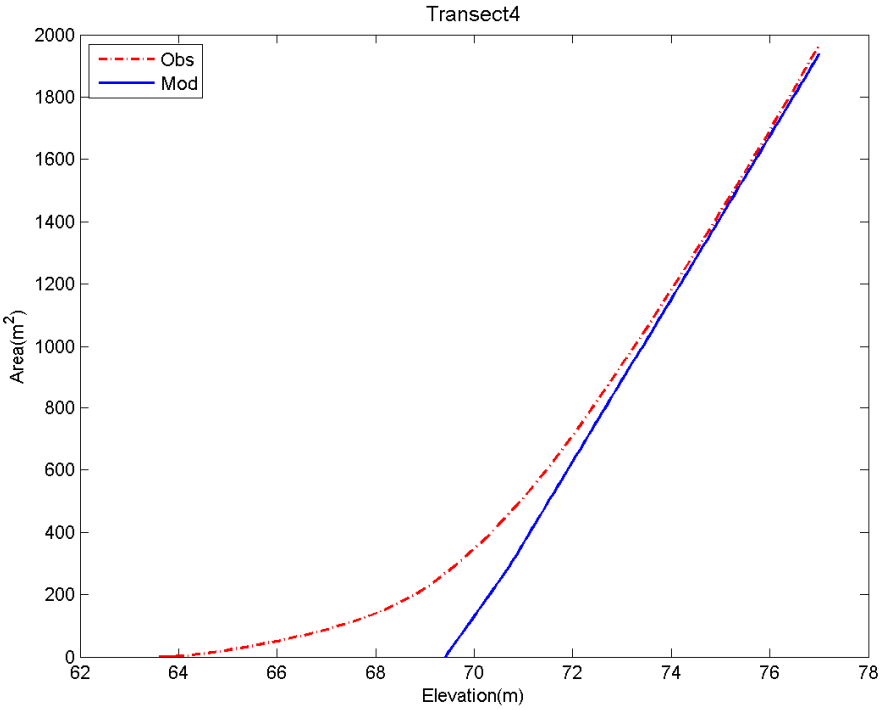
Transect4
Obs
Mod
Area(m2)
Elevation(m)
0
200
400
600
800
1000
1200
1400
1600
1800
2000
62
64
66
68
70
72
74
76
78

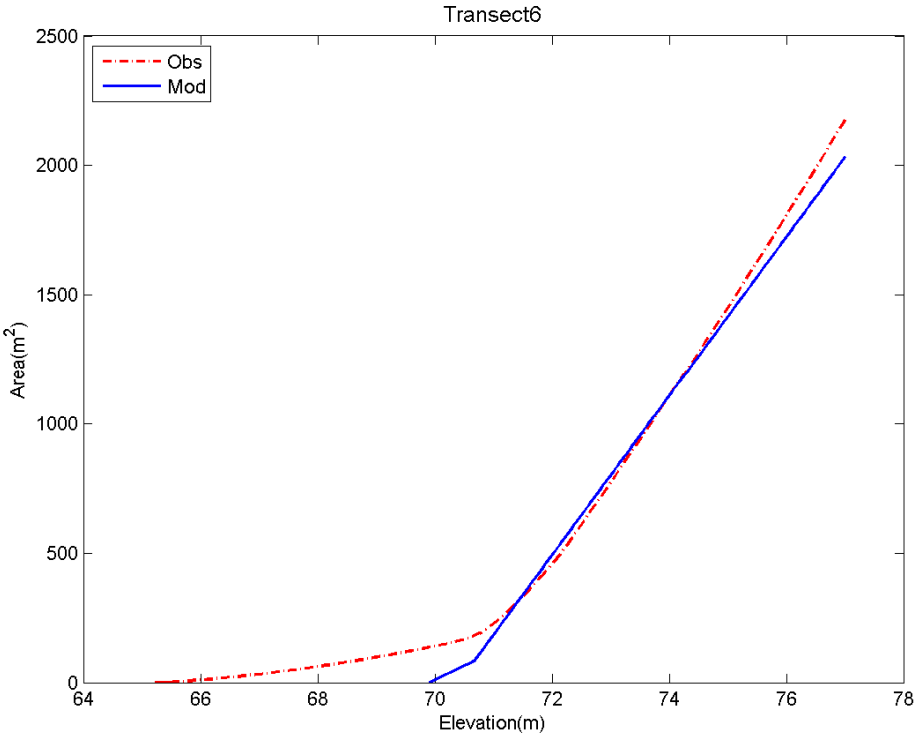
Transect6
Obs
Mod
Area(m2)
Elevation(m)
0
500
1000
1500
2000
2500
64
66
68
70
72
74
76
78

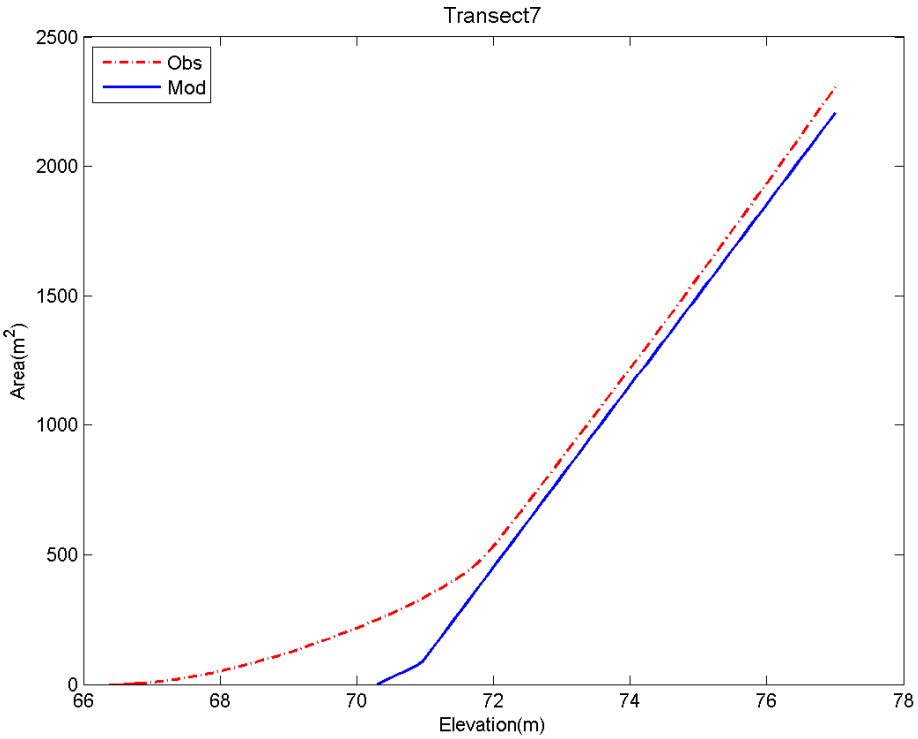
Transect7
Obs
Mod
Area(m2)
Elevation(m)
0
500
1000
1500
2000
2500
66
68
70
72
74
76
78

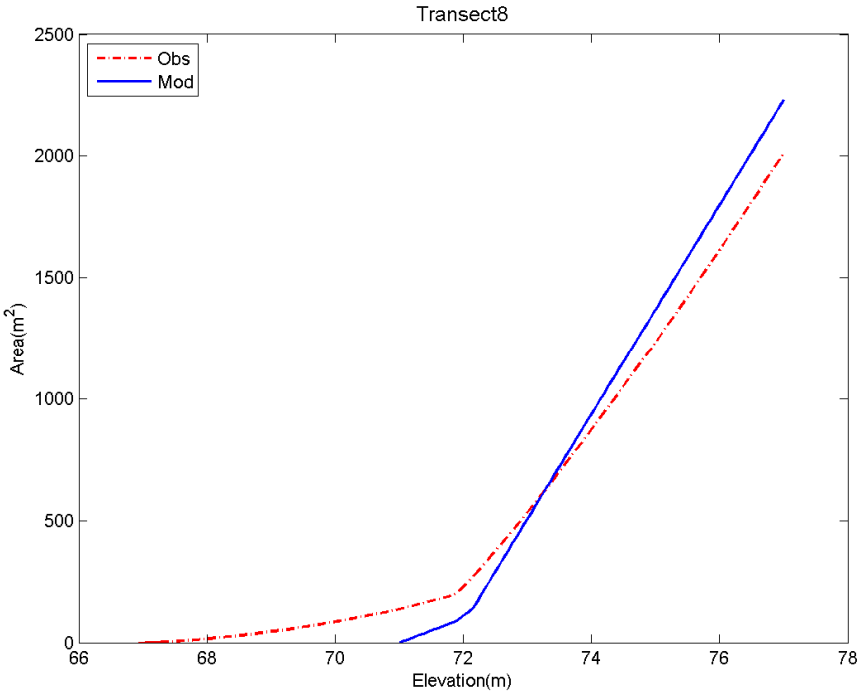
Transect8
Obs
Mod
Area(m2)
Elevation(m)
0
500
1000
1500
2000
2500
66
68
70
72
74
76
78

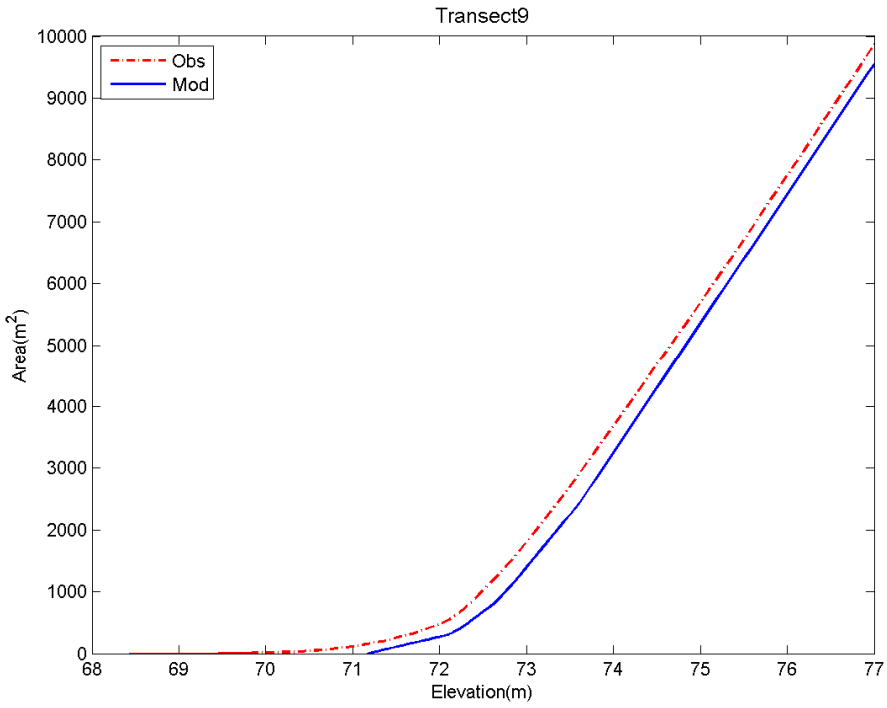
Transect9
Obs
Mod
Area(m2)
Elevation(m)
0
1000
2000
3000
4000
5000
6000
7000
8000
9000
10000
68
69
70
71
72
73
74
75
76
77

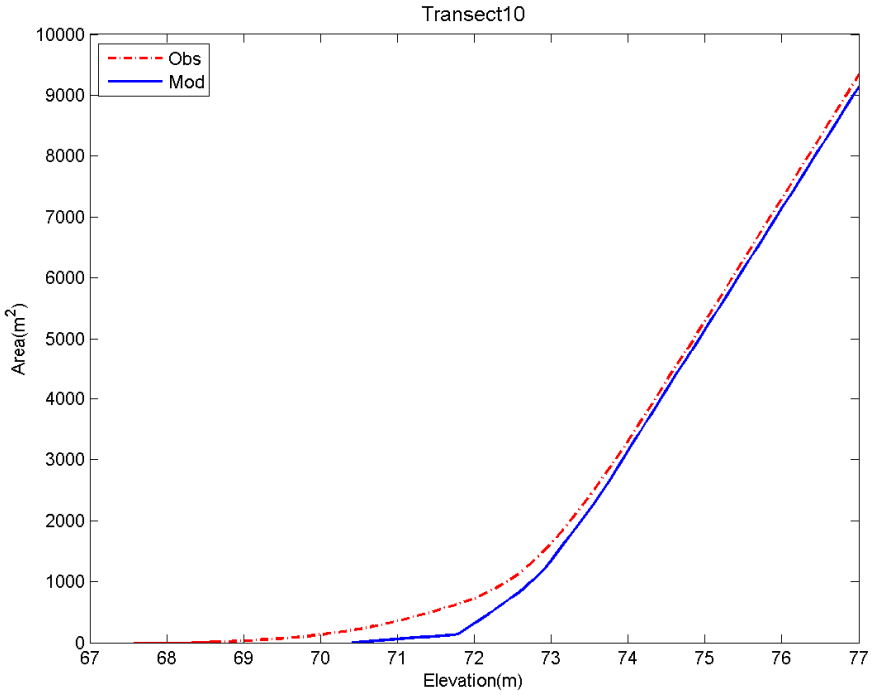
Transect10
Obs
Mod
Area(m2)
Elevation(m)
0
1000
2000
3000
4000
5000
6000
7000
8000
9000
10000
67
68
69
70
71
72
73
74
75
76
77

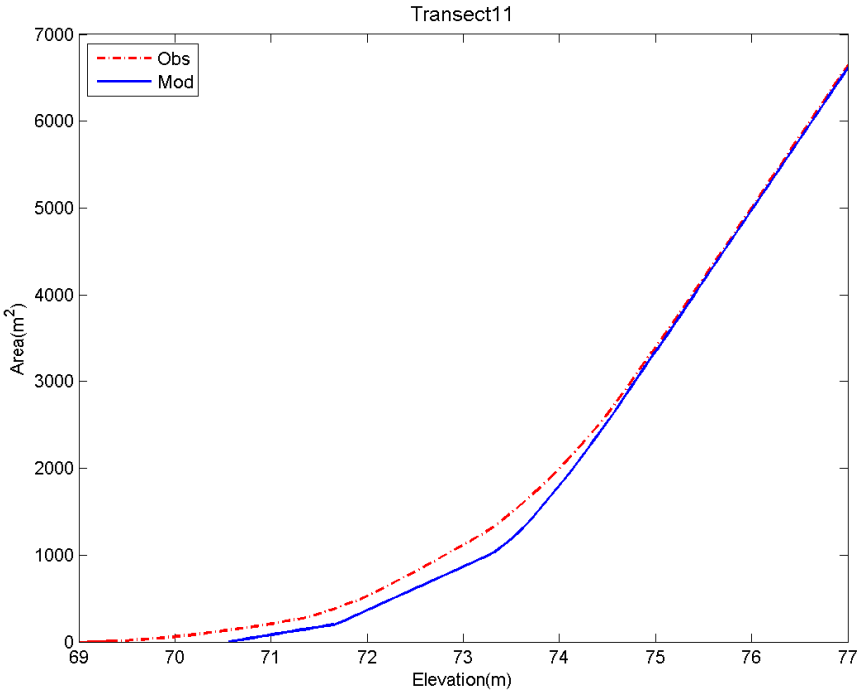
Transect11
Obs
Mod
Area(m2)
Elevation(m)
0
1000
2000
3000
4000
5000
6000
7000
69
70
71
72
73
74
75
76
77

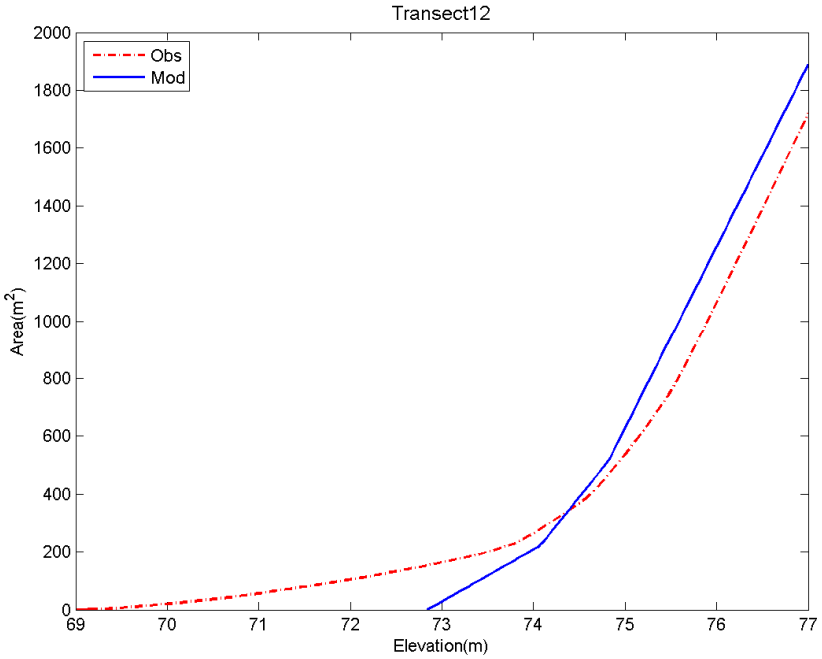
Transect12
Obs
Mod
Area(m2)
Elevation(m)
2000
1800
1600
1400
1200
1000
800
600
400
200
0
69
70
71
72
73
74
75
76
77

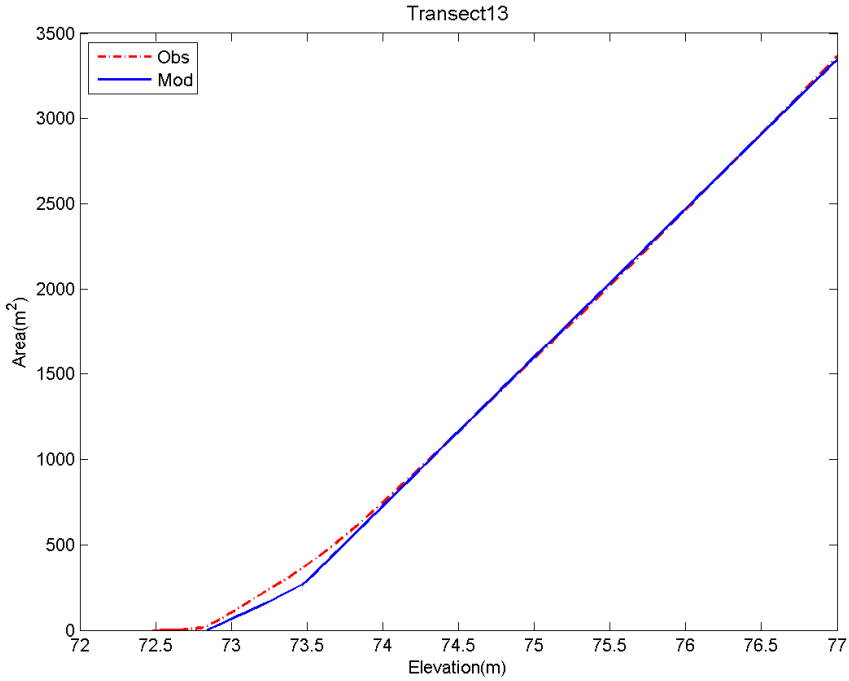
Transect13
Obs
Mod
Area(m2)
Elevation(m)
3500
3000
2500
2000
1500
1000
500
0
72
72.5
73
73.5
74
74.5
75
75.5
76
76.5
77

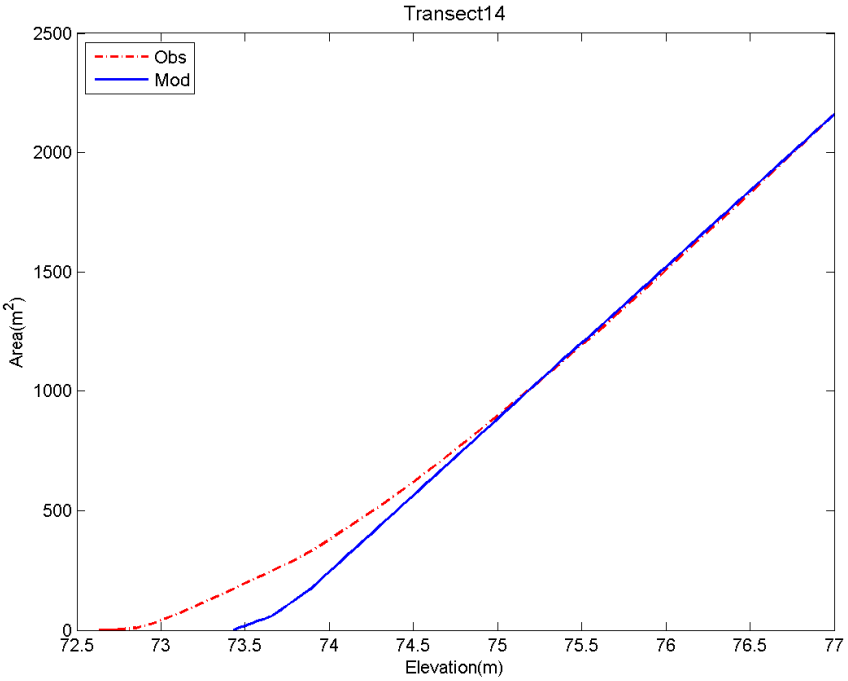
Transect14
Obs
Mod
2500
2000
1500
1000
500
0
Area(m2)
72.5
73
73.5
74
74.5
75
75.5
76
76.5
77
Elevation(m)

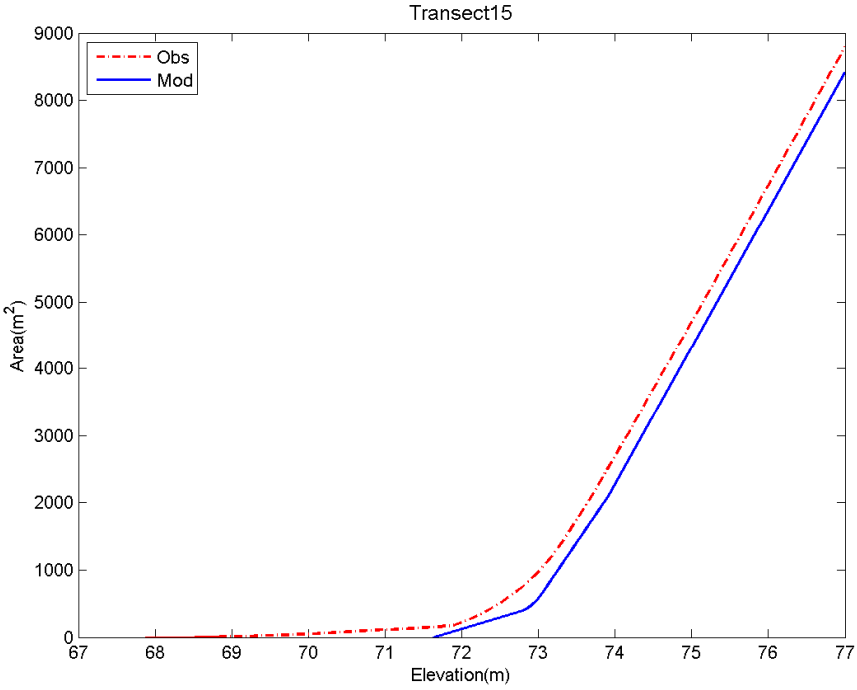
Transect15
Obs
Mod
9000
8000
7000
6000
5000
4000
3000
2000
1000
0
Area(m2)
67
68
69
70
71
72
73
74
75
76
77
Elevation(m)

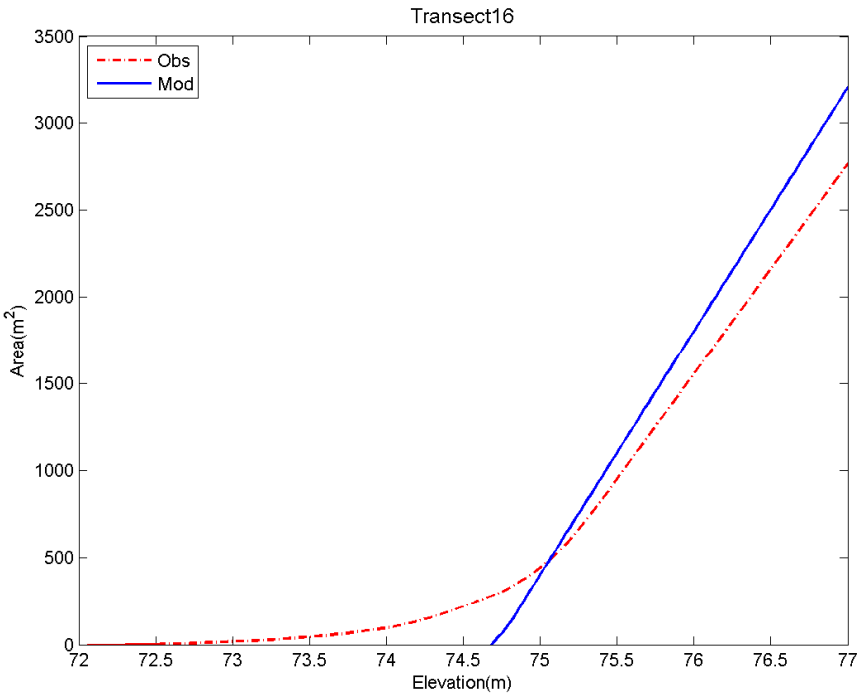
Transect16
Obs
Mod
Area(m2)
Elevation(m)
0
500
1000
1500
2000
2500
3000
3500
72
72.5
73
73.5
74
74.5
75
75.5
76
76.5
77

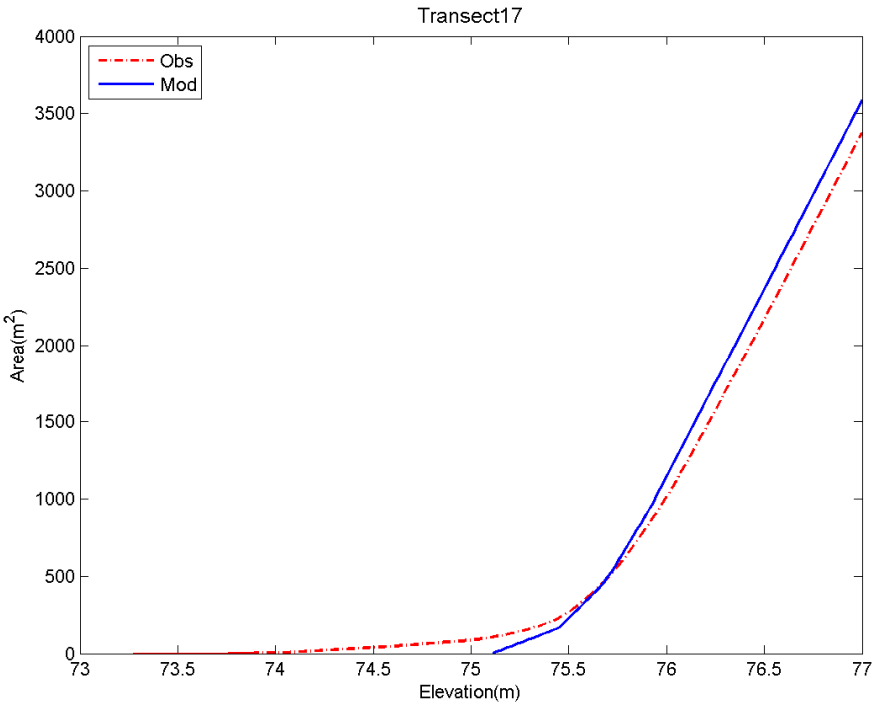
Transect17
Obs
Mod
Area(m2)
Elevation(m)
0
500
1000
1500
2000
2500
3000
3500
4000
73
73.5
74
74.5
75
75.5
76
76.5
77

Appendix B. Model calibration/validation results for water temperature

a. 2005 results (lines – model results; stars – field data) :

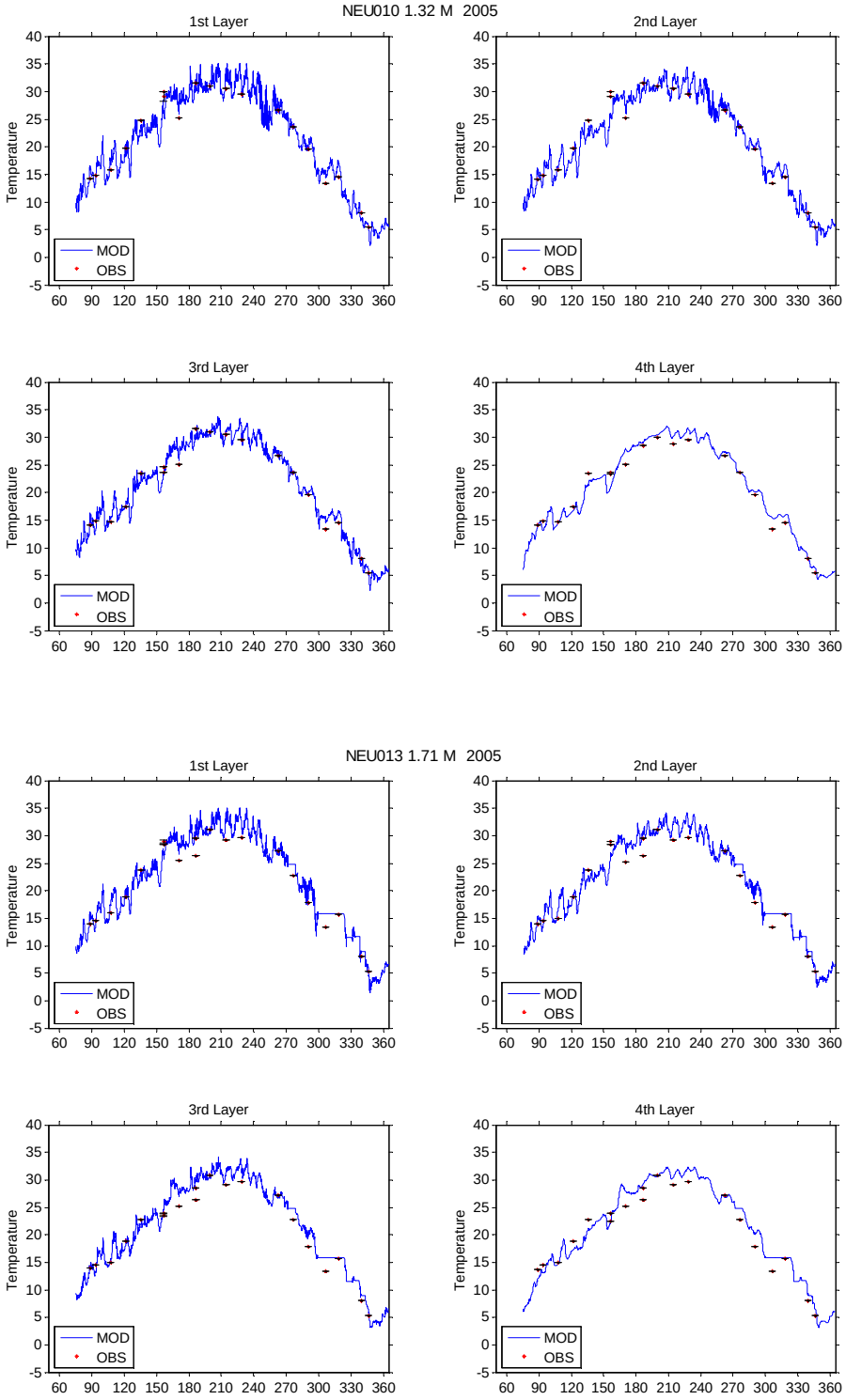

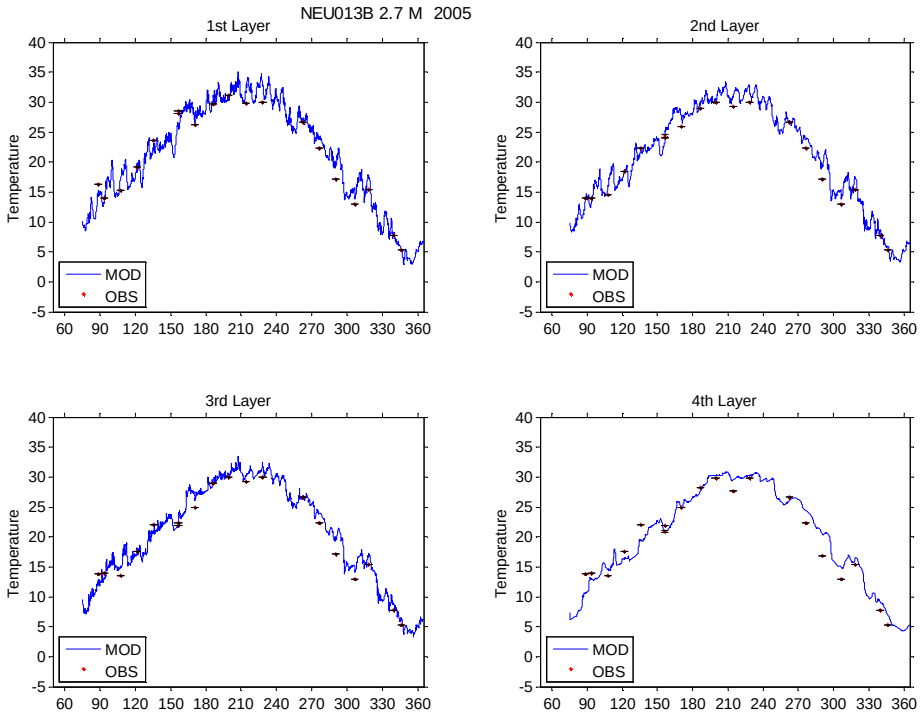
NEU013B 2.7 M 2005
1st Layer
2nd Layer
3rd Layer
4th Layer
Temperature
MOD
OBS

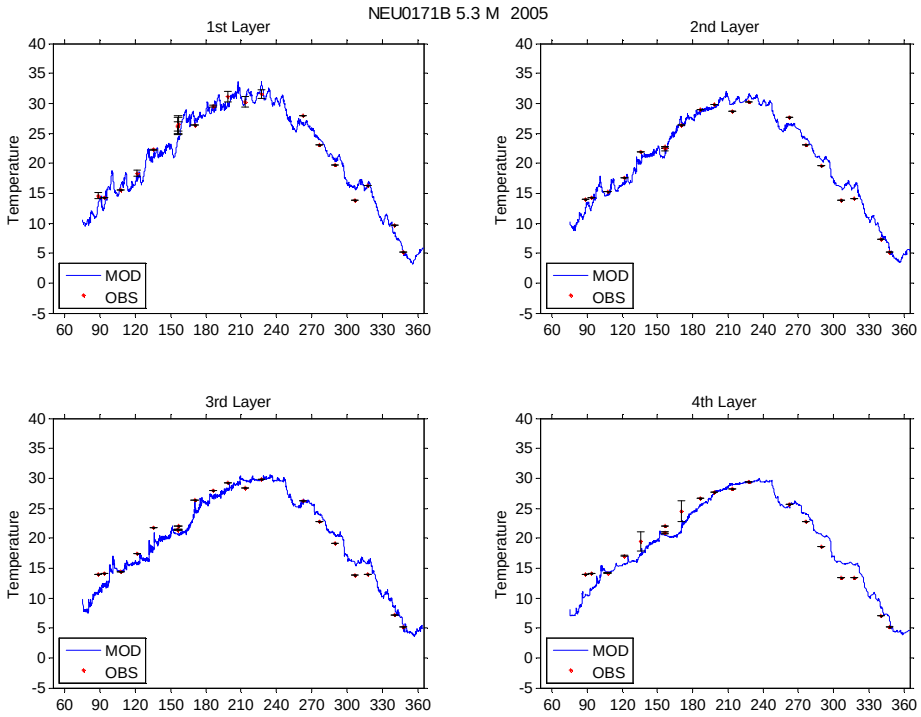
NEU0171B 5.3 M 2005
1st Layer
2nd Layer
3rd Layer
4th Layer
Temperature
MOD
OBS

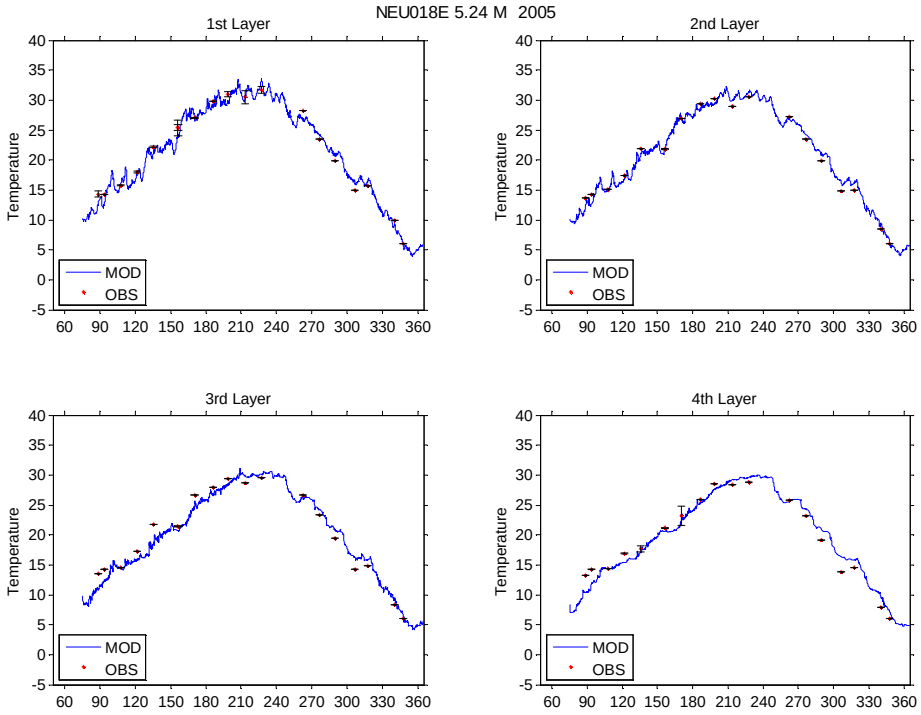
NEU018E 5.24 M 2005
1st Layer
2nd Layer
3rd Layer
4th Layer
Temperature
MOD
OBS

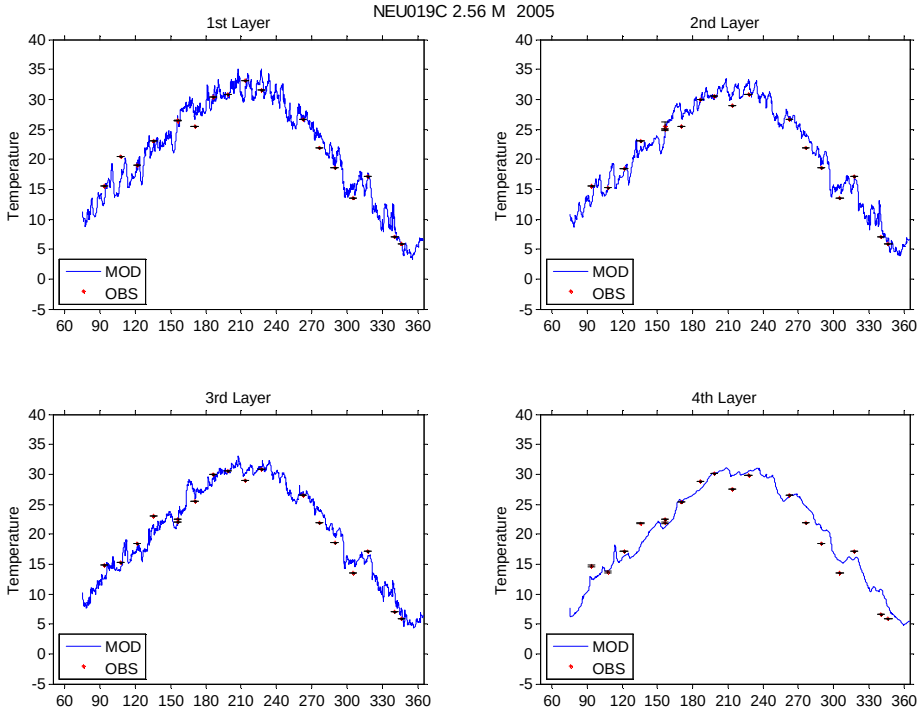
NEU019C 2.56 M 2005
1st Layer
2nd Layer
3rd Layer
4th Layer
Temperature
MOD
OBS

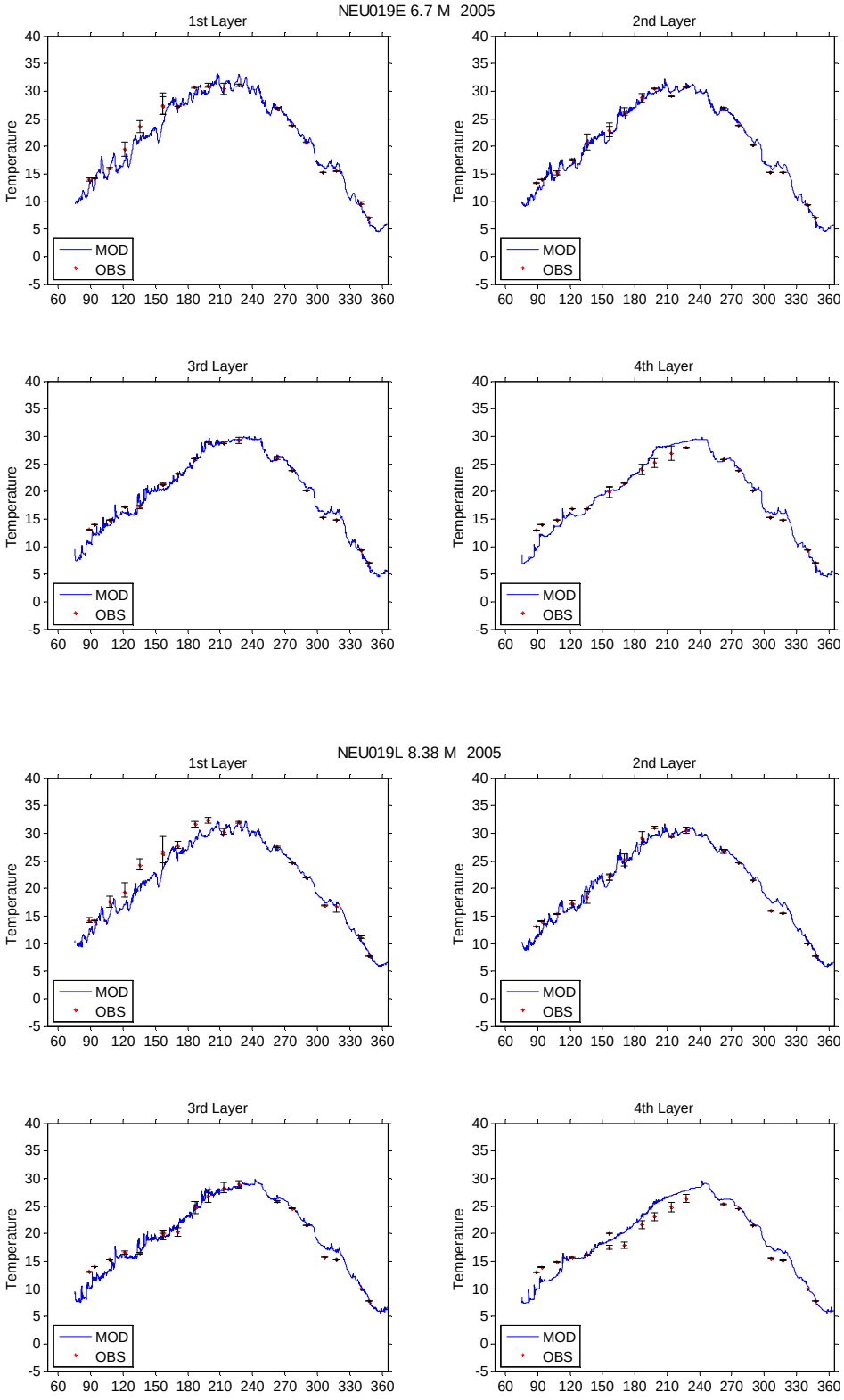
NEU019E 6.7 M 2005
1st Layer
2nd Layer
3rd Layer
4th Layer
NEU019L 8.38 M 2005
1st Layer
2nd Layer
3rd Layer
4th Layer
Temperature
MOD
OBS
40
35
30
25
20
15
10
5
0
-5
60 90 120 150 180 210 240 270 300 330 360

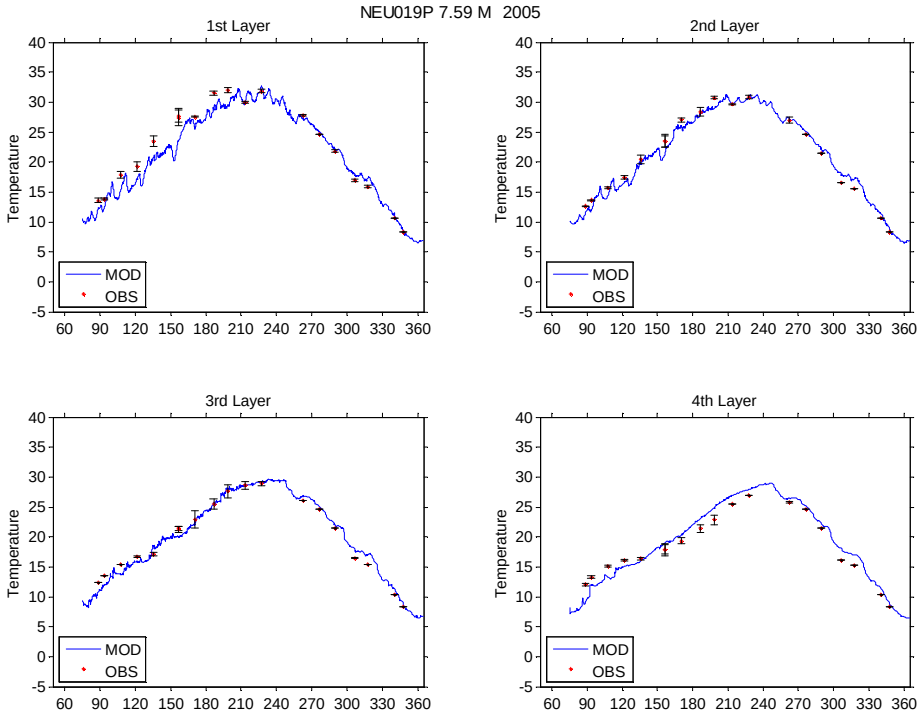
NEU019P 7.59 M 2005
1st Layer
2nd Layer
3rd Layer
4th Layer
Temperature
MOD
OBS

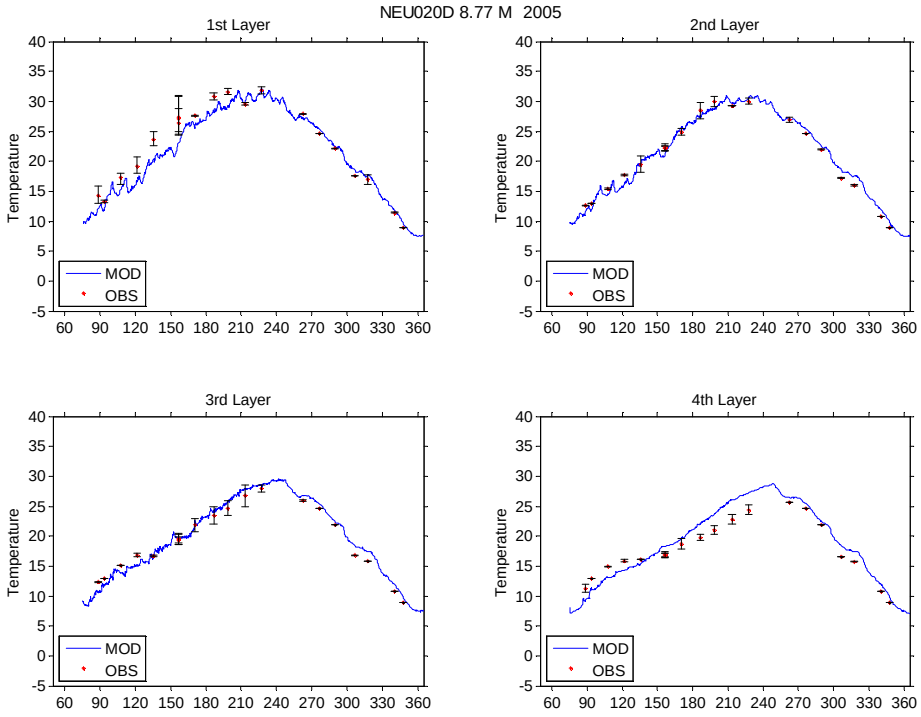
NEU020D 8.77 M 2005
1st Layer
2nd Layer
3rd Layer
4th Layer
Temperature
MOD
OBS

b. 2006 results (lines – model results; stars – field data) :

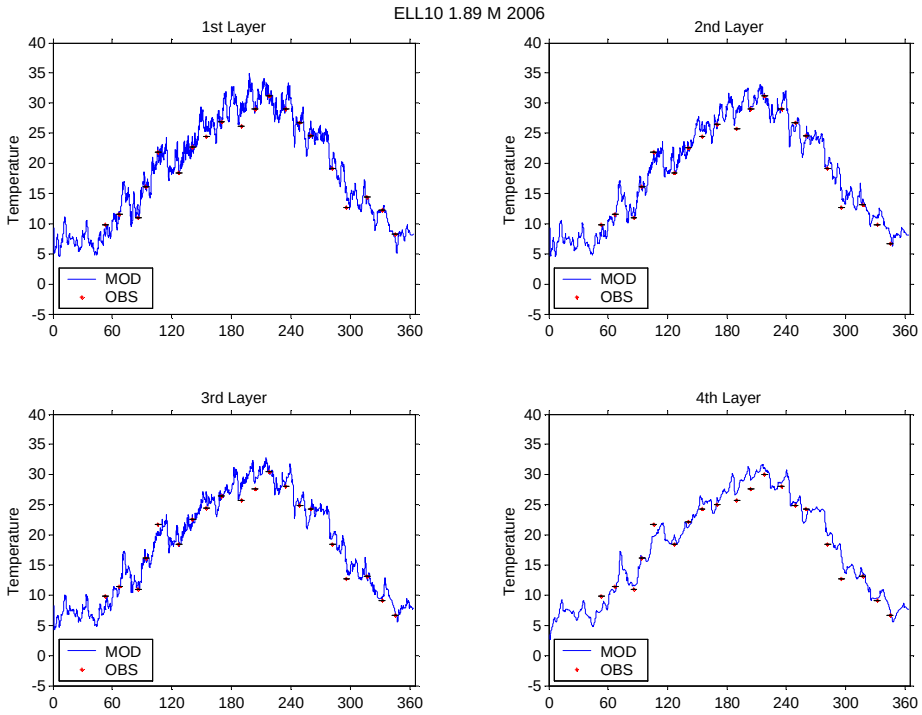

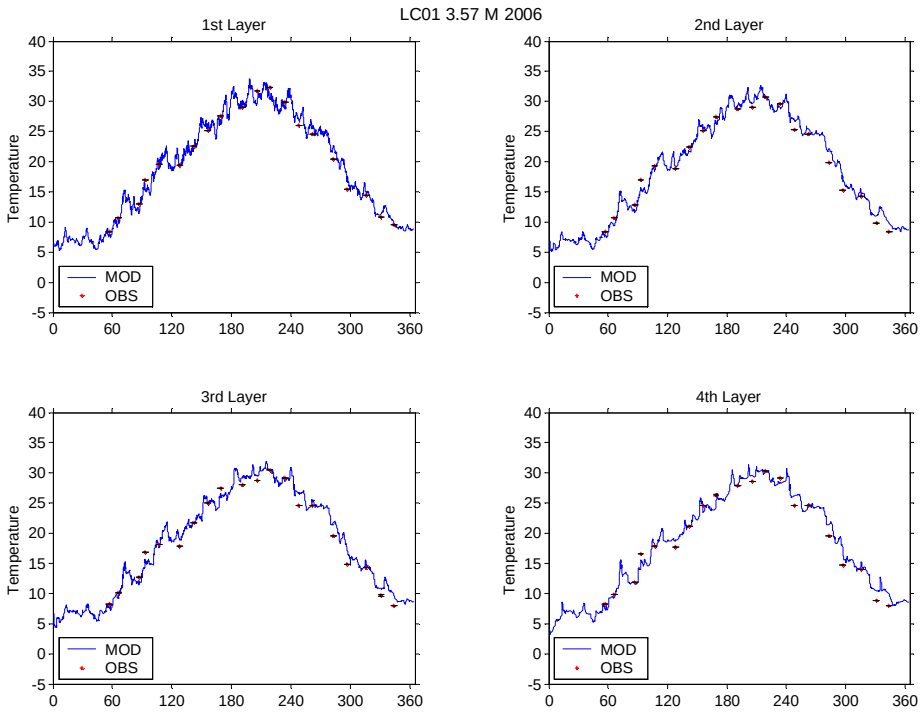

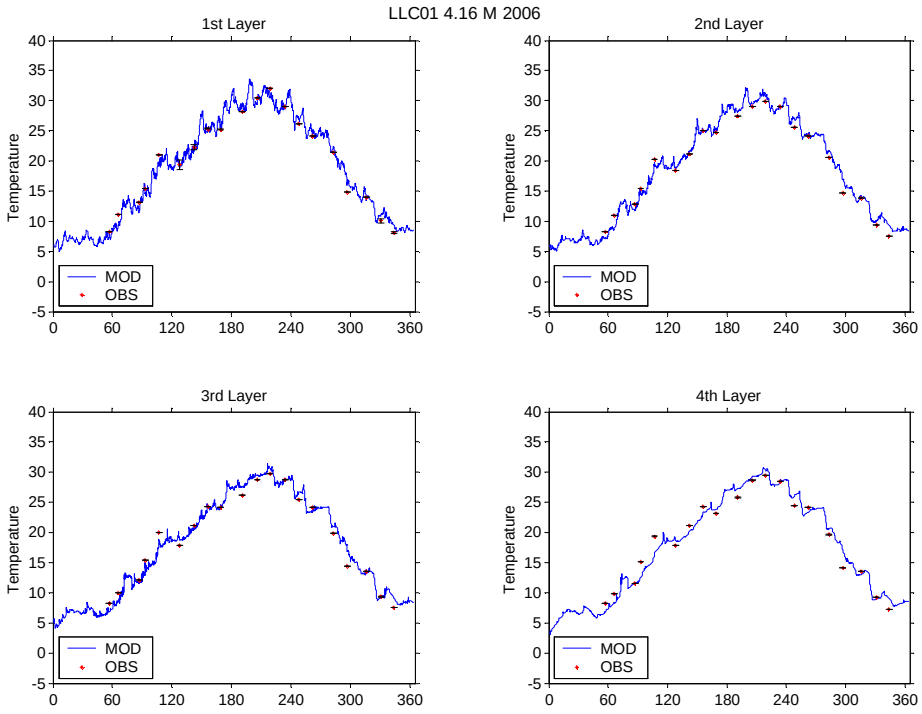
LLC01 4.16 M 2006
1st Layer
2nd Layer
3rd Layer
4th Layer
Temperature
MOD
OBS
0
60
120
180
240
300
360
-5
0
5
10
15
20
25
30
35
40

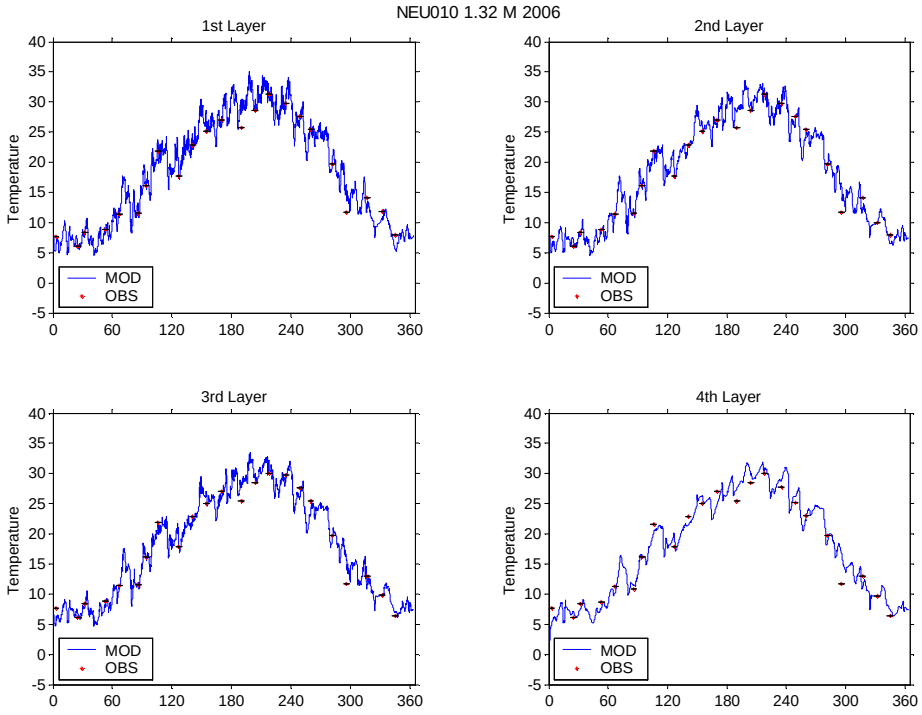
NEU010 1.32 M 2006
1st Layer
2nd Layer
3rd Layer
4th Layer
Temperature
MOD
OBS
0
60
120
180
240
300
360
-5
0
5
10
15
20
25
30
35
40

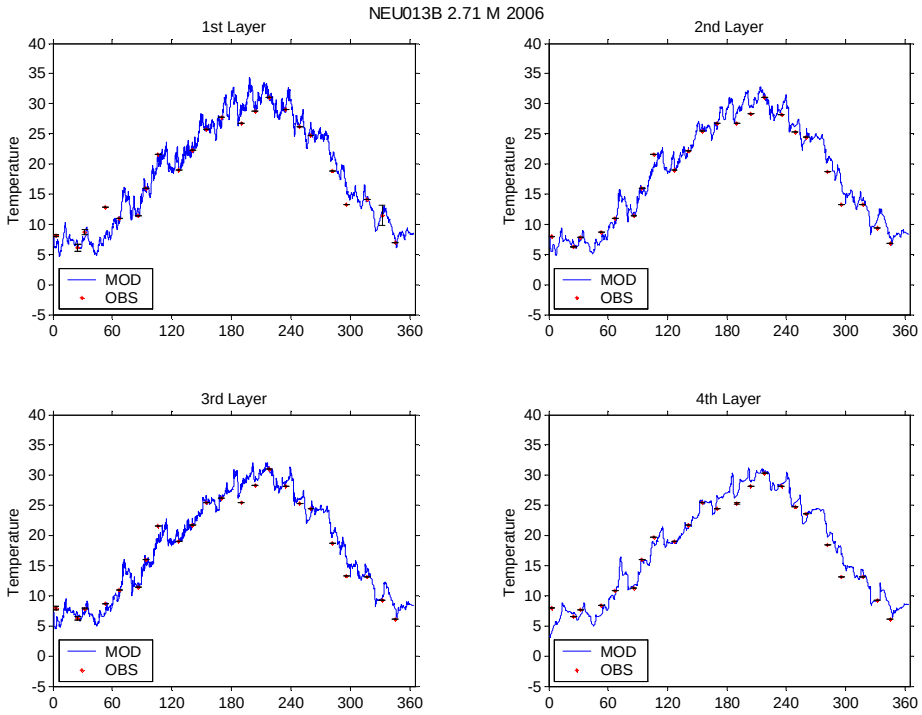
NEU013B 2.71 M 2006
1st Layer
2nd Layer
3rd Layer
4th Layer
Temperature
MOD
OBS

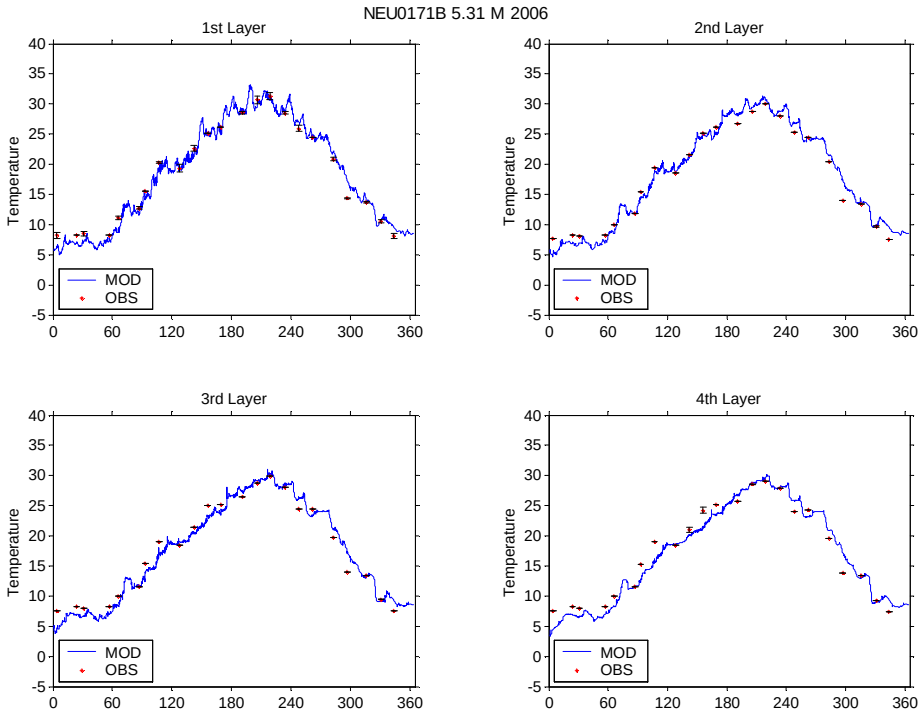
NEU0171B 5.31 M 2006
1st Layer
2nd Layer
3rd Layer
4th Layer
Temperature
MOD
OBS

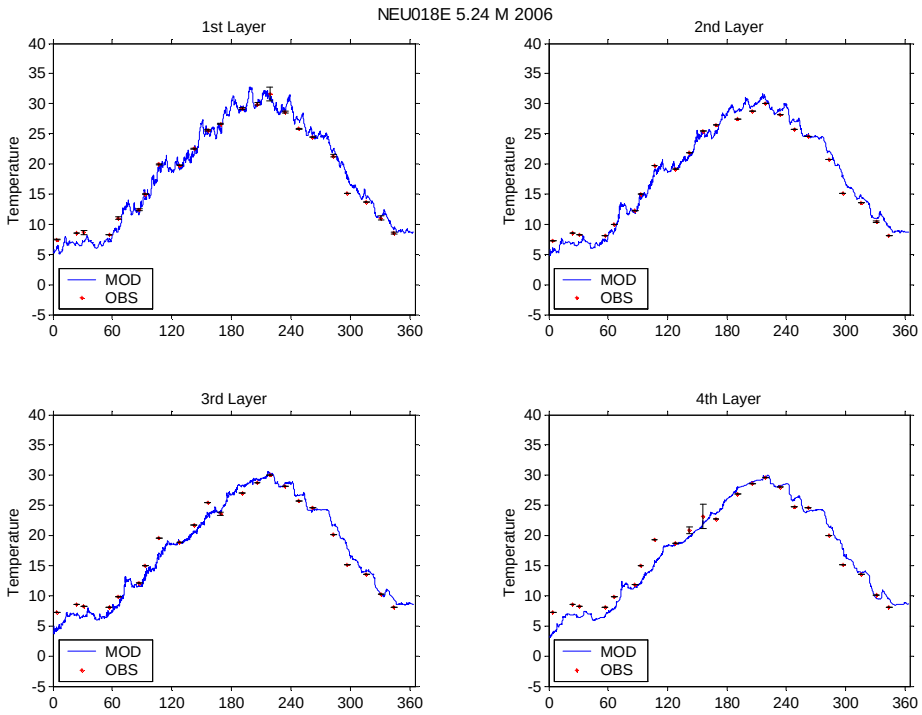
NEU018E 5.24 M 2006
1st Layer
2nd Layer
3rd Layer
4th Layer
Temperature
MOD
OBS

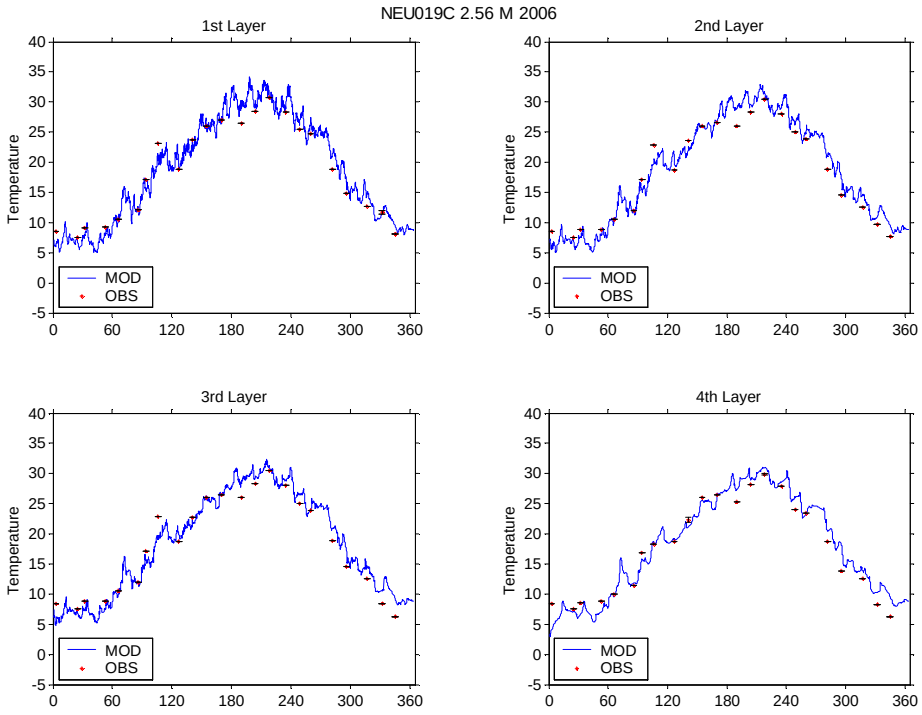
NEU019C 2.56 M 2006
1st Layer
2nd Layer
3rd Layer
4th Layer
Temperature
MOD
OBS

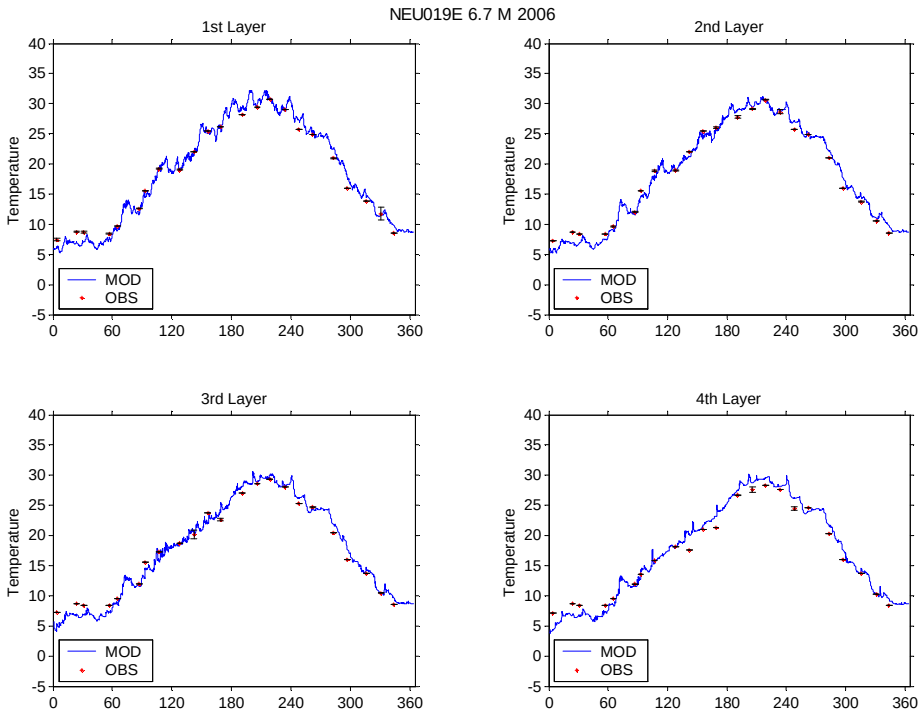
NEU019E 6.7 M 2006
1st Layer
2nd Layer
3rd Layer
4th Layer
Temperature
MOD
OBS

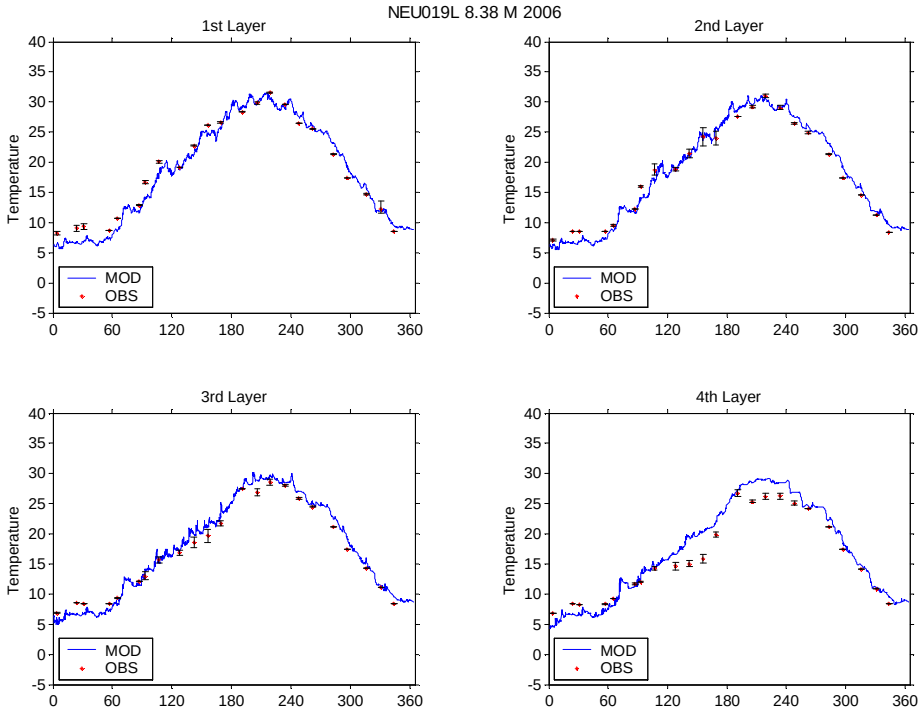
NEU019L 8.38 M 2006
1st Layer
2nd Layer
3rd Layer
4th Layer
Temperature
MOD
OBS

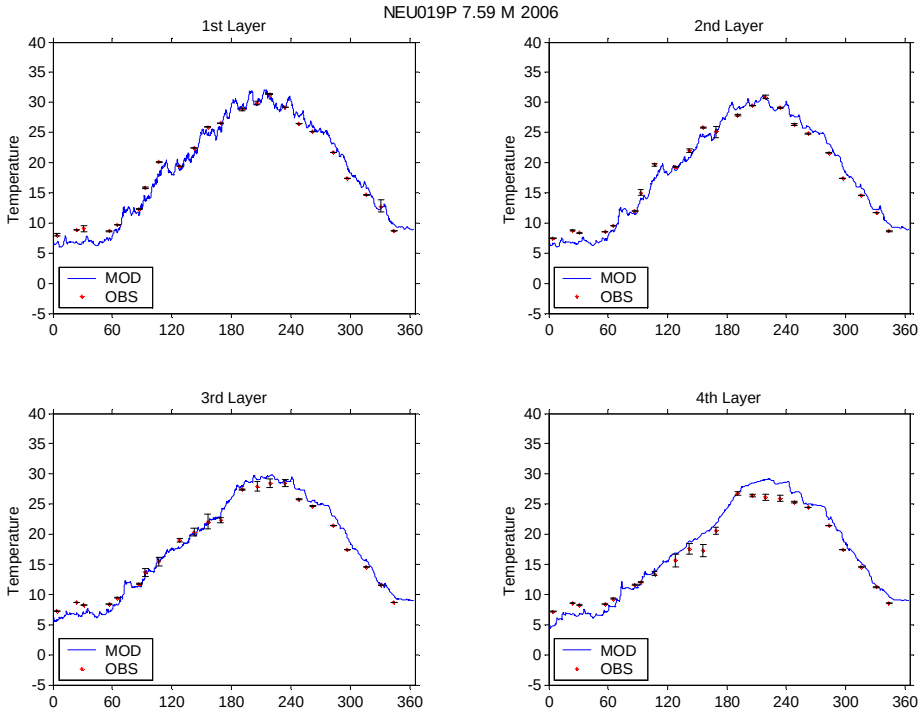
NEU019P 7.59 M 2006
1st Layer
2nd Layer
3rd Layer
4th Layer
Temperature
MOD
OBS

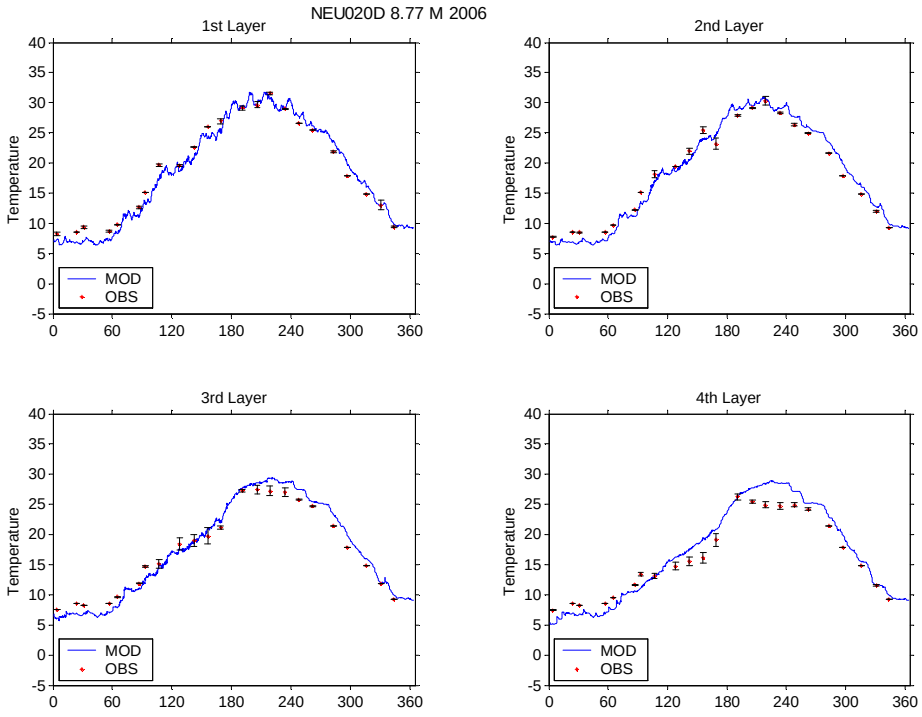
NEU020D 8.77 M 2006
1st Layer
2nd Layer
3rd Layer
4th Layer
Temperature
MOD
OBS

c. 2007 results (lines – model results; stars – field data) :

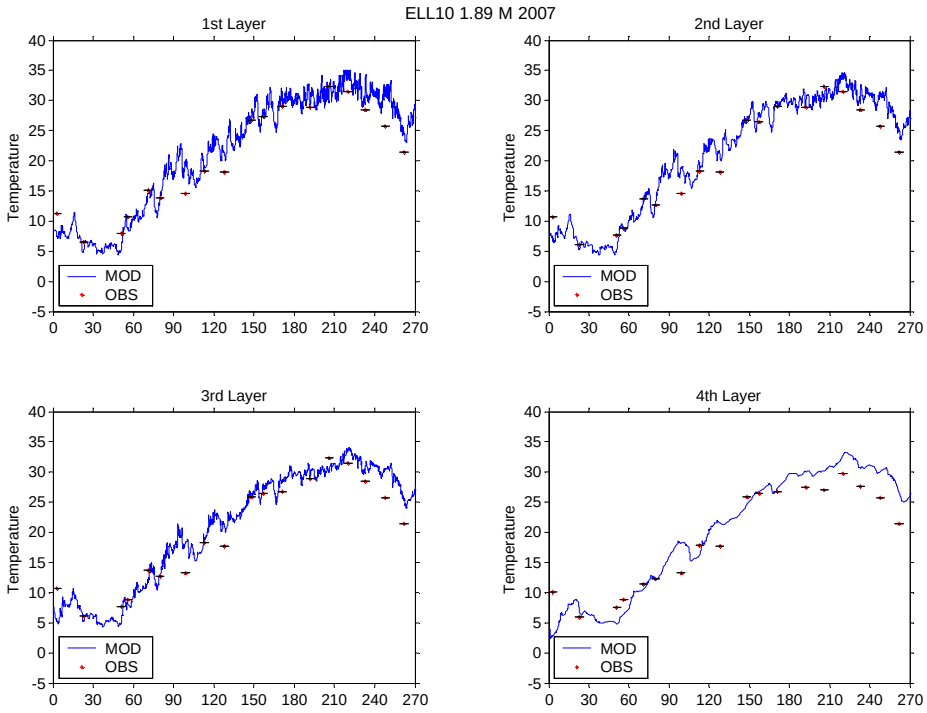

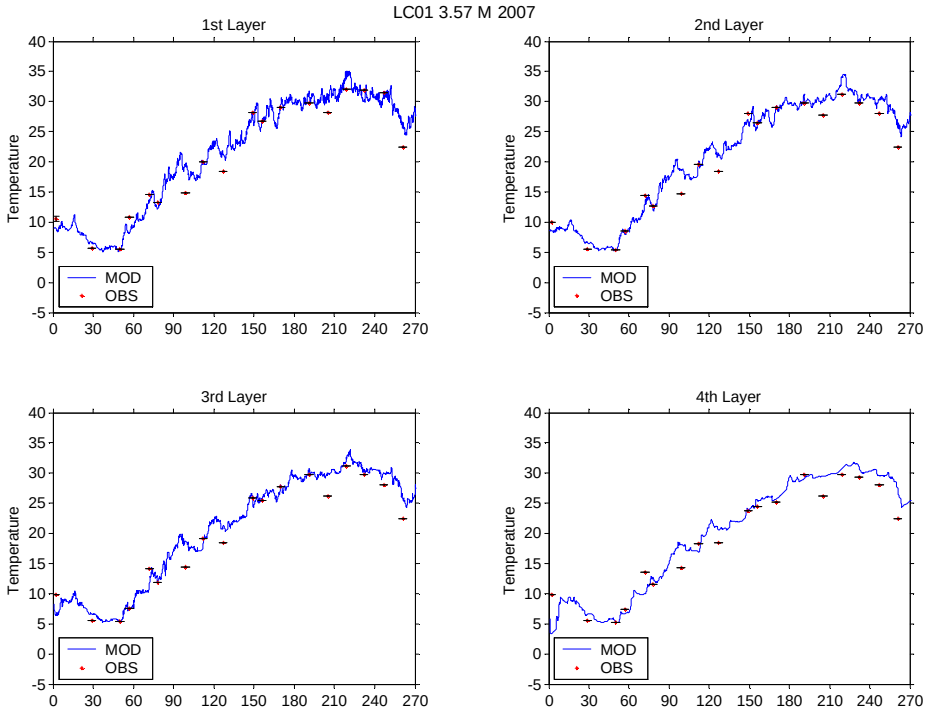

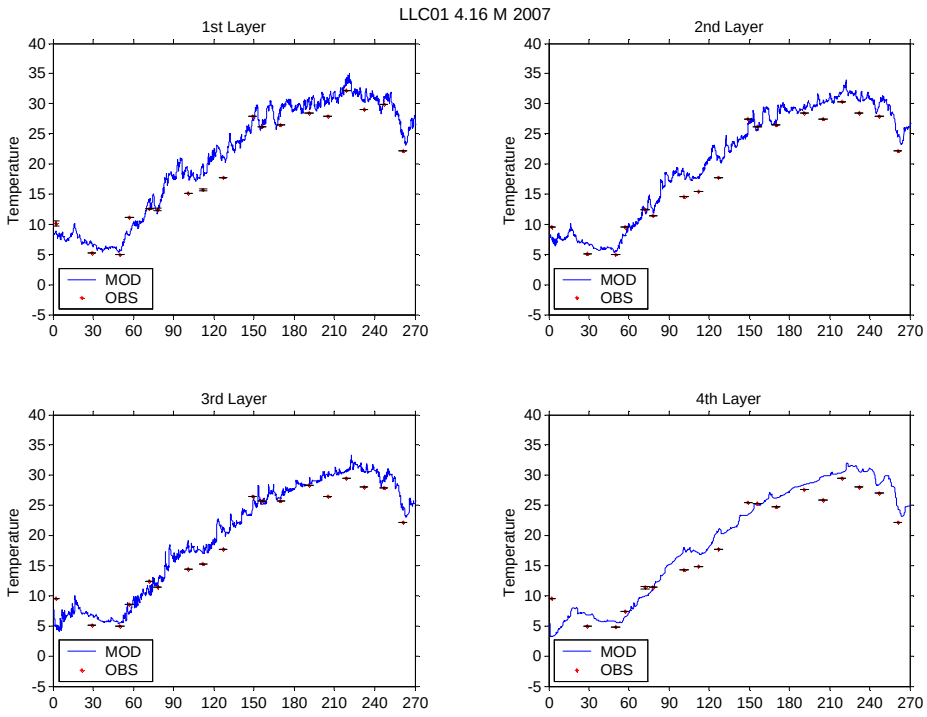
LLC01 4.16 M 2007
1st Layer
2nd Layer
3rd Layer
4th Layer
Temperature
MOD
OBS

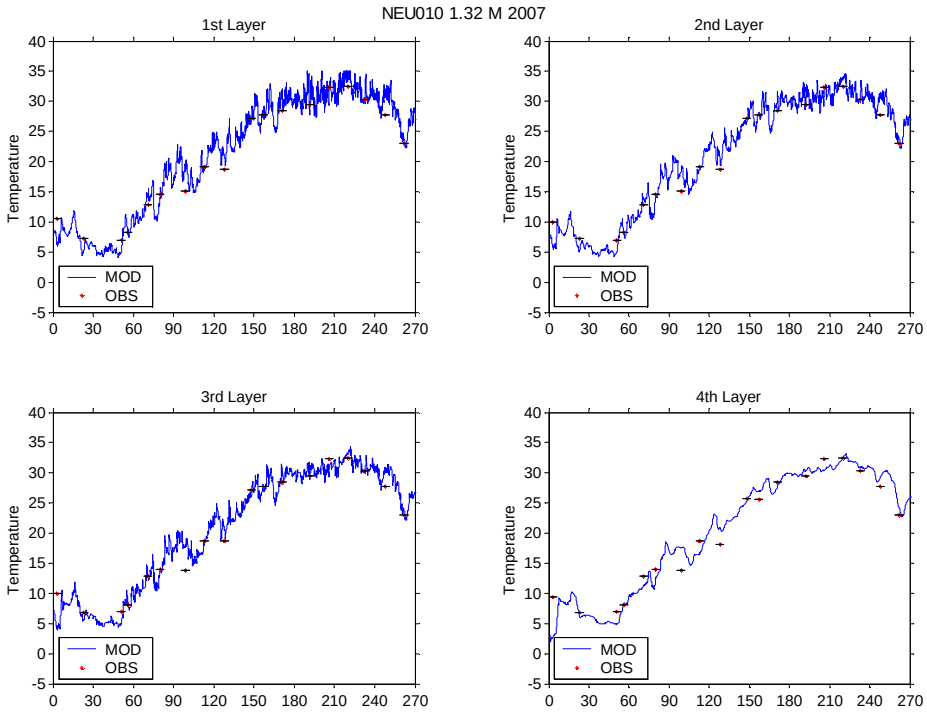
NEU010 1.32 M 2007
1st Layer
2nd Layer
3rd Layer
4th Layer
Temperature
MOD
OBS

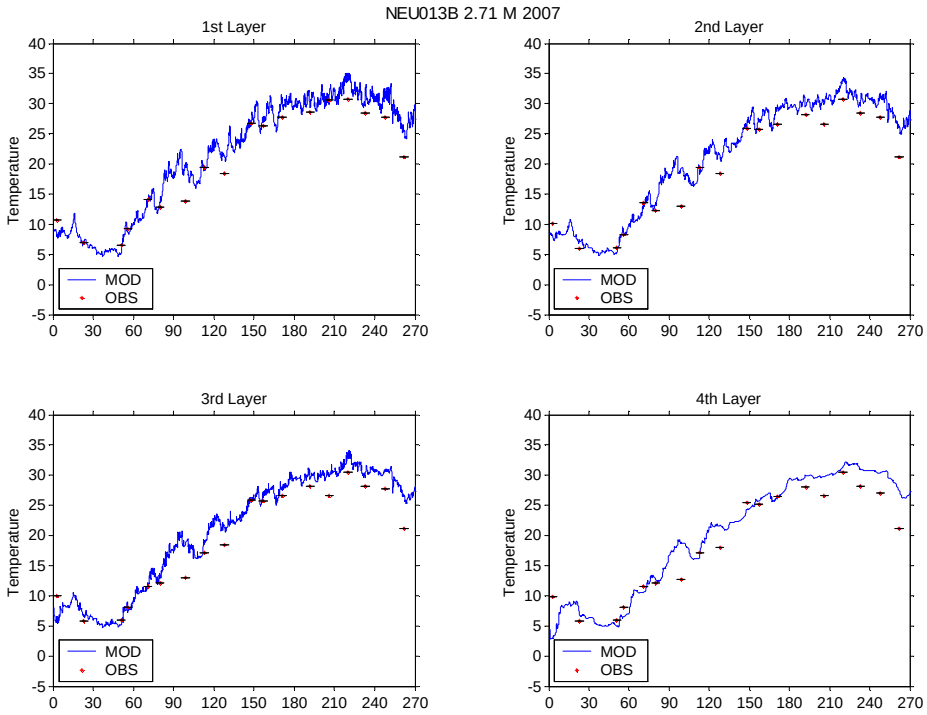
NEU013B 2.71 M 2007
1st Layer
2nd Layer
3rd Layer
4th Layer
Temperature
MOD
OBS
0 30 60 90 120 150 180 210 240 270
-5 0 5 10 15 20 25 30 35 40

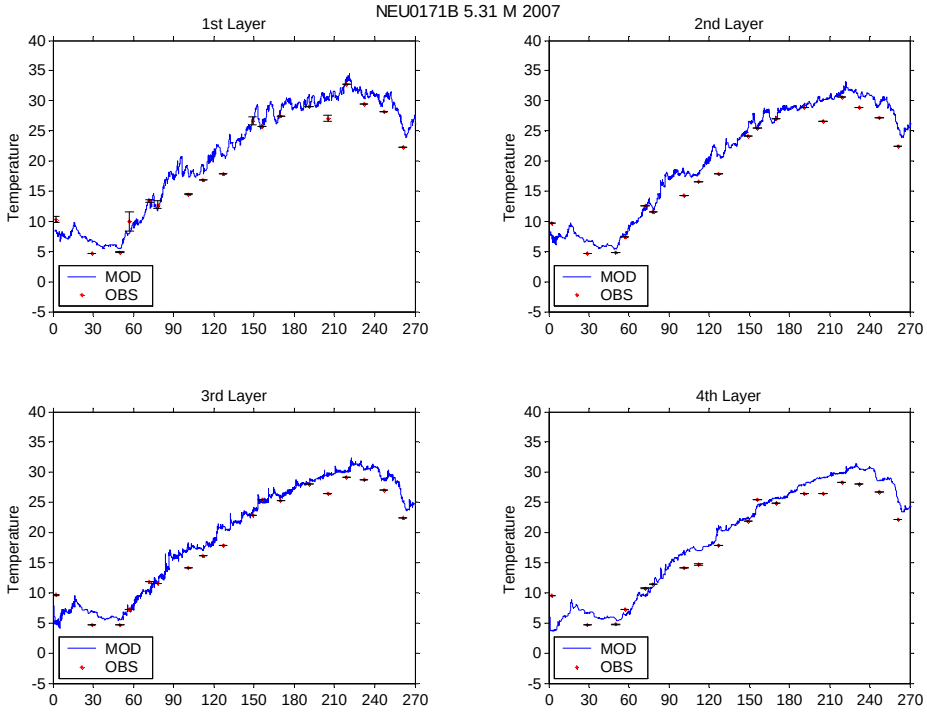
NEU0171B 5.31 M 2007
1st Layer
2nd Layer
3rd Layer
4th Layer
Temperature
MOD
OBS
0 30 60 90 120 150 180 210 240 270
-5 0 5 10 15 20 25 30 35 40

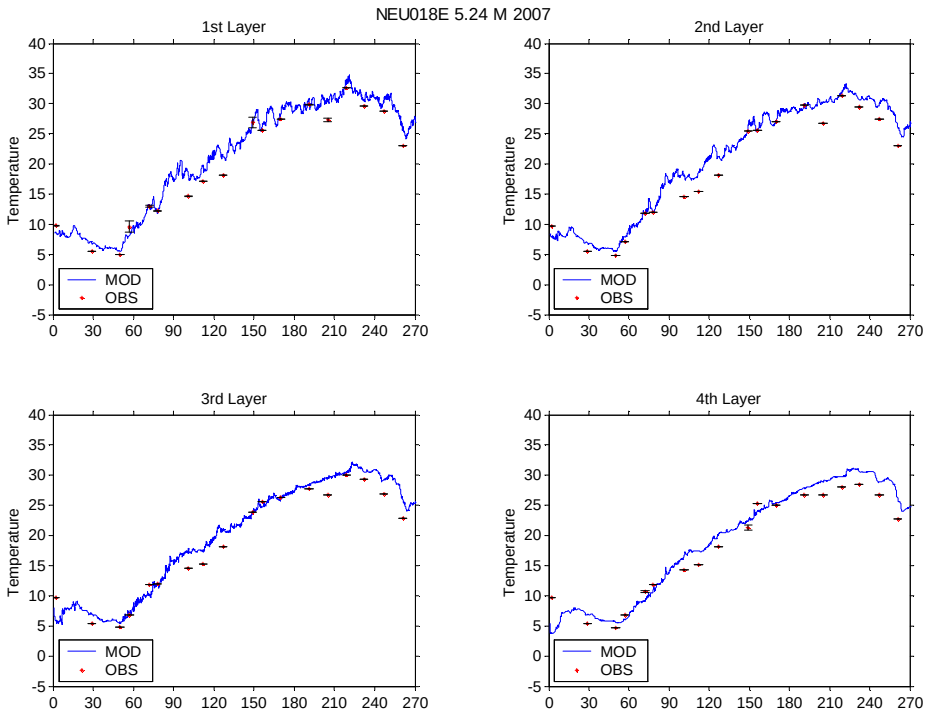
NEU018E 5.24 M 2007
1st Layer
2nd Layer
3rd Layer
4th Layer
Temperature
MOD
OBS

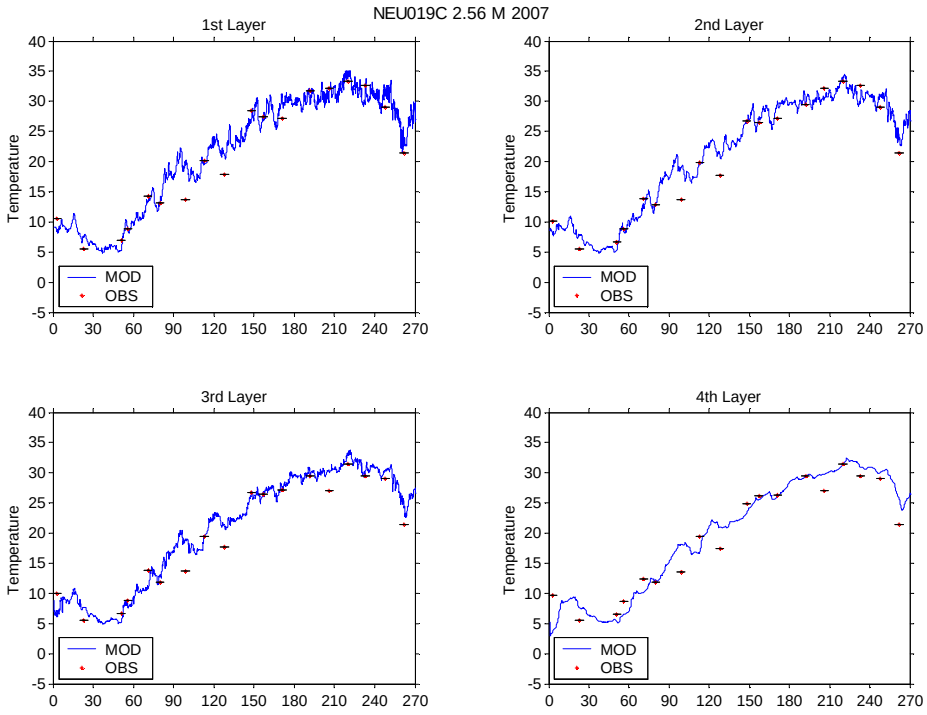
NEU019C 2.56 M 2007
1st Layer
2nd Layer
3rd Layer
4th Layer
Temperature
MOD
OBS

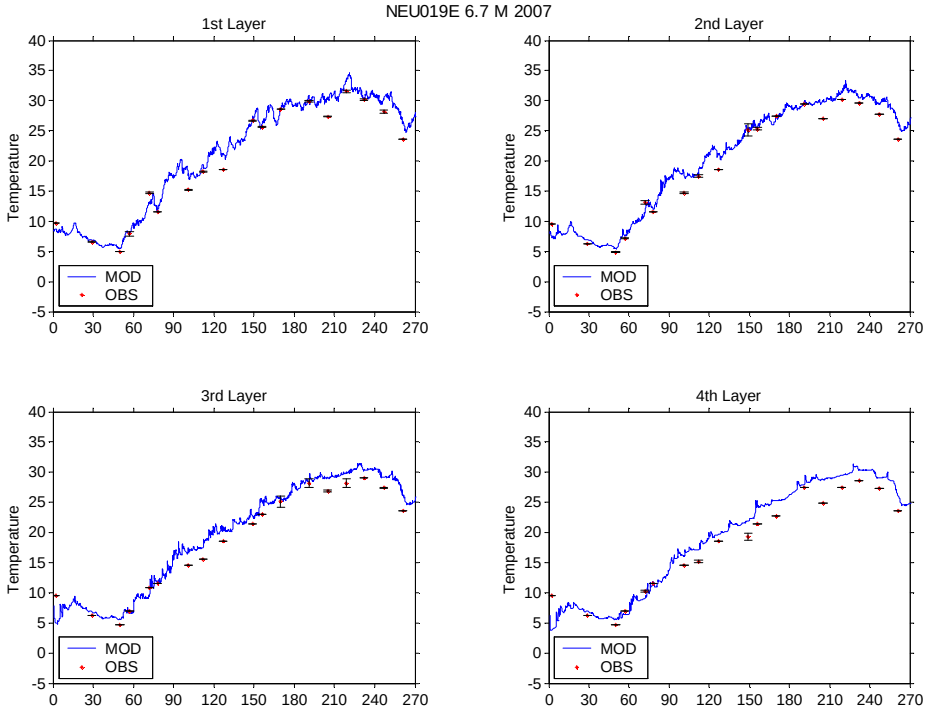
NEU019E 6.7 M 2007
1st Layer
2nd Layer
3rd Layer
4th Layer
Temperature
MOD
OBS

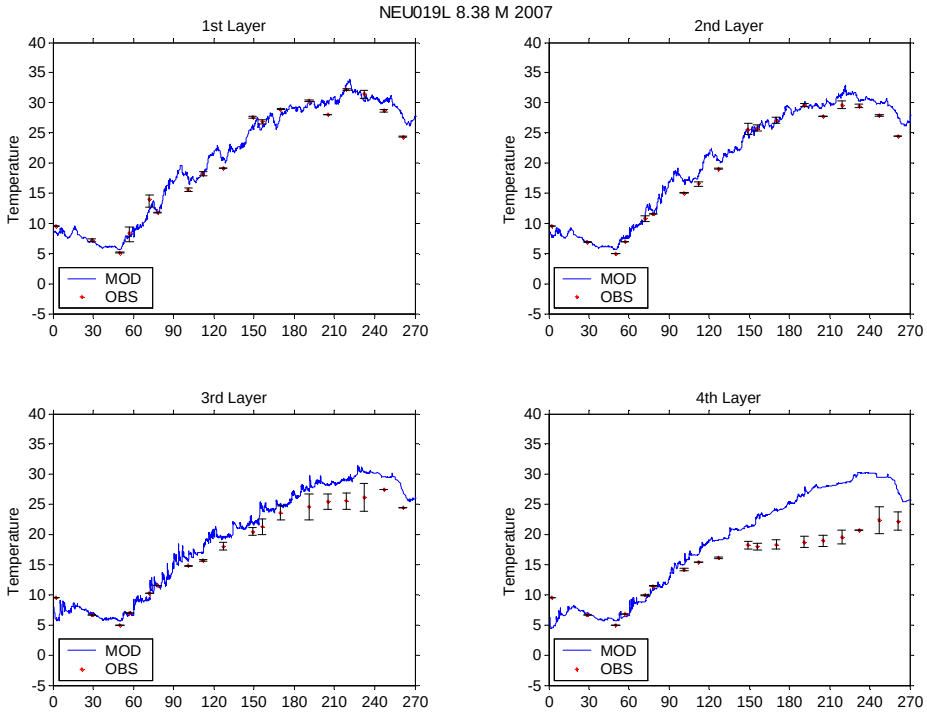
NEU019L 8.38 M 2007
1st Layer
2nd Layer
3rd Layer
4th Layer
Temperature
MOD
OBS

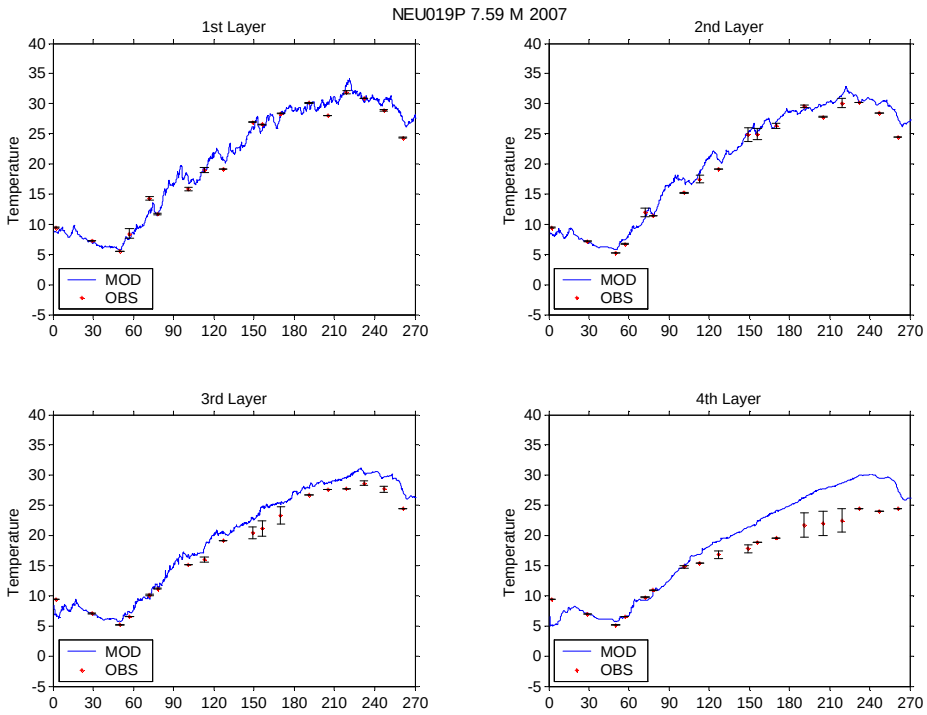
NEU019P 7.59 M 2007
1st Layer
2nd Layer
3rd Layer
4th Layer
Temperature
MOD
OBS

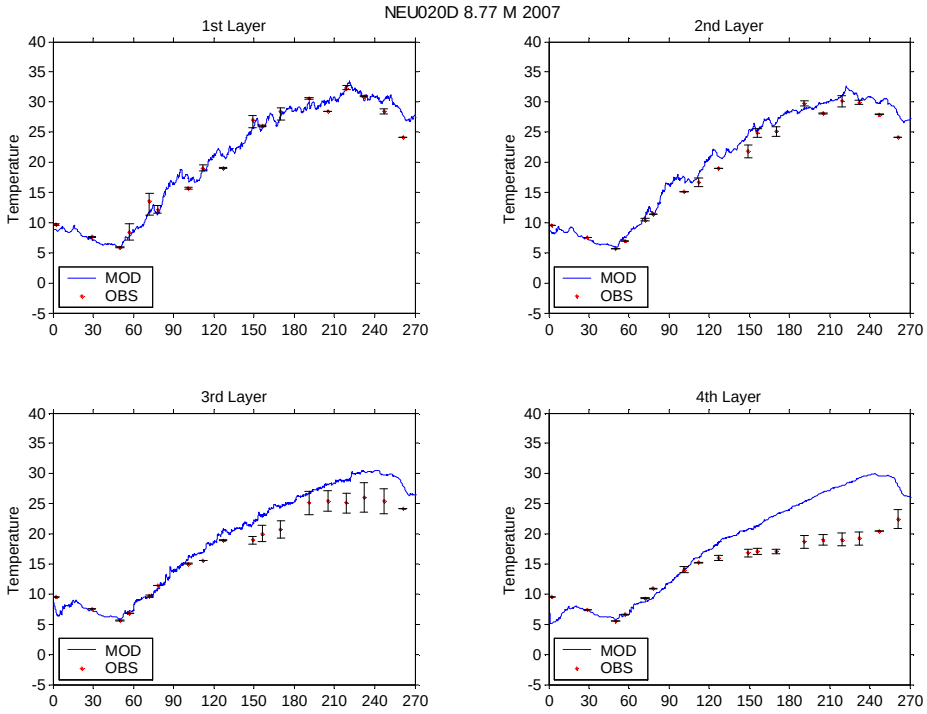
NEU020D 8.77 M 2007
1st Layer
2nd Layer
3rd Layer
4th Layer
Temperature
MOD
OBS

Appendix C. Model modifications

To meet the requirements and configurations for Falls Lake, the EFDC model was modified to better represent the system and its forcing conditions. The following lists the modifications made specifically for Falls Lake Nutrient Response Model:

1. Wave-induced bed shear stress

In the upper portion of the Falls Lake, TSS concentrations were usually very high, ranging from 10 to above 300 mg/l. Sediment resuspension from the bottom as well as river input are probably the primary causes. Wave-induced sediment resuspension may be important in shallow areas. Wave-induced bed shear stress following Lin et al (2003) was added in the model to simulate sediment resuspension due to wind waves. The formulation was illustrated under bullet b of section II-1. The affected model subroutines include SSEDTOX.

2. Time-varying atmospheric deposition

The available information regarding atmospheric deposition of nutrients were assessed by NC Department of Transportation (NCDOT, 2008). The best representation was reported to be time-series of wet and dry atmospheric deposition data from NADP and CASTNET (detailed descriptions under bullet b of section II-2). Constant depositional fluxes were required from the original model (WQWETTS.INP, WQDRYTS.INP). Modifications were made in order to allow for time series input of wet and dry atmospheric depositions. The affected model subroutines include RWQATM and RWQC1.

3. Moving river boundary

During the summer months of 2005 and 2007, when drought condition occurred, many upstream cells were marked as dry cells, not allowing flows coming from or going into the cell when the cell depth fell below a critical value. When such condition occurred at the river boundary cells in the Falls Lake Model, pollutant delivered into the dry cell will be blocked from moving downstream. To avoid such blockage, a moving river boundary was built into the model. An array representing the channel cells from each tributary into the lake was read in from an

input file (QIJMV.INP). If the river boundary cell was marked as dry, its corresponding downstream cells were evaluated one by one until a wet cell was found, and that wet cell served as the new river boundary cell. The model subroutines affected by this modification include RWQPSL, CALBAL3, BUDGET3, CALTRWQ, CALLQS2, CALFQC, CALQVS, CALQS2, CALTRANQ, CALTRANI, CBALEV3, and CBALOD3.

Reference:

Lin, J., H.V. Wang, J.H. Oh, k. Park, S. Kim, J. Shen, and A.Y. Kuo (2003), A new approach to model sediment resuspension in tidal estuaries, *Journal of Coastal Research* 19(1): 76-88.

NCDOT Highway Stormwater Program, (2008), Summary of atmospheric deposition data available for modeling nutrients in the Falls Lake, North Carolina, watershed, Draft Report, May 5, 2008.

Appendix D. Model Review Response

Draft Falls Lake Model documentation was released to Falls Lake Technical Advisory Committee (TAC) on March 23, 2009. A complete copy of the model, including model input files, model code, model executable, model output, and data files, was released to TAC members who requested it on April 1, 2009.

During the model review period, the North Carolina Department of Transportation (DOT) contracted with TetraTech to conduct a thorough review of the lake model. DOT submitted their review comments, together with a report from TetraTech, on May 29, 2009.

In summary, three key recommendations were made by TetraTech:

1. During 2006, rainfall input was based on station “Clay.” Station Clay is not a good representation of the "wet" year of 2006. Data from "RDU" should be used.

Response:
When modelers from Modeling & TMDL Unit (MTU) of DWQ requested data from the State Climate Office, RDU station seemed to have more missing data than Clay; therefore, data from Clay were initially used.

DWQ acknowledges that rainfall recorded at RDU may be a better representation of what happened in the lake area during 2006. The input file was re-generated based on RDU data and data from station Reed (Reedy Creek) were used when missing data were reported for RDU.

2. For dry atmospheric deposition, NH4 flux suggested by a multi-layer-model from CASTNET show much lower values than what the lake model used.

Response:
Literature values from research work at NCSU were originally used for the estimation of depositional velocity, hence the model input of NH4 atmospheric depositional flux. As suggested by TetraTech, the dry deposition input file was re-generated for the model (2005-2007) based on the MLM weekly output from CASTNET.

3. Uncertainty analysis and explicit definition of model goal is needed.

Response:
Discussions were added to the report.

The current draft report reflects model results after the above modifications were made. The reported model scenario runs are based on the newly modified model.